National Science Foundation Graduate Fellowship and Grant ATM-9900929

SATELLITE AND RADAR SURVEY OF MESOSCALE CONVECTIVE SYSTEM DEVELOPMENT

by Israel L. Jirak

William R. Cotton, P.I.

DEPARTMENT OF ATMOSPHERIC SCIENCE

Paper No. 727

SATELLITE AND RADAR SURVEY OF MESOSCALE CONVECTIVE SYSTEM DEVELOPMENT

by

Israel L. Jirak

Department of Atmospheric Science

Colorado State University

Fort Collins, Colorado 80523

Research Supported by

National Science Foundation

under a Graduate Fellowship and Grant ATM-9900929

June 27, 2002

Atmospheric Science Paper No. 727

ABSTRACT

SATELLITE AND RADAR SURVEY OF MESOSCALE CONVECTIVE SYSTEM DEVELOPMENT

An investigation of mesoscale convective systems (MCSs) during the warm seasons (April-August) of 1996-1998 is presented. The MCSs were initially identified and classified by infrared satellite imagery. A satellite classification scheme encompassing MCSs of a wide variety of shapes and sizes is introduced. The classes include *mesoscale convective complexes (MCCs), persistent elongated convective systems (PECSs), meso-β MCCs (MβMCCs), and meso-β PECSs (MβPECSs)* . Definitions, basic characteristics, and examples are provided for each. In addition, the development of each of the systems was analyzed using 2-km national composite radar reflectivity data. A three-level classification process describing MCS development is identified. These levels include determining the *presence of stratiform precipitation, arrangement of convective cells, and interaction of convective clusters* . Each level of the classification process is described and compared in detail, along with examples.

The environment in which each MCS developed was determined from the standard National Weather Service upper-air network. Additionally, the severe weather

reports were logged for each system. The findings of these data are discussed in context of the present classification schemes. Furthermore, composite analyses of the satellite lifecycle and precipitation lifecycle are presented.

Israel L. Jirak
Department of Atmospheric Science
Colorado State University
Fort Collins, Colorado 80523
Summer 2002

ACKNOWLEDGEMENTS

I am grateful to Colorado State University and the Department of Atmospheric Science for providing an educational environment that allowed myself to pursue research in the field of atmospheric science. First of all, I would like to thank my advisor, Dr. William R. Cotton, for his guidance on my research. In addition, I would like to recognize Dr. Steven A. Rutledge and Dr. Jorge A. Ramírez for serving on my committee.

I am truly indebted to Ray McAnelly for all of the help and advice that he offered. Without his expertise, the research presented in this thesis would surely not be the same and certainly would have taken longer to finish. Furthermore, I would like to thank the remaining members of the Cotton group for all of the assistance and support that they have provided.

Infrared satellite data and radar composite data were provided by the Global Hydrology Resource Center. This research was supported by a National Science Foundation (NSF) Graduate Fellowship as well as NSF grant ATM-9900929.

Finally, I would like to thank my family, and especially my wife, Hannah, for her love, support, caring, and understanding in carrying me through this research.

TABLE OF CONTENTS

1 Introduction **1**

2 Background **5**

2.1 Satellite classification of MCSs 6

2.2 Radar classification of MCSs 8

2.2.1 Radar classification by organization 9

2.2.2 Radar classification by development 12

3 Data and methods of analysis **17**

3.1 Study area and period 17

3.2 Satellite data 19

3.2.1 Dataset information 19

3.2.2 Satellite analysis 19

3.3 Radar data 21

3.3.1 Dataset information 22

3.3.2 Radar analysis 22

3.4 Sounding data and severe weather reports 24

4 Satellite classification of MCSs **27**

4.1 Definition of classes 27

4.2 Basic characteristics 30

4.3 Examples of classes 34

5 Radar classification of MCSs **39**

5.1 Classification by organization 39

5.2 Classification by development 43

5.2.1 Definition of classes 44

5.2.2 Basic characteristics 48

5.2.3 Examples of classes 54

6 MCS environment and severe weather **61**
6.1 Average properties of soundings 61
6.2 Properties of average soundings 67
6.3 Severe weather reports 69

7 MCS composite results **81**
7.1 MCS tracks 81
7.2 MCS satellite lifecycle 90
7.3 MCS radar lifecycle 96

8 Summary and conclusions **107**
8.1 Summary 107
8.2 Conclusions 107
8.3 Suggestions for future research 111

A Sounding Indices **113**

LIST OF FIGURES

2.1 Symmetric and asymmetric TS MCS (Houze et al. 1990) 10
2.2 Swiss MCS archetypes (Schiesser et al. 1995) 10
2.3 Linear MCS archetypes (Parker and Johnson 2000) 11
2.4 Classification of squall line development (Bluestein and Jain 1985) 13
2.5 Classification of mesoscale convective patterns (Blanchard 1990) 14
2.6 Paths to asymmetric TS structure (Loehrer and Johnson 1995) 15

3.1 Geographical area of study 18
3.2 Example of an MCC plot of satellite characteristics 21
3.3 Example of an MCC plot of radar characteristics 24

4.1 Distribution of MCSs as a function of size 33
4.2 Distribution of MCSs as a function of initiation time, time of maximum extent, and termination time. 34
4.3 Infrared satellite images of a MCC example 35
4.4 Infrared satellite images of a PECS example 36
4.5 Infrared satellite images of a MβMCC example 37
4.6 Infrared satellite images of a MβPECS example 38

5.1 Radar reflectivity examples of radar organization categories 44
5.2 Classification of MCS development 47
5.3 Radar images of an areal merger example 55
5.4 Radar images of a combination merger example 56
5.5 Radar images of an areal growth example 57
5.6 Radar images of a line merger example 58
5.7 Radar images of an embedded areal merger example 59
5.8 Radar images of an areal isolated example 60

6.1 Scatter plot of maximum area against duration. 63
6.2 Scatter plot of maximum area against total totals index. 64
6.3 Scatter plot of maximum area against precipitable water. 65
6.4 Mean sounding for all systems. 68
6.5 Mean sounding for MCCs. 69
6.6 Mean sounding for PECSs. 71
6.7 Mean sounding for MβMCCs. 72
6.8 Mean sounding for MβPECSs. 74
6.9 Mean sounding for embedded systems. 75
6.10 Mean sounding for systems that were not embedded. 75
6.11 Mean sounding for areal systems. 76
6.12 Mean sounding for line systems. 76
6.13 Mean sounding for combination systems. 77
6.14 Mean sounding for merger systems. 77
6.15 Mean sounding for growth systems. 78
6.16 Mean sounding for isolated systems. 78
6.17 Mean sounding for unclassifiable systems. 79

7.1 Plot of MCS tracks for all systems. 83
7.2 Plot of MCC tracks. 83
7.3 Plot of PECS tracks. 84
7.4 Plot of MβMCC tracks. 84
7.5 Plot of MβPECS tracks. 85
7.6 Plot of MCS tracks for embedded systems. 86
7.7 Plot of MCS tracks for systems that were not embedded. 86
7.8 Plot of MCS tracks for areal systems. 87
7.9 Plot of MCS tracks for line systems. 87
7.10 Plot of MCS tracks for combination systems. 88
7.11 Plot of MCS tracks for merger systems. 88
7.12 Plot of MCS tracks for growth systems. 89
7.13 Plot of MCS tracks for isolated systems. 89
7.14 Infrared satellite lifecycle composite for all systems. 91
7.15 Infrared satellite lifecycle composite for MCCs. 91

7.16 Infrared satellite lifecycle composite for PECSs. 92
7.17 Infrared satellite lifecycle composite for MβMCCs. 92
7.18 Infrared satellite lifecycle composite for MβPECSs. 92
7.19 Infrared satellite lifecycle composite for embedded systems. 93
7.20 Infrared satellite lifecycle composite for systems that were not embedded. 93
7.21 Infrared satellite lifecycle composite for areal systems. 93
7.22 Infrared satellite lifecycle composite for line systems. 94
7.23 Infrared satellite lifecycle composite for combination systems. 94
7.24 Infrared satellite lifecycle composite for merger systems. 94
7.25 Infrared satellite lifecycle composite for growth systems. 95
7.26 Infrared satellite lifecycle composite for isolated systems. 95
7.27 Radar lifecycle composite for all systems. 97
7.28 Radar lifecycle composite for MCCs. 97
7.29 Radar lifecycle composite for PECSs. 98
7.30 Radar lifecycle composite for MβMCCs. 98
7.31 Radar lifecycle composite for MβPECSs. 98
7.32 Radar lifecycle composite for embedded systems. 99
7.33 Radar lifecycle composite for systems that were not embedded. 99
7.34 Radar lifecycle composite for areal systems. 99
7.35 Radar lifecycle composite for line systems. 100
7.36 Radar lifecycle composite for combination systems. 100
7.37 Radar lifecycle composite for merger systems. 100
7.38 Radar lifecycle composite for growth systems. 101
7.39 Radar lifecycle composite for isolated systems. 101

LIST OF TABLES

2.1 Definition of mesoscale convective complex (MCC) (Maddox 1980). . . . 7

2.2 Modified MCC definition (Augustine and Howard 1988). 8

4.1 MCS definitions based upon analysis of infrared satellite data 29

4.2 Distribution of MCS type (1996-1998). 31

4.3 Statistics for each MCS type: means and (standard deviations). 32

5.1 Distribution of radar organization by MCS type (1996-1998). 41

5.2 Distribution of radar organization by month (1996-1998). 42

5.3 Statistics for each radar organization type: means and (standard deviations). 43

5.4 Distribution of MCS development by satellite classification. 49

5.5 Distribution of MCS development by satellite classification broken into the three levels of the classification process. 50

5.6 Distribution of MCS development by month broken into the three levels of the classification process. 52

5.7 Statistics for each radar development level: means and (standard deviations). 53

6.1 Average properties of soundings for the entire MCS sample. Means and (standard deviations). 62

6.2 Sounding properties for each MCS satellite classification: means and (standard deviations). 65

6.3 Sounding properties for each MCS radar classification: means and (standard deviations). 66

6.4 Properties of average soundings for each satellite classification. 67

6.5 Properties of average soundings for each radar classification. 70

6.6 Number of severe weather reports for each MCS satellite classification. . 73

6.7 Number of severe weather reports per MCS for each satellite classification. 73

6.8 Number of severe weather reports for each radar classification. 79

6.9 Number of severe weather reports per MCS for each radar classification. 80

7.1 Total precipitation mass, average motion, and percentage of convective precipitation for the composite of each MCS satellite classification. . . 103

7.2 Total precipitation mass, average motion, and percentage of convective precipitation for the composite of each radar development level. . . . 104

7.3 Composite lifecycle characteristics for each MCS satellite classification. . 106

7.4 Composite lifecycle characteristics for each level of radar development. . 106

Chapter 1

Introduction

Mesoscale convective systems (MCSs) provide a significant portion of the precipitation that falls over the central United States during the critical agricultural growing seasons of spring and summer. In fact, MCSs account for 30% to 70% of the warm-season precipitation in this area (Fritsch et al. 1986). Additionally, MCSs produce a broad range of severe convective weather events (Maddox et al. 1982 and Houze et al. 1990) that can be potentially damaging to crops and society in general. Given that MCSs have such a profound influence on the midlatitudes, it is important to study them and their development process.

Even though the importance of MCSs is well understood, there is much left to learn about the growth and development of these systems. One difficulty in understanding MCSs lies in the fact that often the mesoscale features important to MCS development are not well sampled by the operational large-scale observation network (Stensrud and Fritsch 1994). Thus, due to its global coverage, infrared satellite imagery has been an important means of studying MCSs, particularly mesoscale convective complexes (MCCs) (e.g. Maddox 1980, Maddox et al. 1982, and Maddox 1983). Although satellite images provide an effective way of identifying MCSs, they don't provide much information on the underlying convection. Consequently,

radar data have been used to allow for more detailed studies of MCS convection (e.g. Bluestein and Jain 1985, Bluestein et al. 1987, Houze et al. 1990, and Parker and Johnson 2000).

Using these different sets of data, many studies have been carried out over the years on various types of MCSs covering different geographical areas. There are probably a couple of reasons for the variations in these studies. First of all, the development of technology and the radar network in the U.S. has permitted the study of more systems over a larger area. In addition, the availability and flexibility of digitized data and computing power have allowed studies to become increasingly extensive. Secondly, the assorted definitions of MCSs throughout the years have been relatively vague, as they should be, to include a variety of convective phenomena. For example, Zipser (1982) defined MCSs as, "cloud and precipitation systems, together with their associated circulation systems, which include a group of cumulonimbus clouds during most of the lifetime of the system." Definitions like this one allow for many interpretations, which has resulted in many types of MCS studies.

Certainly, a comprehensive study of MCSs would be helpful in supplementing the various MCS studies done previously. One purpose of this thesis is to provide a more comprehensive study of MCSs than many of the previous MCS studies in terms of number, MCS type, length of study, and geographical area considered. Another purpose of this thesis is to focus on the MCS growth stage to better characterize common patterns of development by which convection becomes organized into mature MCSs. In brief, the warm seasons (April-August) of 1996 through 1998 were examined to provide a large sample of MCSs. A significant portion of the central United States extending basically from the Rocky Mountains in the west to the Appalachian Mountains in the east and from the southern U.S. border to the northern

U.S. border was chosen for this study. Choosing a larger spatial domain was done in hope to expand on previous single-radar studies (e.g. Bluestein and Jain 1985, Bluestein et al. 1987, and Houze et al. 1990). During the identification process, all systems subjectively deemed to be coherent based on infrared satellite imagery were recorded regardless of their size or shape. Again, this was an attempt to be more comprehensive in MCS type by expanding on MCC studies (e.g. Maddox 1980, Maddox 1983, and McAnelly and Cotton 1986), squall line or linear MCS studies (e.g. Bluestein and Jain 1985 and Parker and Johnson 2000), and even large system studies (e.g. Anderson and Arritt 1998). Selecting a wide assortment of MCS types over a large region of the U.S. inherently led to large MCS sample of 514 systems initially identified by infrared satellite imagery.

In addition to the MCSs being classified by their cold cloud top characteristics, their development as seen through radar imagery was categorized. Looking at the development of such a wide variety of systems should complement previous radar studies, such as Bluestein and Jain's (1985) study on the formation of Oklahoma squall lines. In addition, studying the development of different types of MCSs may lead to understanding the differences between the processes governing their development. Finally, representative soundings were examined as in previous MCS studies. The primary purpose for looking at the soundings was to provide some basic information on the environment in which these systems formed and to note obvious differences between systems based on either satellite classification or radar development classification.

The remainder of this thesis provides the details, description, and results of the analysis of this MCS sample. Chapter 2 provides information on relevant observational MCS studies done in the past. The third chapter provides a description of

the data and methods used in this analysis. The infrared satellite classifications are defined and discussed in Chapter 4 along with some basic comparisons and examples. Chapter 5 discusses the method by which the MCSs were categorized according to their development. In addition, this chapter also provides some basic comparisons between each category and examples of each. The sixth chapter briefly discusses the similarities and differences among the environmental conditions of each MCS category as well as severe weather reports. A composite analysis of the MCS sample is discussed in Chapter 7. Finally, Chapter 8 provides a summary, conclusions, and suggestions for future research.

Chapter 2

Background

Several MCS studies performed in the past have attempted to classify MCSs into discrete categories by a variety of different methods and perspectives. The most common methods of MCS classification involve analyzing satellite and radar characteristics of the systems. Similar to past studies, the present study attempts to classify MCSs to better understand the similarities and differences between the systems; however, unlike many past studies, this study will classify each MCS by *both* satellite and radar characteristics. Of course, nature doesn't necessarily make it easy to sort out these systems into categories. In effect, there are numerous ways to analyze and classify MCSs that may be completely appropriate, but the multitude of methods may lead to confusion. The purpose of this chapter is to provide a background on MCS classification to help clarify the relationship among existing schemes, so it will be easy to relate them to the schemes used in this study (see Chapters 4 & 5).

It is necessary to first introduce the ubiquitous term, *squall line*. This term is probably the first instance of MCS "classification" even though it was used well before MCSs were defined. Bluestein and Jain (1985) provide a nice summary of the evolution of this term, noting that it is now loosely applied to both frontal and nonfrontal lines of thunderstorms. The fluctuating nature of the definition of squall

line has led to ambiguity when using the term. Consequently, it has become common for authors to use "linear MCS," for example, instead of "squall line" in an attempt to avoid using the term. In any case, one must be careful when using the term to make sure there is no uncertainty about its meaning. From its inconspicuous beginning, the area of MCS classification has blossomed with the advent of satellites and radar. Several studies on both satellite and radar classifications have emerged in the past twenty years.

2.1 Satellite classification of MCSs

Maddox (1980) was the first to classify a particular type of MCS by means of satellite imagery. He noticed a high frequency of organized, meso-α (see Orlanski 1975) convective weather systems moving across the central U.S. He termed these massive systems "mesoscale convective complexes" (MCCs). He based the definition of MCCs on typical infrared satellite characteristics possessed by systems moving across the central United States (see Table 2.1).

The physical characteristics described in Table 2.1 are somewhat arbitrary, but were chosen to ensure that only large, well-organized, and active systems were classified as MCCs. Although Maddox (1980) focused primarily on MCCs, he does suggest a classification scheme for MCSs based on location (tropics or midlatitudes), shape (linear or circular), and size (meso-α or meso-β). As will be discussed in Chapter 4, the present study uses a very similar infrared satellite classification scheme for the midlatitudes.

The nomenclature "MCC" has been widely used, and its definition has not been abused as is the case with "squall line." There has been one relatively minor

Table 2.1: Definition of mesoscale convective complex (MCC) (Maddox 1980). (based upon analysis of infrared satellite imagery)

Physical characteristics	
Size:	A–Cloud shield with continuously low IR temperature temperature $\leq -32°C$ must have an area $\geq 100,000$ km^2 B–Interior cold cloud region with temperature $\leq -52°C$ must have an area $\geq 50,000$ km^2
Initiate:	Size definitions A and B are first satisfied
Duration:	Size definitions A and B must be met for a period ≥ 6 h
Maximum extent:	Contiguous cold cloud shield (IR temperature $\leq -32°C$) reaches a maximum size
Shape:	Eccentricity (minor axis/major axis) ≥ 0.7 at time of maximum extent
Terminate:	Size definitions A and B no longer satisfied

modification to the definition of MCCs. Augustine and Howard (1988) removed the $\leq -32°C$ size requirement of the cloud shield. They dismissed this criterion for several reasons. First of all, it allows the process to be more automated as often it is much easier to delineate between systems using the $-52°C$ threshold as opposed to the $-32°C$ threshold. Secondly, they added that McAnelly and Cotton (1985) found a majority of precipitation from an MCC falls out of the $-52°C$ region. Finally, they showed that for most MCCs there is a linear relationship between the area of the $-32°C$ threshold and the area of the $-52°C$ threshold. Table 2.2 shows the modified MCC definition. This is probably the more widely used MCC definition today and will be used for this study.

Although MCCs are massive, striking systems, they represent only a small fraction of the total MCSs that exist in nature. Anderson and Arritt (1998) performed a study on MCCs and another large class of MCSs, persistent elongated convective systems (PECS). PECS are what you might call the "linear" version of MCCs. The only difference between a MCC and a PECS is the shape of the system. PECSs

Table 2.2: Modified MCC definition (Augustine and Howard 1988).

Physical characteristics	
Size:	Cloud shield with continuously low IR temperature temperature $\leq -52°C$ must have an area $\geq 50,000$ km^2
Initiate:	Size definition is first satisfied
Duration:	Size definition must be met for a period ≥ 6 h
Maximum extent:	Contiguous cold cloud shield (IR temperature $\leq -52°C$) reaches a maximum size
Shape:	Eccentricity (minor axis/major axis) ≥ 0.7 at time of maximum extent
Terminate:	Size definition no longer satisfied

have eccentricities between 0.2 and 0.7 while MCCs must have eccentricities ≥ 0.7 (see Table 2.2). All of the other criteria (i.e. size and duration) are the same for both MCCs and PECSs. In their study, Anderson and Arritt (1998) found that PECSs occurred about twice as frequently as MCCs, which is not astonishing since the definition of PECS involves the removal of the arbitrary eccentricity stipulation. Due to their potential to produce significant and severe weather, PECSs cannot be ignored just because they do not meet certain shape characteristics of a particular definition. However, there are still many smaller MCSs (e.g. Knupp and Cotton 1987) that have not been addressed by satellite classification. One feature of the present study is to include these smaller systems with the larger systems (MCCs and PECSs) in a MCS study.

2.2 Radar classification of MCSs

In addition to classifying MCSs according to infrared satellite characteristics, there have also been many attempts to classify MCSs by their radar characteristics. However, unlike the satellite classification process where there is a "standard" method of categorizing systems, the radar classification process has been less standardized.

One common method of classifying MCSs by radar has been to look at the arrangement of the convective and stratiform regions of a mature MCS (e.g. Houze et al. 1990 and Parker and Johnson 2000). Another common, yet different, method of MCS radar classification has been to classify MCSs based on their developmental or formational stages (e.g. Bluestein and Jain 1985, Bluestein et al. 1987, and Loehrer and Johnson 1995). It is worth noting that most of these studies have focused on squall lines or linear MCSs. The present study attempts to classify all systems (both linear and circular) focusing on the stages of development (see Chapter 5).

2.2.1 Radar classification by organization

Categorizing MCSs according to their organization deals with the location of the convective line of the storm in relation to the stratiform region of the storm. Houze et al. (1990) performed a single-radar study in Oklahoma looking at "mesoscale precipitation systems" that passed through the area. They categorized the systems based on the degree to which they were of "leading-line trailing-stratiform" (TS) structure and whether or not the systems were deemed to be "symmetric" or "asymmetric" (see Fig. 2.1). They discovered that 42 systems, or two-thirds of the systems in their study, could be considered either weakly, moderately, or strongly classifiable as a TS precipitation system. The remaining systems (21) were regarded to be unclassifiable. Of the classifiable systems, there was approximately an equal number of symmetric, asymmetric, and intermediate systems.

Houze et al. (1990) also looked at previously documented MCCs and their relationship to the systems they were studying. Whenever a MCC passed through the region of interest, a major rain event meeting their criteria occurred. However, 75% of their systems did not occur in conjunction with a cloud shield that met

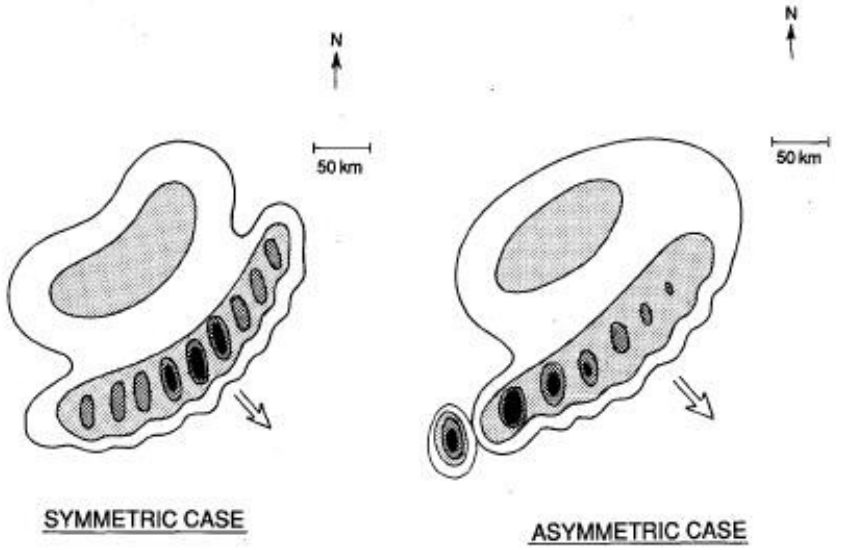

Figure 2.1: Schematic of symmetric (left) and asymmetric (right) leading-line trailing-stratiform MCSs (from Houze et al. 1990).

MCC criteria. This certainly suggests that other MCSs not meeting the strict MCC definition might be important precipitation-producing systems.

In related work, Schiesser et al. (1995) analyzed the structure of "severe precipitation systems" in Switzerland. In addition to the trailing stratiform (TS) systems described by Houze et al. (1990), Schiesser et al. (1995) also documented leading stratiform systems (LS) and systems without a stratiform precipitation region (referred to as none)(see Fig. 2.2).

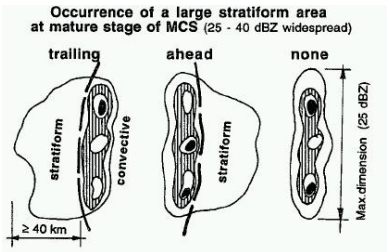

Figure 2.2: Schematic reflectivity drawings of Swiss mesoscale convective systems (from Schiesser et al. 1995).

This work led to a similar study of MCS organization in the central United

States by Parker and Johnson (2000). In addition to the TS and LS archetypes, they added a third mode of MCS arrangement: parallel stratiform (PS) systems (see Fig. 2.3). In fact, Parker (1999) believes that many of the systems classified with no stratiform precipitation in the Schiesser et al. (1995) study may actually correspond to the PS archetype. Parker and Johnson (2000) noted that linear MCSs frequently evolve among the archetypes during their lifecycle; therefore, the systems were classified based upon their predominant organizational mode. They found that the TS archetype was the dominant form of MCS organization in the central U.S. However, both the LS and PS archetypes each accounted for about 20% of the studied population of MCSs. Thus, these systems are very common in the U.S. and necessitate future study.

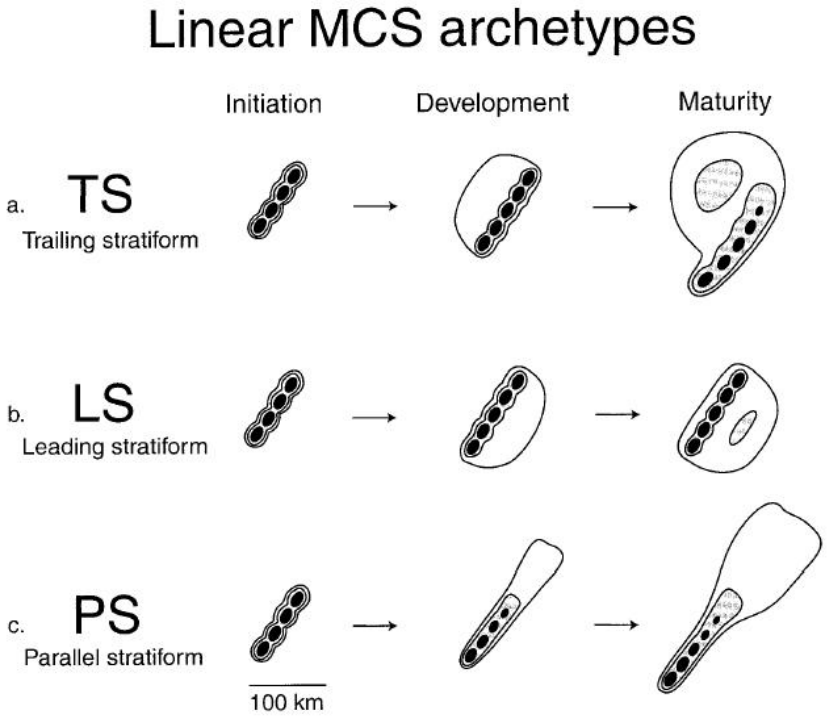

Figure 2.3: Schematic reflectivity drawing of idealized lifecycles for three linear MCS archetypes: (a) TS, (b) LS, and (c) PS (from Parker and Johnson 2000).

Although the primary focus of the present study is not on the radar classification

of MCSs by their organization, each system was casually examined and categorized by their predominant arrangement using the archetypes discussed in Parker and Johnson (2000) (see Chapter 5). It is important to stress that the studies mentioned in this section primarily focused on convective lines, leaving the topic of non-linear convective systems relatively untouched.

2.2.2 Radar classification by development

The concept of classifying MCSs by their development is of greater importance to the focus of the present study. Classifying systems by their *organization* involves looking at the precipitation structure of mature MCSs while classifying systems by their *development* involves tracing back from the mature stages of MCSs to the formative stages to see the arrangement of convection at initiation. The intent of studying the development of MCSs lies in the desire to understand the different types of convective arrangements that ultimately lead to mature MCSs.

Bluestein and Jain (1985) performed the first study of this type seeking to identify common patterns of severe squall line formation. They considered the general definition of squall line (i.e. "a linearly oriented mesoscale convective system"). In their examination of the radar data for Norman, Oklahoma, they broke squall line development into four classifications: *broken line, back building, broken areal, and embedded areal* (see Fig. 2.4). Out of the 52 squall lines they studied, 14 formed by broken line, 13 formed by back building, 8 formed by broken areal, and 6 formed by embedded areal arrangements. The remaining 10 systems did not fit into a classification. Bluestein and Jain (1985) also observed satellite images to determine if the formation of squall lines could be discerned independently of radar. They found that the broken line and back building types of formation were the easiest to distinguish

using satellite imagery. However, they made no attempt beyond this to observe and classify squall lines by satellite characteristics. In a closely related study, Bluestein et al. (1987) studied the formation of non-severe squall lines in Oklahoma. One of the differences is that many more non-severe squall lines formed through the broken areal process and fewer formed by back building as compared to severe squall line formation.

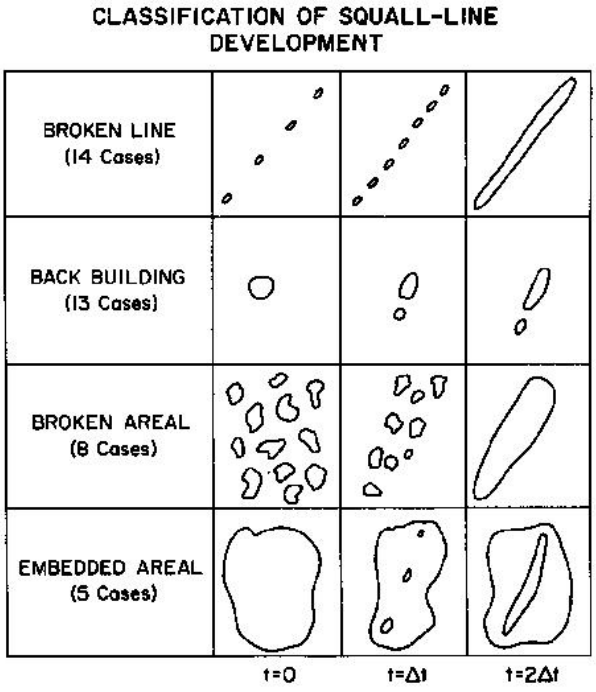

Figure 2.4: Idealized depictions of squall line formation (from Bluestein and Jain 1985).

Another study on the classification of MCS development was done by Blanchard (1990). This study is descended from Bluestein and Jain (1985), but it is unique in its own right. In relation to the present study, the most important feature of the study done by Blanchard (1990) is the inclusion of all types of MCSs in the classification scheme. Unfortunately, however, none of the terminology used by Bluestein and Jain (1985) is repeated. Blanchard (1990) identified three mesoscale convective patterns for

the Oklahoma-Kansas Preliminary Regional Experiment for STORM-central (PRE-STORM) field program: *linear convective systems, occluding convective systems, and chaotic convective systems* (see Fig. 2.5). From the 25 systems studied, 17 were classified as linear convective systems, 2 were classified as occluding systems, and 6 were classified as chaotic systems. This classification scheme is probably not as widely used as other schemes due to vagueness of the categories and terminology (see Doswell 1991 and Parker 1999). More than likely, viewing the cloud shields of these systems with satellite imagery would have cleared up some of the confusion, especially for the chaotic convective systems. Regardless, it was a worthy attempt of classifying *all* types of MCSs.

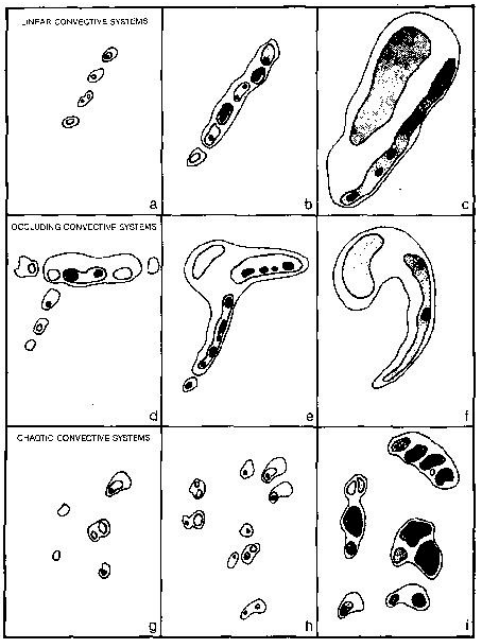

Figure 2.5: Schematic reflectivity evolution of three convective modes during the PRE-STORM program: (a-c) linear convective systems, (d-f) occluding convective systems, and (g-i) chaotic convective systems. (from Blanchard 1990).

A more recent and specific study by Loehrer and Johnson (1995) looked at different development paths of MCSs to reach an asymmetric TS structure. *Disorganized, linear, back-building,* and *intersecting convective bands* were the four types

of development they identified (see Fig. 2.6). The numbers in Figure 2.6 represent the number of systems observed for each classification in the 1985 PRE-STORM field program. Out of the few cases they studied, a dominant evolutionary mode did not emerge. One important aspect of their classification is the idea of interaction between convective bands, which will be implemented into the classification scheme in the present study (see Chapter 5).

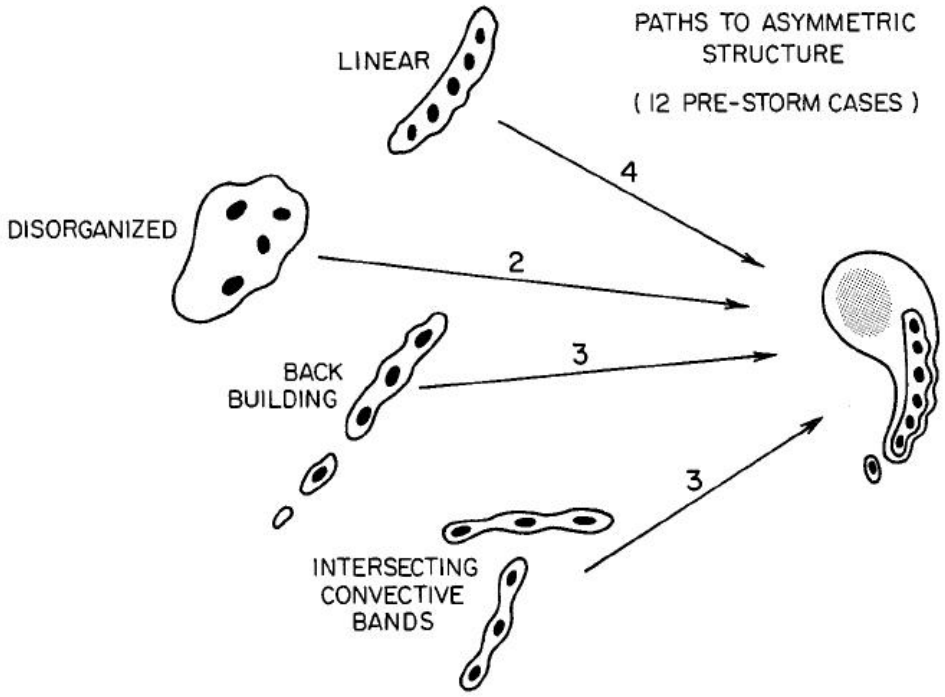

Figure 2.6: Schematic of the paths to reach asymmetric structure observed by Loehrer and Johnson (1995) (from Hilgendorf and Johnson 1998).

In summary, there have been many worthwhile studies on classifying MCSs by either satellite or radar characteristics. The satellite classification schemes have been well-defined by cloud shield characteristics of the system. The radar classification schemes have been much less well-defined due to the complex nature of convection as depicted by radar echoes. In addition, there have been multiple viewpoints on the radar classification of MCSs, which is certainly valid. The present study is another

attempt to create MCS classification schemes that might provide a contribution in understanding these systems by building upon past studies.

Chapter 3

Data and methods of analysis

From this point on, the focus of this thesis shifts from past studies to the present study. This chapter provides basic information about the time period and area of interest for this study. In addition, details are supplied about the different types of data utilized and the way in which they were analyzed. All told, the chapter reviews the approach used to study the sample of MCSs.

3.1 Study area and period

In reality, the time frame and area studied are relatively arbitrary variables that are selected to meet the author's interests and goals. For this study, one goal was to study a large sample of MCSs. Thus, it would make sense to select a reasonably long time period and large domain to reach that goal. In the spirit of Maddox (1980), it was decided to study the majority of the active convective season of the central United States. Based on the number of MCCs he observed per month, the range of April through August seemed appropriate. In addition, the months of April, May, and June analyzed in springtime studies, such as Houze et al. (1990) and Bluestein and Jain (1985), are obviously included in this time frame. Furthermore, a three

year period was selected to try to get a large and varied sample of MCSs and to remove any annual bias. It was desirable to study most of the United States, so only areas west of the Rocky Mountains and east of the Appalachian Mountains were not considered. Additionally, the initiation and development of MCSs is less frequent in these areas as opposed to the central United States. Thus, any MCS that had its convective initiation between $24° - 51°$N and $82° - 115°$W was considered for this study (see Fig. 3.1). The area and period studied proved to be sufficient in achieving a large sample of MCSs as several hundred systems were initially identified during the fifteen months included in the investigation.

Figure 3.1: Geographical area considered in the study.

3.2 Satellite data

The first step in this study was to identify the sample of MCSs using satellite imagery. It is generally easier to identify MCSs by their cold cloud shield than by their radar reflectivity patterns, as the underlying convection can take many forms (see Blanchard (1990)). The cold cloud shield is larger than the area of convection and often is more contiguous making it easier to identify and study a large number of systems. The rest of this section discusses the satellite dataset and the methods used in analyzing the data to obtain information on the lifecycle of the MCSs.

3.2.1 Dataset information

The satellite data for the three-year period (1996-1998) were obtained from the Global Hydrology Resource Center (GHRC) at the Global Hydrology and Climate Center in Huntsville, Alabama. The dataset is comprised of hourly global composite infrared images from four weather satellites in geosynchronus orbit: GMS, GOES-8, GOES-9, and Meteostat. The Storm Prediction Center (SPC) creates the composite image, and the GHRC ingests it real-time. The resolution of the data is 14 km in the horizontal, which is sufficient for identifying MCSs, but does not provide detailed cloud structure information. Occasionally, there were missing data (most notably July 1-7, 1996), but overall it was a consistent dataset that provided fundamental information about each MCS.

3.2.2 Satellite analysis

Naturally, in order to study MCSs, a sample of MCSs needs to be identified. The infrared satellite data were converted from brightness counts into blackbody

temperature, and the hourly files of the region of interest were plotted at three temperature contours ($-52°, -32°,$ and $-10°$C) following Maddox's (1980) MCC study. Two 12-panel plots were created, printed, and reviewed for each day during the 15-month period. As discussed in Section 2.1, the $-52°$C temperature threshold was the primary contour considered when reviewing the satellite images. This initial MCS identification process was very subjective. Any system developing in the region of interest that appeared to have contiguous, coherent structure at the $-52°$C temperature threshold for a few hours was recorded as a MCS. The size and shape of the systems were really not a serious consideration at this point because those issues would be dealt with at a later point. It was important to be lenient in this first stage of identification because a large sample of *all* types of MCSs was desired, and later steps in the classification process were sure to eliminate some systems. Indeed, a total of 643 systems were identified for the three warm seasons after the first step with more steps to come.

The next step was to gather size, centroid, and eccentricity information for each hour during the MCS lifecycle in order to be able to classify the systems. A modified version of a program written by Augustine (1985) was used to document the systems. One modification made to the program allows the user to isolate specific cloud shields by drawing a polygon around them, so that only the system of interest is considered. Thus, each hourly satellite image of the MCS was analyzed with this program to produce information on its lifecycle. With this information, plots of the MCS tracks and area could be produced for each system (e.g. Fig. 3.2). During this stage, several more systems were discarded due to lack of cohesiveness, missing data, or border issues. Consequently, a total of 514 systems were left for the satellite classification process.

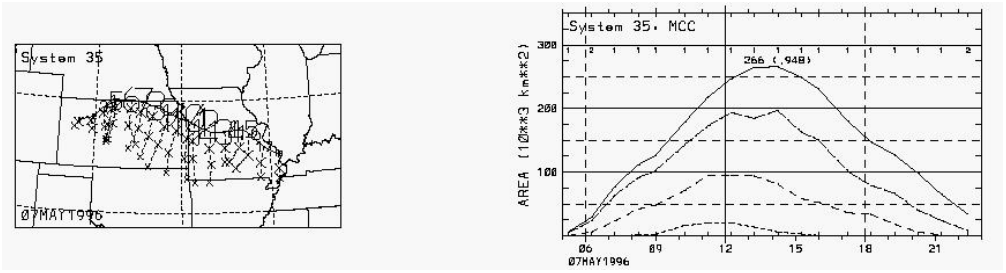

Figure 3.2: Example plot of a MCC track across Kansas and Missouri on May 7, 1996 (left) and its corresponding area over time at the $-52°$, $-58°$, $-64°$ and $-70°$C cloud top temperature thresholds (right).

The remaining systems were classified according to their size, shape, and duration. The categories were devised to be consistent with previous satellite classification studies, so that the results would follow and allow comparison to preceding studies. Ultimately, 465 systems fit into one of four satellite categories. The satellite classification process will be discussed in much greater detail in Chapter 4.

3.3 Radar data

Another important aspect of this study was to address the issue of MCS development. While satellite imagery is useful for getting a broad viewpoint of MCSs, it is not helpful in studying the small-scale structure of MCS development. Therefore, radar reflectivity data were used to examine the systems at a higher temporal and spatial resolution. Since the MCSs had already been identified by means of infrared satellite, the radar data could be used to study the development and arrangement of the underlying convection of these predetermined systems. The remainder of this section will address information on the radar dataset and how the data were analyzed.

3.3.1 Dataset information

The radar data were also obtained from the GHRC. The radar images are national reflectivity composites, which are very convenient images for examining a significant portion of the United States, as in this study. Weather Services International (WSI) generates these composite products (i.e. WSI NOWrad (TM) products) with data from the National Weather Service (NWS) radars in the continental United States. They quality control the images in real-time before the GHRC receives them. The data are arranged into sixteen bins of 5 dBZ intervals with a resolution of 2 km x 2 km and are available at 15-minute intervals. The spatial and temporal resolution is not adequate to follow an individual convective cell throughout its lifecycle; however, the resolution is sufficient for studying the overall organization and evolution of large convective cells and meso-β scale convective clusters. Since the dataset was very consistent with very little missing data, it proved to be a useful tool for viewing the development of MCSs over the central United States.

3.3.2 Radar analysis

With the MCSs already identified by means of satellite imagery, the first stage of radar analysis was to correlate the radar echoes with the cloud shields of the MCSs. As was done with the satellite images, the radar images were plotted at three thresholds to recognize the systems: 20, 30, and 40 dBZ. Once again, two 12-panel plots of hourly radar images were created, printed, and reviewed for each day of the period to identify the MCSs by their radar characteristics. It became obvious after reviewing the radar images that the radar coverage was not sufficient to capture many of the systems, especially into Canada to the north and into Mexico and the

Gulf of Mexico to the south. This was certainly expected as the geographical region considered extends beyond the radar coverage of the continental United States (see Fig. 3.1). For the most part, a significant convective structure on radar imagery could easily be associated with its cloud shield on satellite imagery.

The next step of radar processing was also very similar to that of satellite processing. Another modified version of Augustine's (1985) program was developed to work with the radar data to obtain size, centroid, eccentricity, and reflectivity characteristics for the radar lifecycle of each MCS. This exhaustive process of analyzing each 15-minute image during the lifecycle of every MCS produced a wealth of information about the systems. With this information, plots of the 15 largest convective clusters at a given dBZ threshold were plotted along with the rainfall characteristics of the system (e.g. Fig. 3.3). The Z-R relationship used to calculate the rain rate in this study was proposed by Woodley et al. (1975):

$$Z = 300R^{1.4}. \tag{3.1}$$

This relationship is used by the GHRC when producing composite daily rainfall maps and is also the default algorithm used for the NEXRAD radars (Fulton et al. 1998). Even though the radar images are quality-controlled, it is worth mentioning that there still may be instances of radar attenuation, bright band effects, and anomalous propagation that may alter the actual reflectivity fields. Nevertheless, an attempt was made to minimize these effects by only looking at the averages of a large number of systems. As previously mentioned, many of the remaining systems did not develop and stay within the range of the radar network. Consequently, there was a total of 387 MCSs with a complete set of both satellite and radar data, which is a sufficient number to consider having a "large" sample.

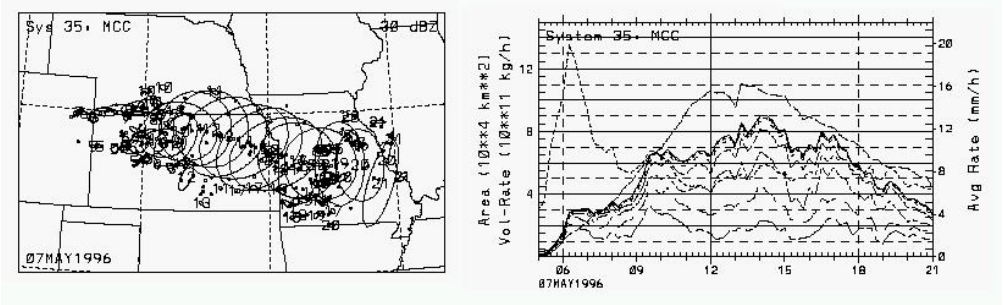

Figure 3.3: Example plot of the same system as Fig. 3.2 with convective cluster (30 dBZ threshold) development over time (left) and the average rain rate (small dashed line), precipitating (i.e.$\geq$ 20 dBZ) area (thick dashed line), and volumetric rain rate (solid line) with contributions from dBZ thresholds at 5 dBZ increments below that (long dashed lines) (right).

Once again, the last step involved classifying the systems. Unlike the satellite classification process, however, the radar classification process was much more subjective. The focus of the radar classification was on the developmental stages of the MCSs, so it was the intent to incorporate as much as possible from similar previous studies (see Section 2.2.2) into the classification scheme. The best way to view the systems and classify them was to animate the 15-minute images and analyze the system's development many times. This process and the resulting classification scheme will be discussed in much more detail in Chapter 5.

3.4 Sounding data and severe weather reports

Sounding data were the last type of data used in analyzing the MCS sample. It is noteworthy that examining the soundings of these systems was not an initial goal of the study, but it was performed to provide some information on the environment in which the MCSs formed. The NWS sounding data were obtained from an online archive maintained by the University of Wyoming Department of Atmospheric Science. Similar to previous MCS studies (e.g. Rasmussen and Wilhelmson 1983,

Houze et al. 1990, and Parker and Johnson 2000), an individual sounding was chosen to be the most representative sounding of the airmass in which the MCS formed and was used without modification. Further efforts to interpolate nearby soundings (see Bluestein and Parks 1983 and Bluestein and Jain 1985) or to modify operational soundings with numerical models (see Brooks et al. 1994) were not undertaken due to the large volume of MCSs studied and the fact that it wasn't the primary focus of the study. The data were processed in order to construct average soundings. In doing this, the mandatory and significant-level information were interpolated to get levels at 25 mb intervals from the surface to 100 mb. The soundings were then grouped according to their radar and satellite classifications and analyzed by looking at both the average properties of the soundings and the properties of the average soundings. In addition, severe weather reports for this time period were obtained from the Storm Prediction Center and recorded for each MCS. A detailed discussion of the results is provided in Chapter 6.

Chapter 4

Satellite classification of MCSs

Classification of MCSs by satellite characteristics has certainly been done in the past (see Section 2.1); however, there has been little recognition of *all* types of MCSs when viewing satellite imagery. In order to produce a useful and commendable taxonomy, it is important to build upon and be consistent with previous studies. The satellite classification scheme presented in this chapter is an attempt to do just that. In addition, it was developed to be more inclusive of MCSs, especially smaller systems. The rest of the chapter provides a description of the classification scheme, presents some basic characteristics of each category, and offers some examples.

4.1 Definition of classes

The cornerstone of MCS classification by satellite imagery is the definition of MCCs by Maddox (1980). Thus, the method he used to define MCCs was the basis of the classification scheme presented in this chapter. It is noteworthy to mention an alternative definition for MCCs set forth by Cotton et al. (1989) that defines a MCC as a "nearly geostrophically-balanced MCS with a horizontal scale comparable to or larger than the Rossby radius of deformation, λ_R." For this study, however, it was

more convenient and practical to use Maddox's (1980) MCC definition as the basis for defining the other types of MCSs. Essentially, the systems were classified according to their size, duration, and eccentricity of the $-52°$C cloud-top temperature threshold (see Table 2.2). As discussed in Section 2.1, the large systems, *MCCs and PECSs* , have been well defined and documented. Consequently, these two types of systems comprise two of the four categories. The relatively undocumented systems are the smaller MCSs; therefore, categories should be defined to include these systems.

Since the large MCSs are discriminated by shape (i.e. MCC for circular systems and PECS for linear systems), it is natural to create two categories for smaller MCSs: one for circular systems and one for linear systems. Consequently, the eccentricity criterion will be the same for the smaller systems as for the larger systems. The only criteria that are left to be set for the smaller systems are the size and duration of the cloud shield at the $-52°$C threshold. These minimum criteria are important because they basically set the definition of a MCS for this study. As discussed in Parker and Johnson (2000), the appropriate MCS time scale is f^{-1} , which is approximately 3 hours for the midlatitudes. Thus, the duration criterion for the smaller MCSs was set at ≥ 3 h.

The size criterion was somewhat more difficult and arbitrary to assign for the smaller systems than the time scale. Some studies have suggested an MCS length scale of 100 km (e.g. Houze 1993 and Parker and Johnson 2000). This seems appropriate, but they were considering the scale of convective radar echoes, and cloud shields grow much larger than the area of the underlying convection. Hence, a somewhat larger scale was desired. The reexamination of several of the small systems led to the conclusion that the most coherent systems reached an area of at least 30,000 km^2.

Thus, the size criterion for the smaller systems was set at $\geq 30,000$ km^2 with the caveat that their maximum size must be at least 50,000 km^2 as a way of connecting the definition of the smaller systems to the larger systems. To keep the naming convention as simple as possible, the smaller circular systems are referred to as *meso-β MCCs* (*MβMCCs*) and the smaller linear systems are called *meso-β PECSs* (*MβPECSs*). From Orlanski's (1975) definitions of meteorological scales, the larger MCSs fit more appropriately into the meso-α scale while the smaller MCSs fit more appropriately into the meso-β scale, hence the reasoning for the nomenclature. Table 4.1 shows the definitions of the four classes of MCSs according to infrared satellite characteristics: *MCC, PECS, MβMCC, and MβPECS.*

Table 4.1: MCS definitions based upon analysis of infrared satellite data

MCS Category	*Size*	*Duration*	*Shape*
MCC	Cold cloud region ≤ -52°C with area $\geq 50,000$ km^2	Size definition met for ≥ 6 h	Eccentricity ≥ 0.7 at time of maximum extent
PECS	Cold cloud region ≤ -52°C with area $\geq 50,000$ km^2	Size definition met for ≥ 6 h	$0.2 \leq$ Eccentricity < 0.7 at time of maximum extent
MβMCC	Cold cloud region ≤ -52°C with area $\geq 30,000$ km^2& maximum size must be $\geq 50,000$ km^2	Size definition met for ≥ 3 hours	Eccentricity≥ 0.7 at time of maximum extent
MβPECS	Cold cloud region ≤ -52°C with area $\geq 30,000$ km^2& maximum size must be $\geq 50,000$ km^2	Size definition met for ≥ 3 hours	$0.2 \leq$ Eccentricity < 0.7 at time of maximum extent

Reviewing Table 4.1 shows that many shapes and sizes of MCSs are included in the classification scheme. The MCC definition is the modified version of Maddox's (1980) definition (see Table 2.2) as set forth by Augustine and Howard (1988)

while the PECS definition is that as defined by Anderson and Arritt (1998). As was discussed above, MβMCCs and MβPECSs are just smaller, abbreviated versions of their namesakes. Including such a broad range of systems led to a large MCS sample, which was desired for this study. The classification scheme presented here will be used throughout the rest of the paper.

4.2 Basic characteristics

As discussed in Section 3.2.2, a total of 514 systems were identified and subjected to the classification scheme. During the classification process, it was expected to eliminate some systems due to the way in which the systems were subjectively identified. In fact, a total of 49 systems were removed from consideration through the classification process. Two systems were removed because their eccentricity was < 0.2, twenty-two systems were removed because they failed to reach a maximum size of 50,000 km^2 even though they met the duration requirement at the size of 30,000 km^2, and twenty-five systems were removed because they did not meet the duration criteria of ≥ 3 hours at a size of 30,000 km^2. Consequently, a total of 465 classifiable systems remained.

Table 4.2 provides a breakdown of MCS frequency for each of the five months during the three-year period. Looking at the totals, more systems fit into the larger MCS classifications (MCCs and PECSs) than the smaller MCS classifications (MβMCCs and MβPECSs). MCCs and PECSs accounted for 64% of the MCSs during the study period. PECSs were by far the most common type of MCS accounting for 40% of the sample total. As far as the monthly totals are concerned, May, June, and July were about equally the most common months for MCS occurrence. April was by far the

least likely month for an MCS to develop accounting for less than 10% of the total sample. Another interesting observation is that the greatest frequency of smaller systems tended to occur later in the season as opposed to the larger systems. The larger MCSs had a peak frequency in May while the smaller MCSs had a peak frequency in July.

Table 4.2: Distribution of MCS type (1996-1998).

MCS Type	April	May	June	July	August	Total
MCC	8	32	20	29	22	111
PECS	20	53	45	40	29	187
MβMCC	3	10	20	21	17	71
MβPECS	11	16	25	28	16	96
Total	42	111	110	118	84	**465**

Average statistics for each MCS class can be found in Table 4.3. Obviously, the larger systems had much larger average maximum areas than the smaller systems. The PECS had the largest average maximum area at over 200,000 km^2 while the smaller systems had average maximum areas under 100,000 km^2. However, the extremely massive systems skew the average maximum size as shown by the large standard deviations. When the distribution of all MCSs is plotted as a function of size (see Figure 4.1), there is an exponential decrease in the number of systems when moving toward larger systems. The tail would be much longer than this, but 30 systems were left off as the largest system grew to over 800,000 km^2. Even though the average maximum size of all the systems was around 160,000 km^2, about 2/3 of the systems were smaller than the average. Thus, it is more common to observe a system smaller than average as opposed to a system larger than average even though more systems fall into the larger MCS categories of MCCs and PECSs.

Table 4.3: Statistics for each MCS type: means and (standard deviations).

MCS Type	Maximum Area (km^2)	Duration (h)	Eccentricity
MCC	193,282(108,146)	10.9(3.9)	0.83(0.09)
PECS	213,473(130,020)	10.6(3.8)	0.50(0.13)
MβMCC	74,696(21,540)	6.1(2.2)	0.84(0.08)
MβPECS	85,195(29,786)	6.7(2.1)	0.53(0.11)
All MCSs	160,980(116,140)	9.2(3.9)	0.64(0.19)

The average duration of each type of MCS can also be found in Table 4.3. The larger systems persisted longer than the smaller systems as would be expected due to the nature of the duration criteria in their definitions. Given that a system is classified as a larger system or smaller system, the shape didn't appear to have much influence on the duration of the system as MCCs and PECSs had nearly identical durations, and MβMCCs and MβPECSs also had very similar durations. The larger systems lasted more than 10 hours on average while the smaller systems lasted more than 6 hours on average. The average lifetime of all MCSs was over 9 hours.

The average and standard deviation of the eccentricities for each type of MCS are listed in Table 4.3. The circular systems, MCCs and MβMCCs, had very similar eccentricities, and the linear systems, PECSs and MβPECSs, also had very similar eccentricities. The circular systems had an average eccentricity of around 0.83 with a small standard deviation as required by their definition. The linear systems had an average eccentricity around 0.50.

The distribution of times at which these systems formed, matured, and dissipated can be found in Figure 4.2. The frequency of times at which the MCSs first

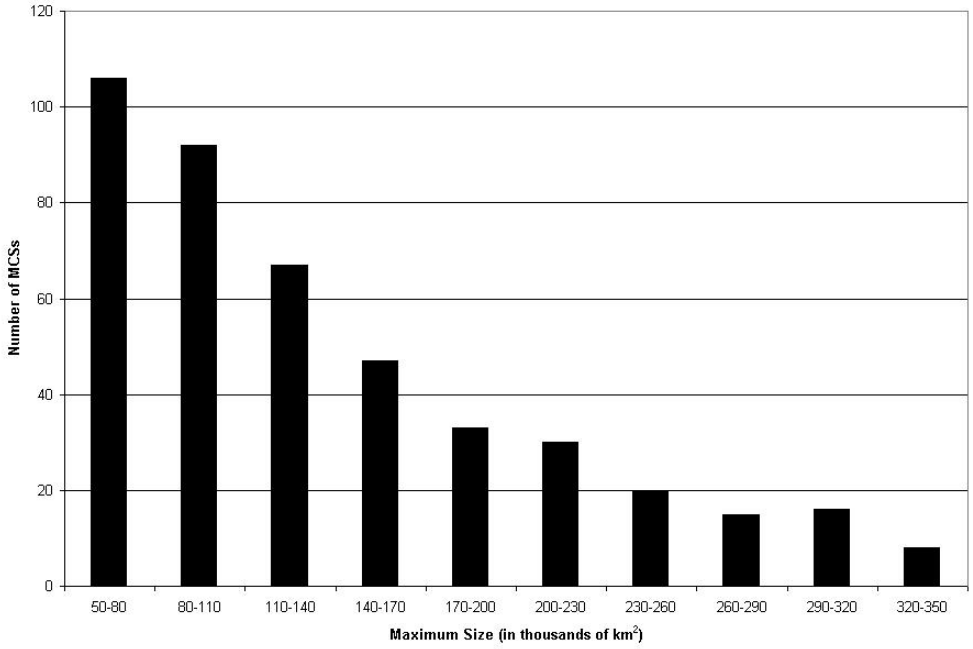

Figure 4.1: Distribution of all MCSs as a function of size.

met their definition is displayed at the front of Figure 4.2. The distribution of initiation time for the MCSs in this sample was close to normal. Nearly 60% of all MCSs initiated between 2000 UTC and 0300 UTC. This corresponds to 3 p.m. to 10 p.m. CDT for the central United States during the warm season. Thus, these systems primarily initiated during the afternoon and evening hours. Figure 4.2 also shows the distribution of times of maximum extent for all MCSs. The times that the MCSs reached their maximum extent also produced a nearly normal distribution. About 60% of the systems reached their maximum size between 0200 UTC and 0900 UTC, or about six hours after initiation. This time frame corresponds to 9 p.m. to 4 a.m. CDT. Finally, the last set of data at the back of Figure 4.2 shows the distribution of times of termination for the MCS sample. Most of the systems dissipated between 0700 UTC and 1500 UTC (2 a.m. to 10 a.m. CDT). Consequently, a majority of the systems in this study formed in the late afternoon and evening hours, reached their

maximum size during the night, and dissipated in the early morning hours, which is consistent with Maddox's (1980) MCC study and other MCS studies.

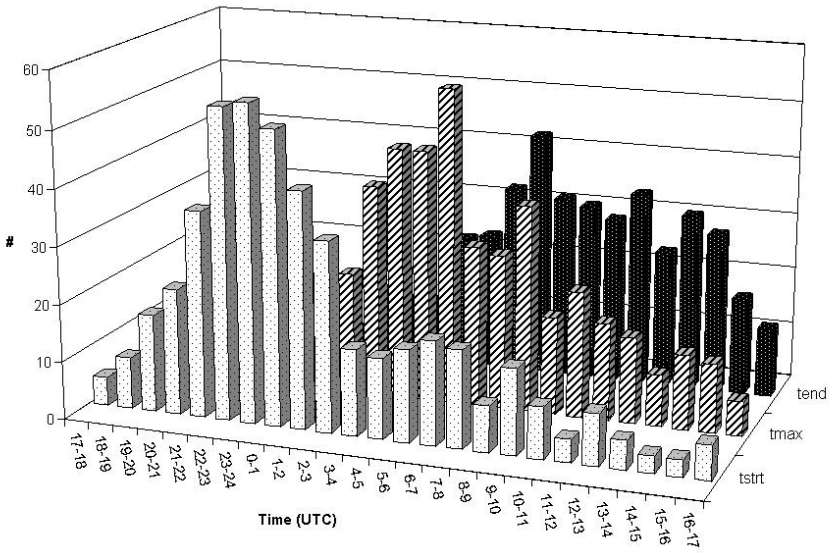

Figure 4.2: Distribution of all MCSs as a function of initiation time (tstrt), time of maximum extent (tmax), and termination time (tend).

4.3 Examples of classes

In order to show what some of these systems actually look like in nature, this section provides infrared satellite images for examples of each type of MCS. The duration and maximum size are also provided to help understand their lifecycle. The examples supplied in this section were selected because they were representative of their respective categories.

MCCs are probably the most striking systems due to their large size and circular shape. Figure 4.3 shows an example of a MCC as it moved across Kansas and Missouri on May 7, 1996. The top left panel was taken at 0615 UTC and shows two cloud clusters in northwest Kansas just before they merged and reached MCC status. The MCC had begun to grow by 0900 UTC and moved eastward across Kansas (top right

panel). The MCC had just about reached its maximum area of 266,000 km^2 at the -52°C threshold by 1215 UTC (bottom left panel). At this time, the system was very circular with an eccentricity of 0.95. The bottom right panel shows the system eight hours later as it dissipated to barely meet MCC criteria. Overall, the system had a duration of over 15 hours.

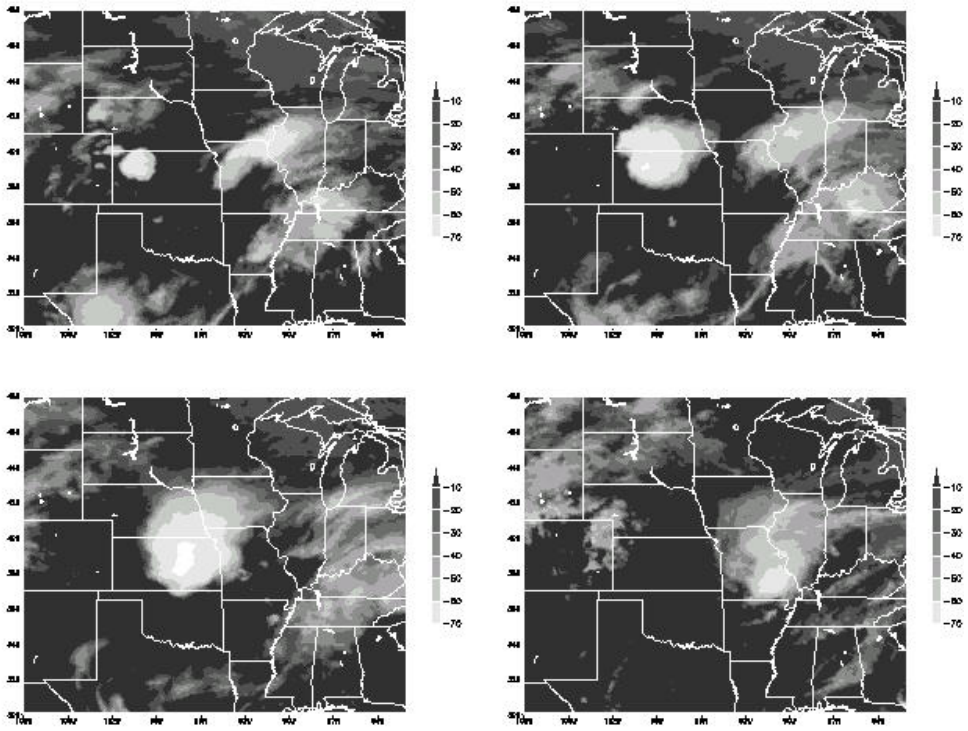

Figure 4.3: The development and dissipation of a MCC that traversed across Kansas and Missouri on May 7, 1996, as seen by infrared satellite imagery. The images are from 0615 UTC (top left), 0900 UTC (top right), 1215 UTC (bottom left), and 2015 UTC (bottom right).

Although MCCs are massive systems in their own right, PECSs can also reach very large sizes. Infrared satellite images of a PECS are shown in Figure 4.4. The system started to develop at 0045 UTC on June 20, 1998, as small cloud clusters began to grow (top left panel). By 0445 UTC (top right panel), the cloud clusters had merged over Missouri creating an oblong system that met the PECS criteria.

The bottom left panel shows that five hours later the system had just about reached its maximum extent of 253,000 km^2. By 1645 UTC (bottom right panel), the system could still be classified as a PECS, but it was well into its dissipation stage. This system persisted as a PECS for more than 17 hours without moving significantly.

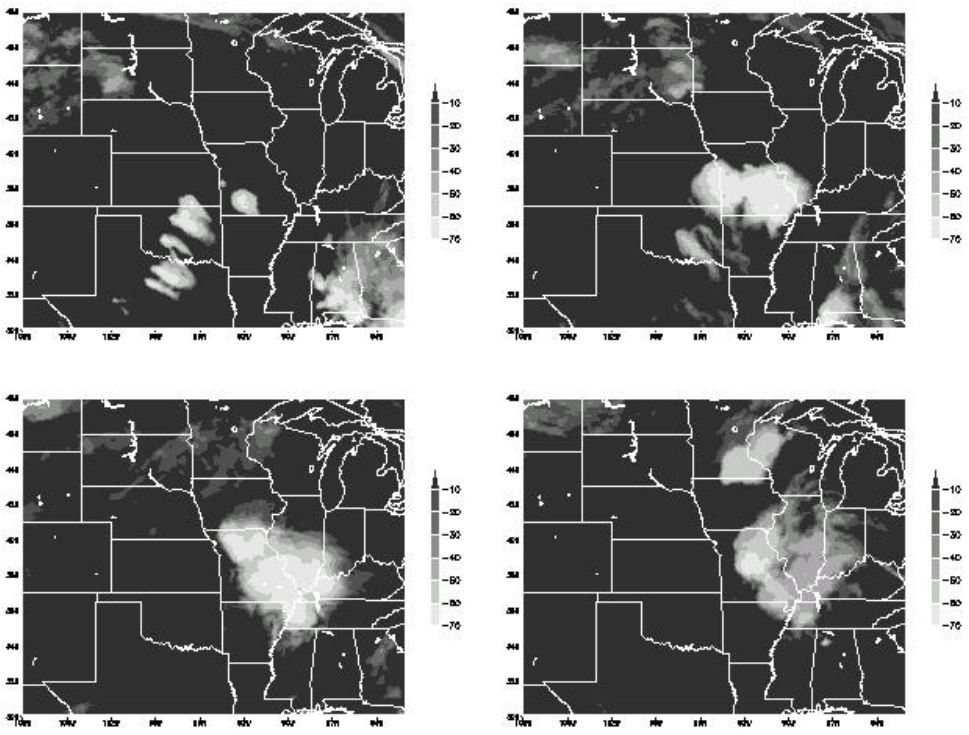

Figure 4.4: The development and dissipation of a PECS that formed over Missouri on June 20, 1998, as seen by infrared satellite imagery. The images are from 0045 UTC (top left), 0445 UTC (top right), 0945 UTC (bottom left), and 1645 UTC (bottom right).

Smaller versions of MCCs, MβMCCs, can also be very coherent and well-organized systems as seen in this example. Figure 4.5 shows a MβMCC that developed along the Oklahoma-Kansas border on July 19, 1997. The top left panel shows the system in its early stages at 0445 UTC. Just two hours later, the system had grown to meet MβMCC criteria (top right panel). At 0845 UTC (bottom left panel), the system had reached its maximum size of 71,000 km^2. The system began to dissipate

by 1245 UTC as seen in the bottom right panel. This system was also relatively stationary and endured for over 8 hours.

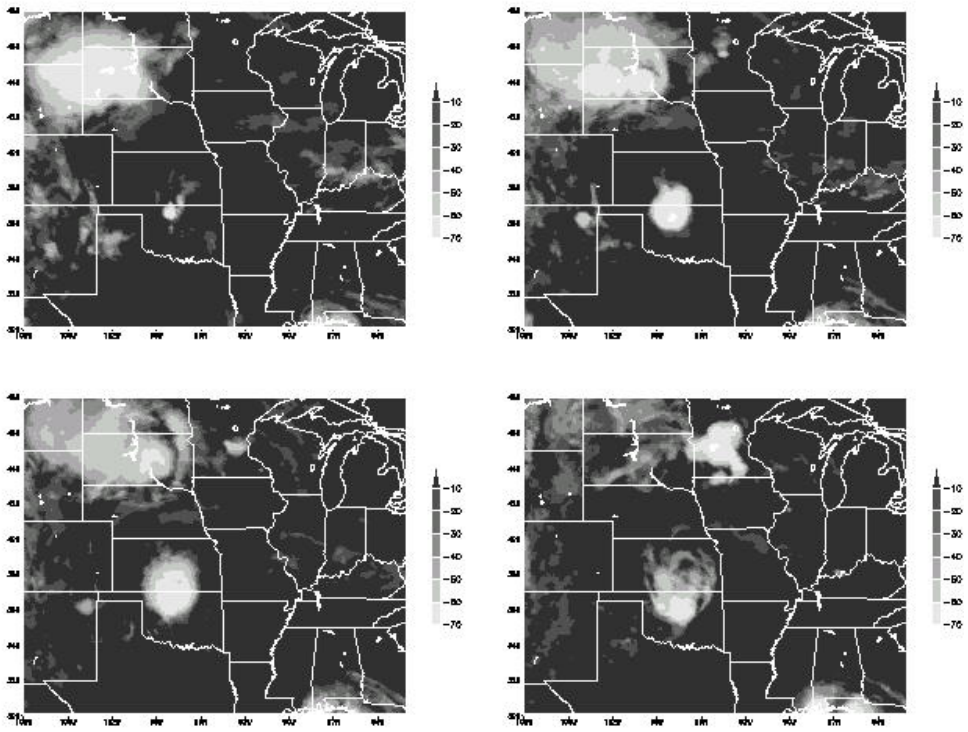

Figure 4.5: The development and dissipation of a MβMCC that formed along the Oklahoma-Kansas border on July 19, 1997, as seen by infrared satellite imagery. The images are from 0445 UTC (top left), 0645 UTC (top right), 0845 UTC (bottom left), and 1245 UTC (bottom right).

The last MCS type for which an example needs to be provided is the MβPECS category. Infrared satellite images of a MβPECS that formed on June 19, 1996, can be found in Figure 4.6. This system began to form at 1845 UTC along the South Dakota-Minnesota border and in northern Nebraska as seen in the top left panel. Two distinct cloud clusters can be seen in the top right panel at 2000 UTC. The cloud clusters eventually merged together to form a mature, oblong system. The MβPECS had just about reached its maximum size of 110,000 km^2 by 2200 UTC (bottom left panel). At 0100 UTC on June 20, 1996 (bottom right panel), the system began to

dissipate after almost 7 hours of existence.

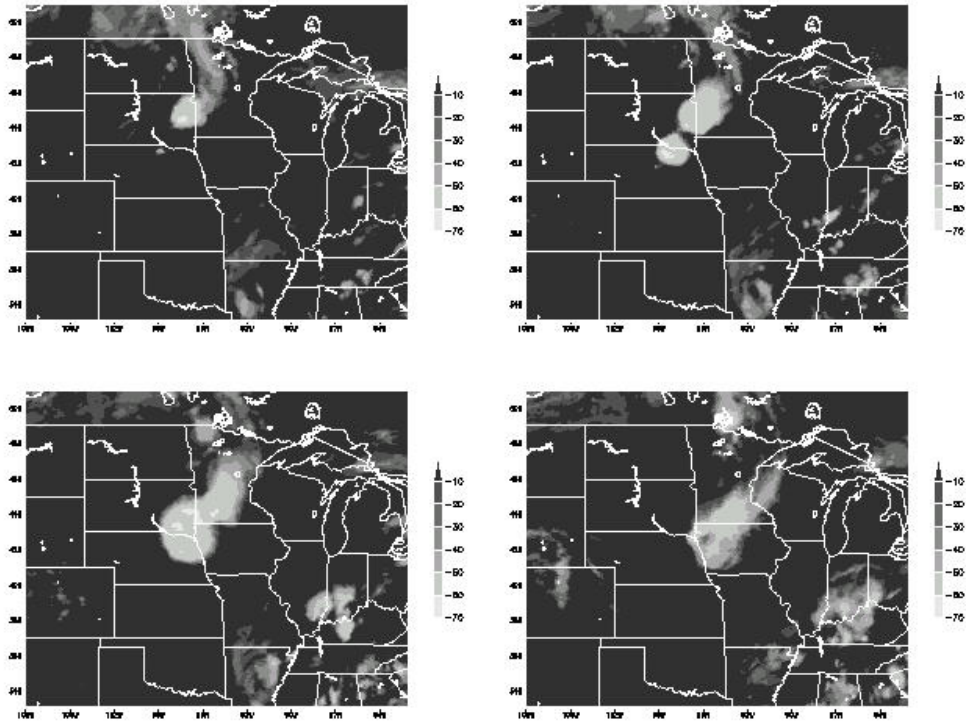

Figure 4.6: The development and dissipation of a MβPECS that formed from Minnesota to Nebraska on June 19, 1996, as seen by infrared satellite imagery. The images are from 1845 UTC (top left), 2000 UTC (top right), 2200 UTC (bottom left), and 0100 UTC (20 June 1996) (bottom right).

Chapter 5

Radar classification of MCSs

Similar to classifying MCSs by satellite characteristics, there have been many studies on classifying MCSs by radar characteristics (see Section 2.2). Unfortunately, the radar studies have not been well connected with one another or with the satellite classification studies. In addition, convective lines were often the only types of MCSs considered in the radar studies. As was mentioned earlier, two primary types of radar classification schemes emerged from previous studies. One scheme involves classifying mature MCSs by their arrangement of convective and stratiform precipitation. This type of classification was not of primary importance for this study, but it will be discussed in this chapter. The other radar classification scheme, which was the focus of the present study, examines the developmental stages of MCS growth. A classification scheme was devised for this study to classify a wide range of MCSs by their development and will be presented later in this chapter.

5.1 Classification by organization

The analysis process of each 15-minute radar field allowed time to observe the organization of each MCS. As previously mentioned, this wasn't a major priority of

the study, so each system was examined only once to assign it to an organizational class. The systems were divided into four categories as set forth by Parker and Johnson (2000): trailing stratiform (TS), leading stratiform (LS), parallel stratiform (PS), and unclassifiable (U). In order for a system to be classified as a linear system by radar characteristics (i.e. TS, LS, or PS), it had to have a contiguous chain of convective echoes that formed a straight or curved line. Once a system was deemed to be linear, then it was classified according to the predominant arrangement of its convective and stratiform areas over its lifetime. This definition of a convective line is somewhat more restrictive than that used by Parker and Johnson (2000). Thus, it was expected for a smaller percentage of systems to meet the linear system criteria. In addition, TS systems generally have a stronger and more contiguous convective line making them more easily identifiable than LS and PS systems.

Table 5.1 shows the distribution of radar organization according to MCS satellite classification. The U and TS categories accounted for nearly 90% of the MCSs. Keep in mind that Parker and Johnson (2000) classified only linear MCSs, so basically any system without a convective *line* (i.e. nonlinear system) would be considered unclassifiable for this study. Thus, in looking at the totals, about half of the systems were linear and about half were nonlinear according to their radar organization. Don't forget about the possibility of a system being classified as circular according to satellite characteristics, but linear according to radar characteristics. Certainly, it appears that there is not an overwhelming relationship between the shape of the cloud shield and the existence of an underlying convective line. The larger systems (MCCs and PECSs) tended to have at least one convective line a majority of the time with PECS having the greatest percentage of convective lines (57%). The smaller systems definitely were less likely to have a contiguous convective line (only about 40% of the

time). The LS and PS categories combined accounted for over 20% of the linear convective systems, which is about half of that found by Parker and Johnson (2000). However, a more lenient interpretation of a convective line might have increased this percentage.

Table 5.1: Distribution of radar organization by MCS type (1996-1998).

MCS Type	TS	LS	PS	U	Total
MCC	37	3	7	43	90
PECS	66	9	10	64	149
MβMCC	17	5	4	39	65
MβPECS	23	2	5	53	83
Total	143	19	26	199	**387**

Table 5.2 breaks down the classification of radar organization by month. The most striking feature of these data was the transition from a higher percentage of linear systems early in the season to a lower percentage of linear systems late in the season. From April through June, more than half of the systems contained a convective line while only about 40% of the systems were linear during July and August. This is consistent with a shift from strong synoptic and baroclinic forcing early in the convective season to weaker baroclinic (or more barotropic) forcing late in the season.

A unique subset of radar organization that was not included in the study by Parker and Johnson (2000) is the bow echo. These systems have a curved or "bowed" convective line and often produce strong winds and downbursts (Fujita 1978). A total of 20 well-defined bow echoes were recorded for this study. These systems were equally common among the satellite classifications of MCC, PECS, and MβMCC while only

Table 5.2: Distribution of radar organization by month (1996-1998).

Month	TS	LS	PS	U	Total
April	14	2	4	16	36
May	40	3	6	47	96
June	44	4	7	42	97
July	27	9	4	53	93
August	18	1	5	41	65
Total	143	19	26	199	**387**

one bow echo was classified as a MβPECS. Nearly all of the systems formed from the merger of multiple convective clusters with the bow echo signature occurring just after the system reached full maturity. Finally, all but one bow echo had the TS arrangement with one system having the LS arrangement (see bottom left panel of Fig. 5.1).

The satellite lifecycle characteristics of the MCSs are broken down in Table 5.3 by type of radar organization. The TS archetype encompasses a wide range of systems making it the most variable category. Nevertheless, the TS systems were statistically larger and longer-lived than the PS and LS systems. This agrees with the results of Parker and Johnson (2000) that TS systems had a mean duration almost twice that of the PS and LS systems. The results of this study are not as dramatic, but remember that they defined the duration of the systems by *radar* characteristics and not *satellite* characteristics, as was done in this study.

To provide an idea of what each category of radar organization looks like, examples are provided in Figure 5.1. These radar reflectivity images are representative examples of each category. The images chosen were taken at approximately the time

Table 5.3: Statistics for each radar organization type: means and (standard deviations).

MCS Type	Maximum Area (km^2)	Duration (h)	Eccentricity
TS	194,148(137,716)	10.5(4.3)	0.62(0.20)
PS	142,643(60,803)	8.2(2.5)	0.66(0.19)
LS	156,341(78,249)	9.2(3.8)	0.68(0.14)
U	133,927(102,260)	8.1(3.5)	0.64(0.20)

of maximum extent for the system. The upper left panel shows a MCC with a TS organization that moved across Missouri on May 5, 1996. The upper right panel is an example of a PS system. This PECS moved through the Nebraska panhandle and northeastern Colorado on August 16, 1996. An example of a LS system is shown in the bottom left panel. This MβMCC moved across Nebraska on July 1, 1997. Finally, an example of an unclassifiable system is provided in the bottom right panel. This system was also a MβMCC that remained stationary over northern Louisiana on May 21, 1997. Notice the absence of a contiguous convective line.

5.2 Classification by development

Although the arrangement of MCSs provides some valuable information, the primary focus of this study was on the development stages of MCSs. Again, it was important to try to be consistent with previous studies using similar terminology wherever possible to avoid confusion. The foundation of the classification scheme presented in this section was provided by Bluestein and Jain (1985). However, since they only considered squall lines, the scheme needed to be expanded to accommodate all types of MCSs. The idea was to try to explain what the convection looked like

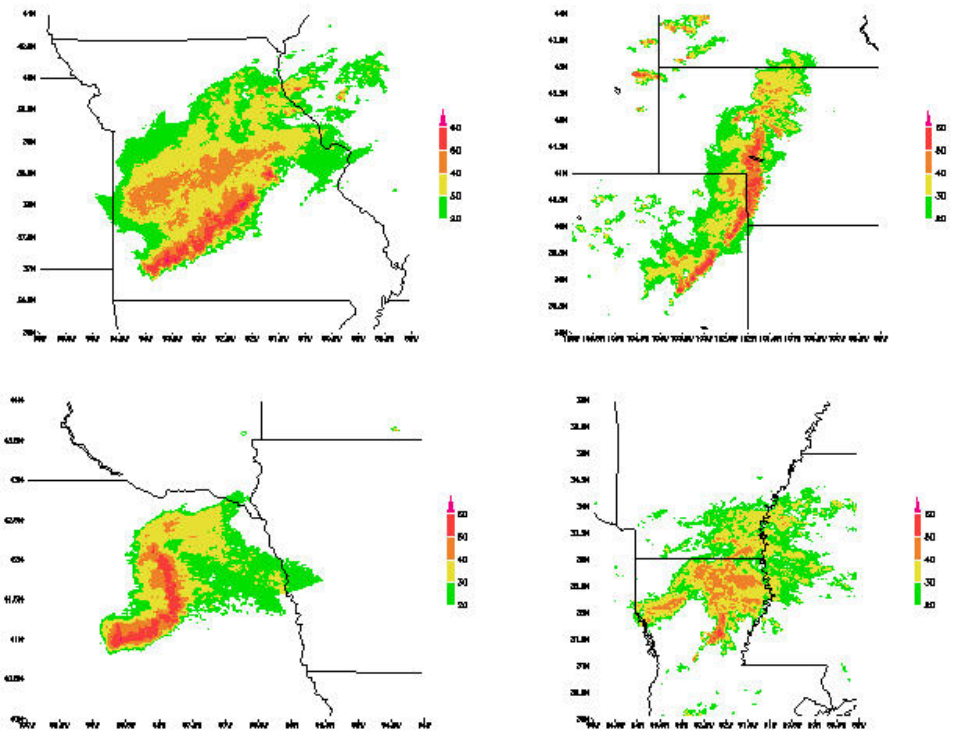

Figure 5.1: Radar reflectivity examples of radar organization categories. Top left is a TS system from 1600 UTC 5 May 1996, top right is a PS system from 0100 UTC 16 August 1996, bottom left is a LS from 0600 UTC 1 July 1997, and bottom right is an unclassifiable system from 1200 UTC 21 May 1997.

under the cloud shield and how the convective cells and clusters interacted with one another.

5.2.1 Definition of classes

Bluestein and Jain (1985) used four classes to describe squall line development: broken line, back building, broken areal, and embedded areal (see Fig. 2.4). The terms *embedded, areal,* and *line* were recycled from this scheme and implemented into the current scheme. Some important factors that were considered in creating the scheme included the orientation, number, and interaction of cells and clusters as well as the presence of stratiform precipitation. Motivated from these factors came a classification scheme of three *levels*. First of all, the systems were categorized based

on whether or not there was preexisting stratiform precipitation in the area where convection initiated. Secondly, the systems were sorted by whether the initial cellular convection was arranged in the form of a line or was scattered out over an area. Finally, the systems were classified by the number of convective clusters and how they interacted. The rest of the section will provide more detail on each level of this classification scheme.

Presence of stratiform precipitation

The first level in the classification process involved determining whether or not the initial convection occurred in an area of stratiform precipitation. This step follows directly from the embedded areal category of Bluestein and Jain (1985) and was included due to anticipated differences between these systems and those that formed in non-precipitating areas. This step was generally straight-forward because the systems usually either formed in echo-free regions or in areas with significant stratiform precipitation. As seen in Figure 5.2, if a system initiated in a region of stratiform precipitation, it was tagged with the term *embedded* . If it did not form in a region of stratiform precipitation, the system was not named for this level (to eliminate usage of a term such as *non-embedded*).

Arrangement of convective cells

The next level in the classification process described the arrangement of convective cells at initiation. Once again, this follows closely from Bluestein and Jain (1985) who basically broke cellular arrangement into line and areal categories. Thus, this step involved analyzing the early stages of convection to determine whether or not the cells were arranged in a line. Figure 5.2 shows that systems with convection

organized in a linear fashion received the term *line* while systems with convection not arranged linearly received the term *areal* . If a system showed both types of cellular arrangement, it was given the term *combination* . Keep in mind that this step does not necessarily provide information on the shape of the MCS at its maturity. As Bluestein and Jain (1985) showed, areal systems can develop into squall lines. This step was somewhat more subjective than the first one, but generally it was apparent whether or not the cells were organized in a line.

Interaction between convective clusters

The final level in the classification process involved observing how the convective cells grew into clusters and interacted with other convective clusters. Please note that this step occurred later in the lifecycle of the MCSs. This was by far the most subjective step in the classification process. The term *cluster* is referring to a meso-β grouping of convective cells that are contiguous or nearly contiguous. Often, it was difficult to distinguish between cells forming independent clusters that merged and cells that grew to form a single convective cluster. The criteria used to identify convective clusters included separation between convection, orientation different from surrounding convection, and initiation of convection at different times. Three major features emerged, and the systems were categorized accordingly. One type of interaction is just the growth of convective cells into a single convective cluster. These systems were termed *growth* systems (see Fig. 5.2). Another type of interaction is the development of multiple independent convective clusters that merge into a single entity. These systems were given the name *merger* systems. Finally, if individual convective clusters developed close enough to one another to share a common cloud

shield, but did not physically merge as seen by radar, then they were called *isolated* systems.

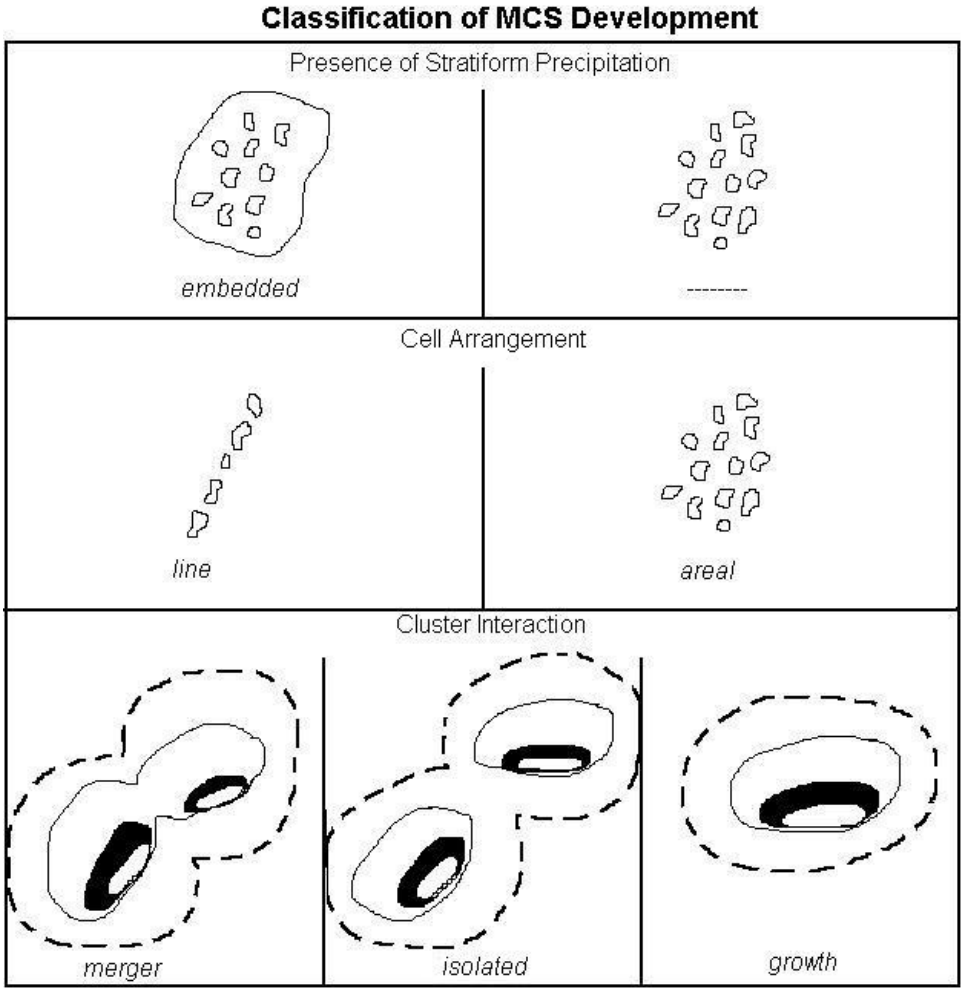

Figure 5.2: Idealized depiction of the three-level classification process used to categorize MCS development as seen by radar. The solid lines and contours represent relative reflectivity levels while the dashed lines represent the outline of the cold cloud shield.

The nature of the classification process as seen in Figure 5.2 leads to 17 categories. Not obvious from this figure is the *unclassifiable* category and four *combination* categories, in which the clusters have developed from a mixture of line and areal arrangements. Growth systems could not have a combination category since they develop from a single convective cluster. Of course, not all categories are guaranteed to

be significant since this was a classification *process* rather than just a list of the most important categories. The next section will discuss the distribution and frequency of the MCSs according to their developmental classification.

5.2.2 Basic characteristics

As was discussed in Section 3.3.2, a total of 387 systems remained after the final stages of radar analysis and screening. The radar images were animated and observed for the lifecycle of each system. In addition, the classification scheme was used to scrutinize, analyze, and ultimately categorize the development of each system. Even though there was much subjectivity involved in the classification process of this MCS sample, useful results can still be obtained through careful and *consistent* analysis. Regardless of the results for this study, hopefully the classification process used will prove to be flexible and functional for future studies.

Table 5.4 lists the distribution of MCS development according to each system's satellite classification. First of all, look at the totals for each development category. The *areal merger* and *combination merger* development categories alone accounted for more than half of the MCSs. Clearly, the MCSs in this study had a propensity to form by a merger of convective clusters. The next most common types of development were the *areal growth* and *line merger* categories. However, each of these categories only accounted for less than 10% of the total MCS sample. Also, it is obvious that the *embedded isolated* systems were not significant types of development in this sample.

Another method that makes it easier to view the results is to break the data into the three levels of the classification process. Table 5.5 presents the data in this fashion. First of all, *embedded* systems accounted for only 17% of the total MCS

Table 5.4: Distribution of MCS development by satellite classification.

Development Type	MCC	PECS	MβMCC	MβPECS	Total
embedded line merger	1	4	0	1	6
embedded areal merger	6	6	7	6	25
embedded combination merger	3	7	1	4	15
embedded line isolated	0	0	0	0	0
embedded areal isolated	0	0	0	1	1
embedded combination isolated	0	0	0	0	0
embedded line growth	0	1	2	1	4
embedded areal growth	3	3	4	4	14
line merger	4	20	2	5	31
areal merger	26	34	20	25	105
combination merger	27	41	9	16	93
line isolated	0	3	0	1	4
areal isolated	4	7	6	4	21
combination isolated	3	3	0	0	6
line growth	3	7	2	6	18
areal growth	9	8	10	7	34
unclassifiable	1	5	2	2	10
Total	90	149	65	83	**387**

sample. It was more common for the smaller systems (MβMCCs and MβPECSs) to be embedded than the larger systems (MCCs and PECSs). The middle section of Table 5.4 shows that more than half of the initial convection was arranged in an *areal* fashion. Not too surprisingly, the linear systems according to satellite imagery (PECS and MβPECSs) were more likely to have the initial convection arranged in a *line* than the circular systems (MCCs and MβMCCs). In fact, more than 20% of the linear systems had its initial cellular convection arranged in a line compared to less than 10% of the circular systems. Finally, *merger* systems were by far the most

common type of cluster interaction accounting for over 70% of all MCSs. Although the *isolated* systems are an interesting class of MCS development, they only occurred about 8% of the time. The data also shows that single clusters, i.e. *growth* systems, more commonly developed into smaller systems (MβMCCs and MβPECSs). About one-fourth of the smaller systems were growth systems while only 15% of the larger systems consisted of a single convective cluster. Similarly, McAnelly and Cotton (1986) noted that smaller MCCs tended to develop from a single meso-β convective cluster.

Table 5.5: Distribution of MCS development by satellite classification broken into the three levels of the classification process.

Development Type	MCC	PECS	MβMCC	MβPECS	Total
embedded	13	21	14	17	65
not embedded	76	123	49	64	312
unclassifiable	1	5	2	2	10
Total	90	149	65	83	387
line	8	35	6	14	63
areal	48	58	47	47	200
combination	33	51	10	20	114
unclassifiable	1	5	2	2	10
Total	90	149	65	83	387
merger	67	112	39	57	275
isolated	7	13	6	6	32
growth	15	19	18	18	70
unclassifiable	1	5	2	2	10
Total	90	149	65	83	387

Table 5.6 lists the distribution of MCS development by month arranged into the

levels of the classification process. Looking at the presence of stratiform precipitation, more than 36% of the MCSs in April were *embedded* compared to only 15% of the systems throughout the remainder of the convective season. The month of April accounted for less than 10% of the total MCS sample, but comprised 20% of the embedded systems. Once again, the month of April stands out when considering the arrangement of convective cells. Due to the strong baroclinic forcing early in the season, one-third of all April MCSs initiated in a linear fashion while only 15% of the systems were arranged linearly throughout the rest of the convective season. Finally, it also appears that single-cluster systems were more likely early in the season with nearly half of the *growth* systems occurring in April and May.

The satellite lifecycle statistics for each main group of radar development are provided in Table 5.7. MCSs that initiated in stratiform precipitation developed into smaller systems at maturity than MCSs that developed in clear air. When looking at the statistics for the different types of cell arrangement, the areal systems were smaller and shorter-lived than both line and combination systems at greater than the 99% confidence level. This suggests that if you know the arrangement of the initial convection, you have some relative information about the duration and maximum size that a system may attain. Also, not surprisingly, systems that had initial convection arranged in a line were more likely to have a linearly shaped cloud shield. The interaction among convective clusters also provides some information on the size of MCSs. If a MCS evolved from a single convective cluster (i.e. growth systems), it was likely to be smaller than a multiple cluster system (i.e. isolated or merger system) at better than the 99% confidence level. This was also seen in the fact that growth systems were more likely to fall into the satellite classification of smaller systems (MβMCCs and MβPECS).

Table 5.6: Distribution of MCS development by month broken into the three levels of the classification process.

Development Type	April	May	June	July	August	Total
embedded	13	13	16	12	11	65
not embedded	22	80	77	79	54	312
unclassifiable	1	3	4	2	0	10
Total	36	96	97	93	65	387
line	12	17	13	10	11	63
areal	13	48	53	50	36	200
combination	10	28	27	31	18	114
unclassifiable	1	3	4	2	0	10
Total	36	96	97	93	65	387
merger	24	59	72	73	47	275
isolated	1	12	8	6	5	32
growth	10	22	13	12	13	70
unclassifiable	1	3	4	2	0	10
Total	36	96	97	93	65	387

The results provided in this section seem to follow intuition.

- When MCSs developed in areas of stratiform precipitation and grew from a single cluster, they tended to be smaller systems.

- Linear systems tended to develop from convection that initiated in a line.

- Linear systems were most common early in the convective season due primarily to the existence of strong baroclinic frontal systems.

- Convection arranged in an areal fashion tended to develop into smaller and

Table 5.7: Statistics for each radar development level: means and (standard deviations).

Development Type	Maximum Area (km^2)	Duration (h)	Eccentricity
embedded	130,072(94,786)	9.3(4.8)	0.66(0.22)
not embedded	162,581(120,256)	9.0(3.7)	0.64(0.19)
line	191,393(122,282)	9.3(3.3)	0.54(0.19)
areal	129,768(96,761)	8.4(3.8)	0.69(0.18)
combination	185,688(133,784)	10.2(4.1)	0.63(0.19)
merger	162,819(117,531)	9.3(3.9)	0.64(0.19)
isolated	184,195(165,548)	9.0(4.3)	0.61(0.21)
growth	121,577(73,629)	8.3(3.6)	0.68(0.18)
unclassifiable	191,401(121,890)	8.9(5.4)	0.60(0.18)

shorter-lived systems.

- The most common type MCS development was the merging of multiple convective clusters.

The rest of the chapter will provide some examples of the most common types of MCS development.

5.2.3 Examples of classes

In order to show how some of these systems actually develop in nature, this section provides radar imagery for examples of some of the most common types of MCS development. The examples supplied in this section were selected to provide a clear idea of how the MCSs were classified. Each category in every development level is represented at least once by the examples provided in this section. The examples will be discussed in order of most common to least common.

Areal mergers were the most frequent type of MCS development for this study. It is certainly a fairly broad category, and the systems that fit into this family take on a variety of forms. A typical areal merger system occurred on June 20, 1996, as shown in Figure 5.3. The top left panel shows the initial convection in southern Arkansas and northern Louisiana at 0000 UTC. Notice that the convection developed in clear air and was not arranged in a linear fashion, hence the classification as an areal system. Two hours later, as seen in the upper right panel, there were three distinct convective clusters extending from south central Arkansas to northeastern Louisiana. Note that the solid black contour in these plots represents the cloud shield outline at the $-52°C$ blackbody temperature. By 0400 UTC (bottom left panel), the two northernmost clusters had begun to merge and shared a common cloud shield.

Finally, the bottom right panel shows the mature MβMCC at 0900 UTC moving to the southwest.

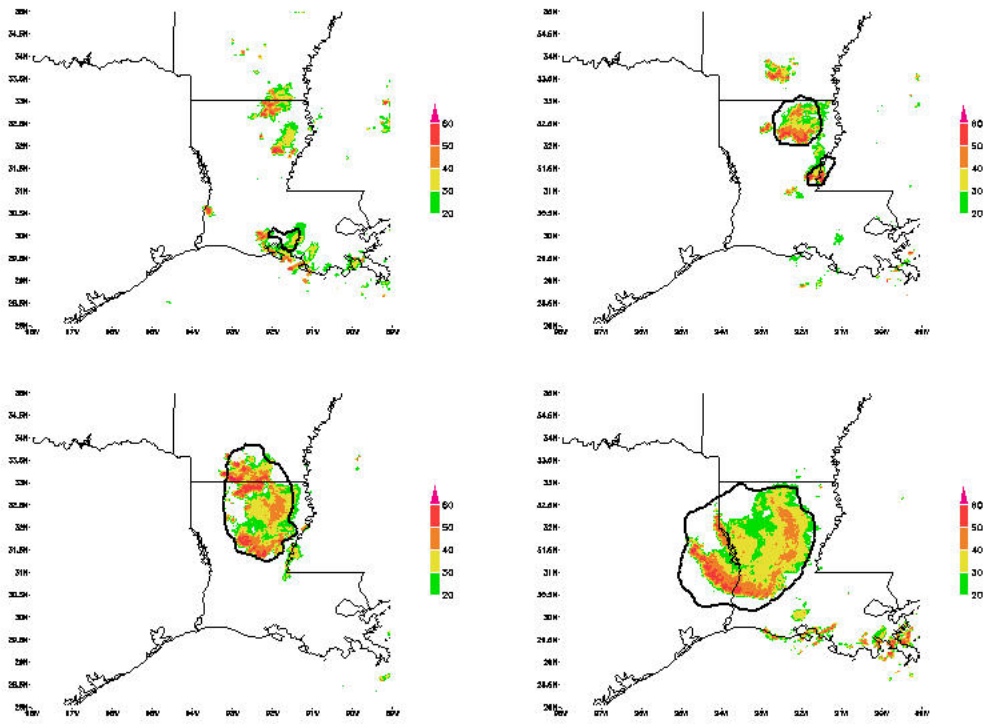

Figure 5.3: Areal merger development of a MβMCC that occurred in southern Arkansas and northern Louisiana on June 20, 1996, as seen by radar imagery. The images are from 0000 UTC (top left), 0200 UTC (top right), 0400 UTC (bottom left), and 0900 UTC (bottom right). The solid black contours represent the outline of the -52°C cloud shield.

Closely related to the areal merger system is the combination merger system, which was the second most common type of MCS development found in this study. The only difference between these types of development is that some of the initial convection in a combination merger system is arranged in a line. Figure 5.4 shows an example of such a system that occurred on June 24-25, 1997. The early stages of convection can be seen in the top left panel, which is from 2215 UTC on June 24. Obviously, the convection in southeastern Colorado was of the areal variety while the convection extending from northern Kansas to southern Nebraska was of the linear

variety; thus, it was a combination system. There were several distinct convective clusters three hours later throughout Colorado, Kansas, and Nebraska as seen in the upper right panel. The clusters had begun to merge by 0315 UTC on June 25 (lower left panel). The bottom right panel taken at 0515 UTC shows the mature PECS with a contiguous area of precipitation and cold cloud shield extending from the Kansas-Colorado border into Iowa.

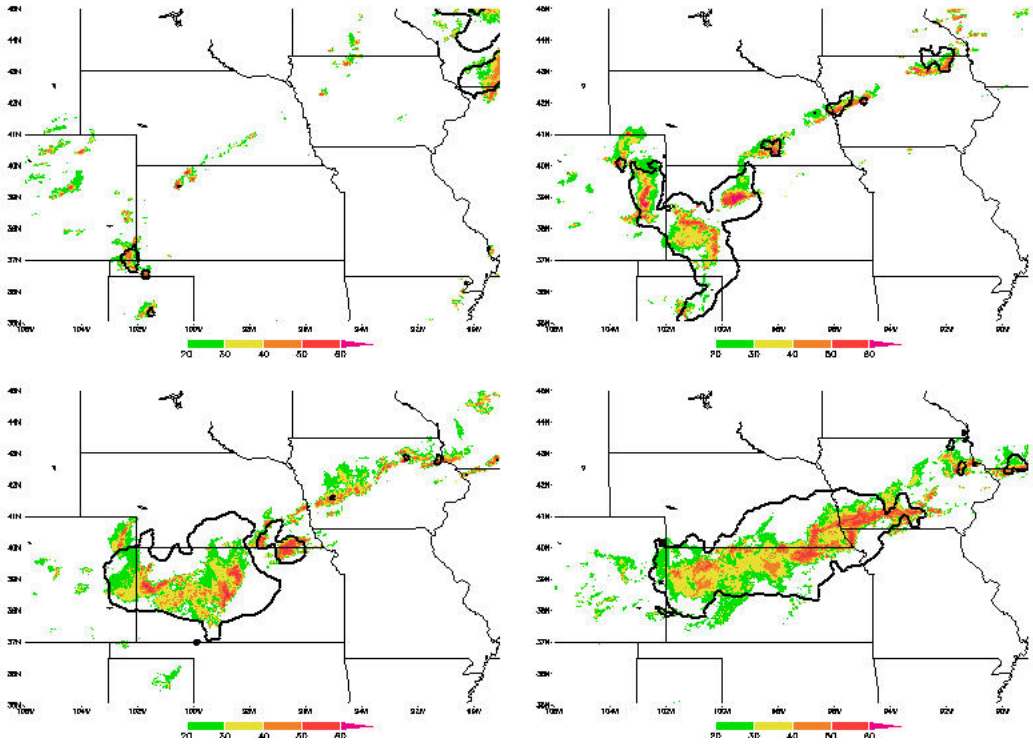

Figure 5.4: Combination merger development of a PECS that occurred throughout Colorado, Kansas, and Nebraska on June 24-25, 1997, as seen by radar imagery. The images are from 2215 UTC (top left), 0115 UTC (top right), 0315 UTC (bottom left), and 0515 UTC (bottom right). The solid black contours represent the outline of the -52°C cloud shield.

The next most common type of development was the areal growth systems. These are systems that basically evolve from a single convective cluster that was formed by scattered convection. An example of this type of system is provided in Figure 5.5. This system developed in northern Texas on the June 4-5, 1996. At 2130

UTC (upper left panel), the convection was arranged in an areal manner. By 0100 UTC, two distinct convective clusters had emerged along the Texas-Oklahoma border as seen in the upper right panel, but the northernmost cluster dissipated rapidly and had little effect on the development of the other cluster. Just over two hours later, the cluster had grown producing a large cloud shield (lower left panel). Finally, the bottom right panel shows the mature MCC at 0800 UTC as it moved to the south-southeast. This system would most likely have fit into the broken areal category of Bluestein and Jain (1985).

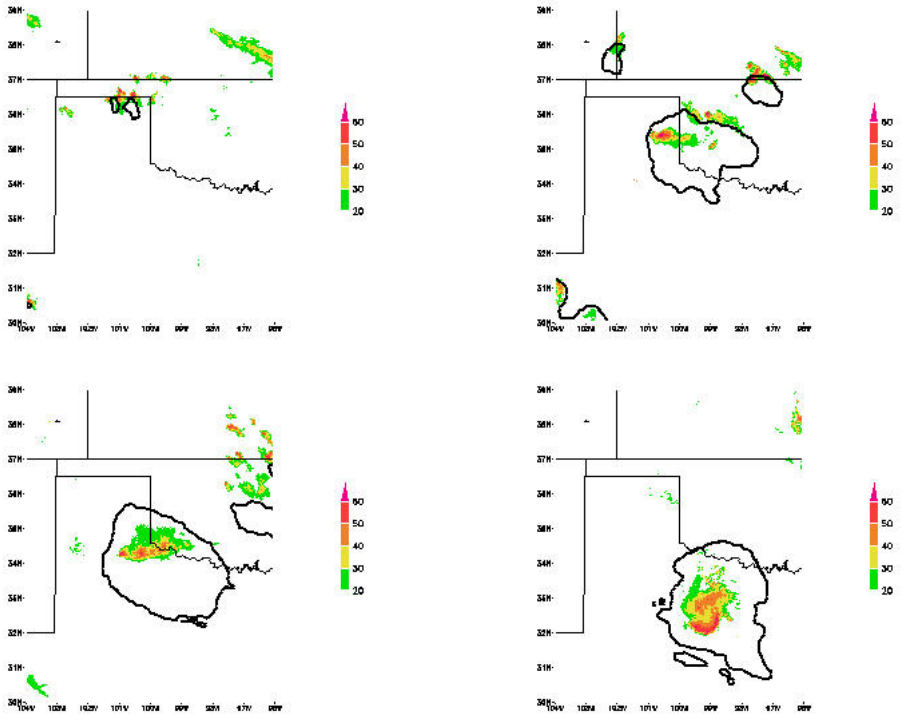

Figure 5.5: Areal growth development of a MCC that occurred in northern Texas on June 4-5, 1996, as seen by radar imagery. The images are from 2130 UTC (top left), 0100 UTC (top right), 0315 UTC (bottom left), and 0800 UTC (bottom right). The solid black contours represent the outline of the $-52°$C cloud shield.

Line mergers are the next category of interest. A representative line merger system occurred on June 21-22, 1997, in the upper Midwest as seen in Fig. 5.6. At 2000 UTC (upper left panel), there was linearly arranged convection in Michigan

and Indiana. The top right panel shows that several distinct convective clusters had formed two hours later extending into Illinois. The clusters began to merge at 2315 UTC (lower left panel) already sharing a contiguous cloud shield. By 0100 UTC, the system had developed into a PECS with a well-defined TS arrangement. Using Bluestein and Jain's (1985) classification scheme, this massive system would most likely have been a combination of the broken line and back building categories.

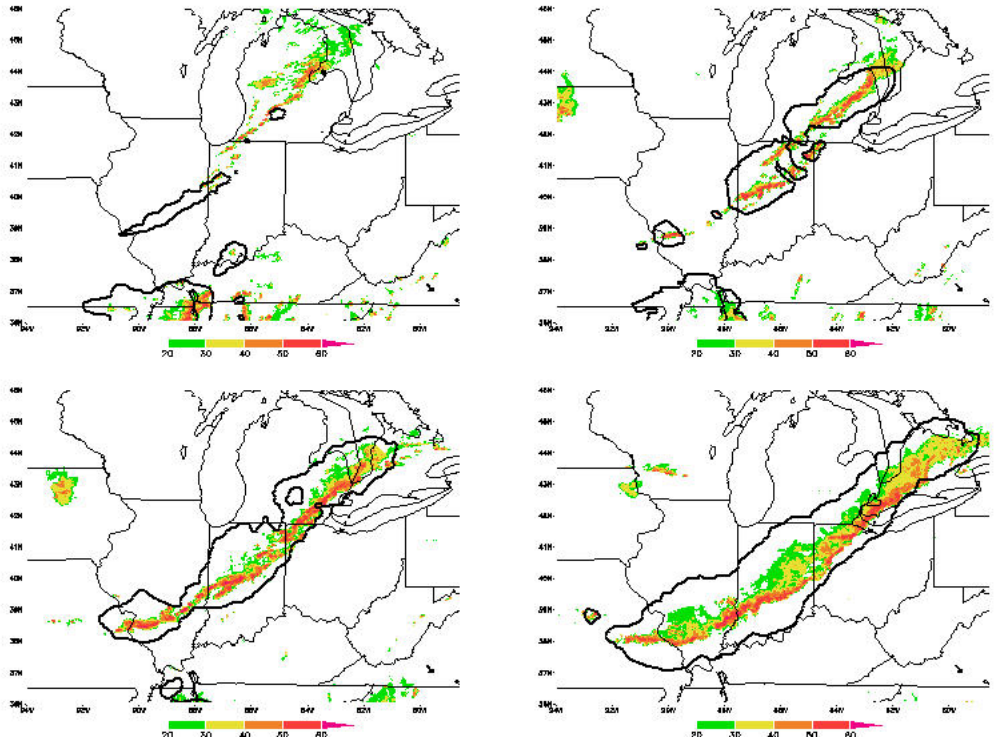

Figure 5.6: Line merger development of a PECS that occurred in the upper Midwest on June 21-22, 1997, as seen by radar imagery. The images are from 2000 UTC (top left), 2200 UTC (top right), 2315 UTC (bottom left), and 0100 UTC (bottom right). The solid black contours represent the outline of the $-52°$C cloud shield.

Embedded areal mergers were the next most common type of MCS development and will provide an example of the appearance of embedded systems in general. The example presented occurred in South Dakota on August 25, 1997. As seen in the upper left panel of Fig. 5.7 at 0100 UTC, the initial convection developed in a general area of

stratiform precipitation separating itself as an embedded system. Nearly three hours later, distinct convective clusters could be observed in central and western South Dakota (top right panel). By 0645 UTC (bottom left panel), the clusters had begun to merge and share an oblong cloud shield. The mature MβMCC at 1045 UTC can be seen in the lower right panel with a unique reflectivity arrangement and a highly organized circular cloud shield. Notice that the cloud shield of this system did not encircle the radar reflectivity echoes as well as the previous examples. This was a common feature of the embedded systems.

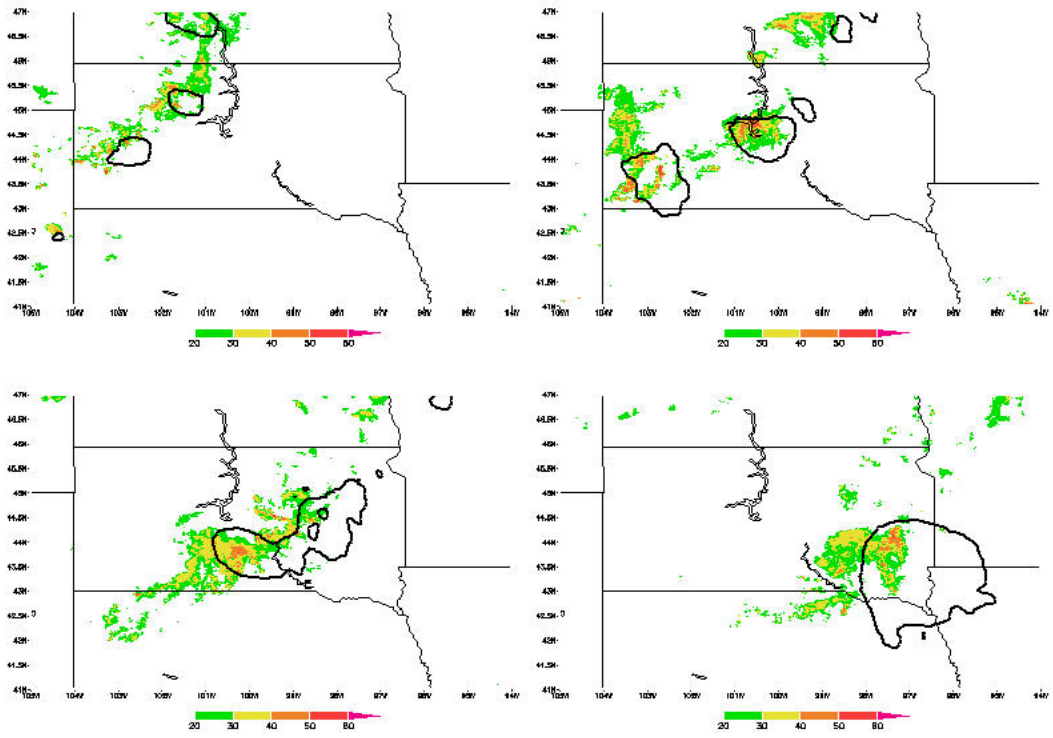

Figure 5.7: Embedded areal merger development of a MβMCC that occurred in South Dakota on August 25, 1997, as seen by radar imagery. The images are from 0100 UTC (top left), 0345 UTC (top right), 0645 UTC (bottom left), and 1045 UTC (bottom right). The solid black contours represent the outline of the -52°C cloud shield.

The final example of MCS development is an areal isolated system. This example will offer some idea of what these unique and interesting systems look like.

This particular MCS occurred on May 26-27, 1998, along a line east of the Rocky Mountains. Figure 5.8 shows that at 2045 UTC (top left panel), there was much scattered convection throughout Wyoming and Colorado. Even though there is a long stretch of convection, the individual convective cells are arranged in an areal fashion. The result was a line of areal clusters by 2245 UTC as seen in the upper right panel. Interaction occurred between these clusters as their cloud shields began to merge by 0045 UTC (bottom left panel). However, the convection itself did not merge resulting in isolated clusters sharing a common cloud shield. An image of this mature PECS taken at 0245 UTC can be seen in the lower right panel.

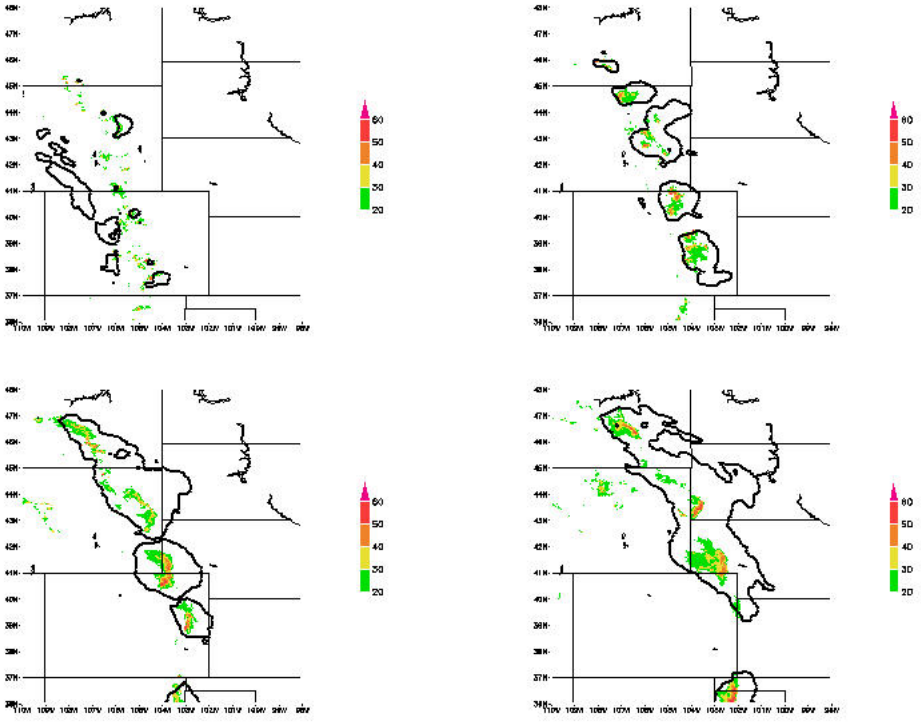

Figure 5.8: Areal isolated development of a PECS that occurred east of the Rocky Mountains on May 26-27, 1998, as seen by radar imagery. The images are from 2045 UTC (top left), 2245 UTC (top right), 0045 UTC (bottom left), and 0245 UTC (bottom right). The solid black contours represent the outline of the $-52°C$ cloud shield.

Chapter 6

MCS environment and severe weather

In addition to the analyses of the MCSs by satellite and radar data, the environment and severe weather production of each MCS were also analyzed. In an effort to learn something about the environmental differences, a sounding was selected as the most representative for each system as discussed in Section 3.4, and the soundings were grouped according to each system's satellite and radar classifications. Similarly, the severe weather reports were logged for each system to study the relationship between severe weather and the various MCS categories. The first section in this chapter discusses the average properties of individual soundings for each group of MCSs while the second section discusses the properties of the average soundings for each MCS category. Finally, the chapter will conclude with a discussion of the severe weather reports for each MCS classification.

6.1 Average properties of soundings

The average properties of the soundings for the entire MCS sample will be discussed first. Table 6.1 lists the average and standard deviation of some common environmental parameters for the entire sample. The average value of each of the

severe weather parameters (i.e. LI, SWEAT, KI, and TT (see Appendix)) indicate a moderate potential for thunderstorms (RAOB Program 1997). In addition, the average convective available potential energy (CAPE) is also of moderate value for convective storms, but keep in mind that this is the average of 387 MCSs. The average bulk Richardson number (BRN), which is a ratio of the amount of CAPE to the amount of shear in the lower troposphere (lowest 6 km for this case), was around 74, which Weisman and Klemp (1982, 1984, 1986) found to be a value favorable for the formation of multicell storms. Certainly, nearly every MCS in this sample was multicellular. Finally, the average precipitable water (PW) of more than 36 mm was relatively high for such a large sample.

Table 6.1: Average properties of soundings for the entire MCS sample. Means and (standard deviations).

Lifted Index (LI)	-4.1(3.9)
SWEAT Index	316(127)
K Index (KI)	32.0(8.3)
Total Totals Index (TT)	50.7(5.1)
Convective Available Potential Energy (CAPE) (J/kg)	1626(1189)
Convective Inhibition (CIN) (J/kg)	80(102)
Equilibrium Level (EL) (mb)	212(98)
Level of Free Convection (LFC) (mb)	741(98)
Bulk Richardson Number (BRN)	74.1(120.5)
Precipitable Water (PW) (mm)	36.7(10.9)

A few interesting relationships were found by producing scatter plots of the maximum area of each system against various parameters. Figure 6.1 shows that, in general, larger systems persist longer than shorter systems even though the relationship is not perfectly linear. The range of the Total Totals Index (TT) appears to shift

toward larger values while moving toward larger systems as seen in Fig. 6.2. In fact, the average TT of systems with a maximum size less than 200,000 km^2 is 50.1 with a standard deviation of 5.0 while systems with a maximum size greater than 200,000 km^2 had an average TT of 52.4 and a standard deviation of 4.9. Finally, the plot of maximum area against precipitable water produces a very interesting shape (Fig. 6.3). Notice that nearly all of the systems would fit within a triangle, which means that the spread of precipitable water values decreases with larger systems. Actually, the standard deviation decreases from 11.4 mm for systems smaller than 200,000 km^2 to 9.4 mm for systems larger than 200,000 km^2 indicating this "narrowing" of PW values for larger systems.

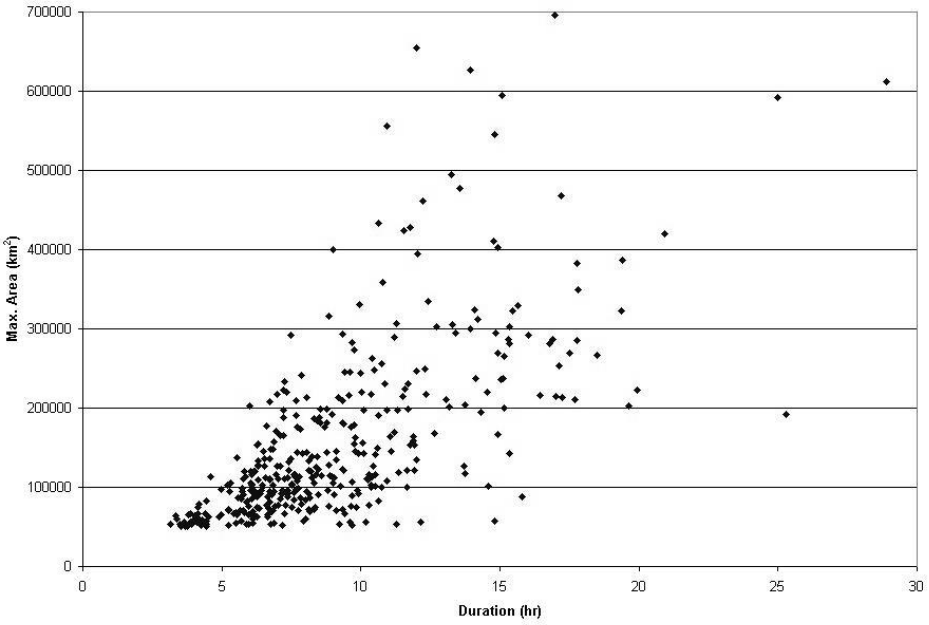

Figure 6.1: Scatter plot of maximum area against duration.

In order to investigate possible differences among the environments of different MCS categories, the averages of these sounding properties were also calculated for each classification. Table 6.2 shows the statistically significant sounding parameters for the MCS satellite classifications. The MβPECSs stood out from the other types of

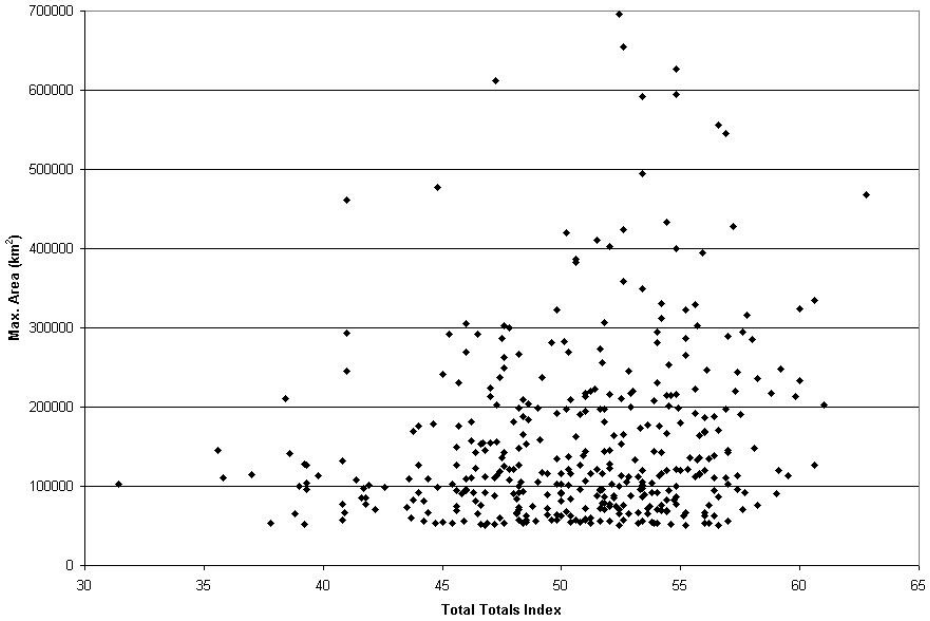

Figure 6.2: Scatter plot of maximum area against total totals index.

MCSs. These systems tended to occur in more stable environments shown by a higher LI and lower CAPE at the 95% confidence level. In addition, they had a lower average BRN than the other satellite categories at the same confidence level. The SWEAT index shows a statistical difference between the larger MCSs (MCCs and PECSs) and the smaller systems (MβMCC and MβPECS). At the 95% confidence level, the smaller MCSs have a lower SWEAT index than the larger systems. This indicates that the SWEAT index, which was created to help forecast tornadic thunderstorms by including wind shear in the calculation (see Appendix), may provide some information in predicting the maximum size of a MCS. Forty-three percent of the larger systems had a SWEAT index greater than 350 while only one-fourth of the smaller systems had a SWEAT index of 350 or greater.

In a similar manner, Table 6.3 contains average sounding properties for each classification of MCS development. There is a significant difference between the environments of embedded systems and those that do not form in areas of stratiform

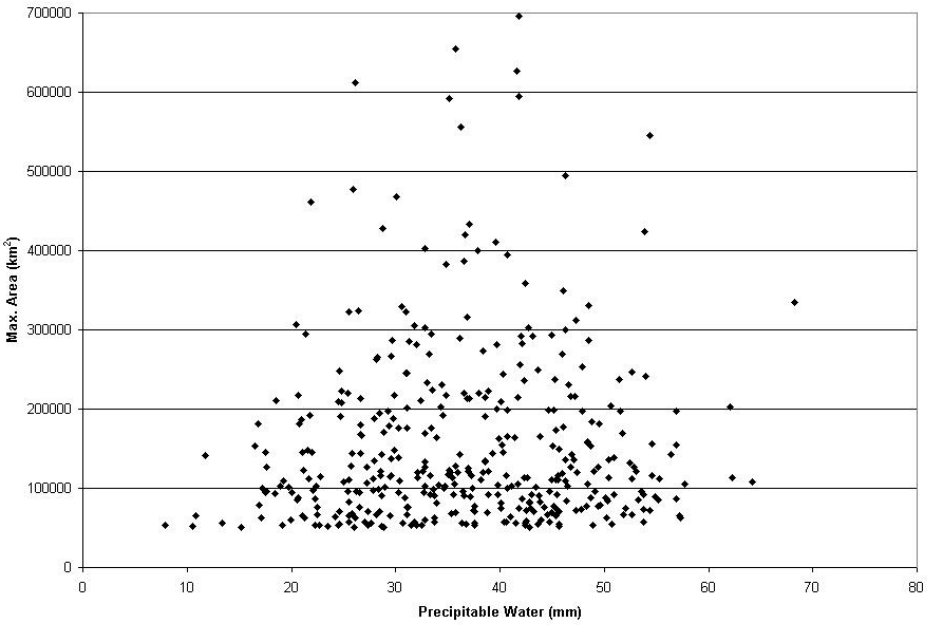

Figure 6.3: Scatter plot of maximum area against precipitable water.

precipitation. As expected, the environments of embedded systems are much more stable as shown by a higher LI and lower CAPE at greater than the 99% confidence level. In addition, embedded systems have a statistically (at the 95% level) lower average BRN and PW value. The sounding average differences are much less pronounced when dividing the systems according to their cell arrangement. The combination systems tended to form in slightly more unstable environments with a lower LI and a

Table 6.2: Sounding properties for each MCS satellite classification: means and (standard deviations).

Classification	LI	SWEAT	CAPE (J/kg)	CIN (J/kg)	BRN	PW (mm)
MCC	-4.3(3.7)	322(128)	1681(1059)	84(104)	79(129)	36.0(8.6)
PECS	-4.4(4.0)	339(132)	1769(1303)	70(100)	81(133)	37.2(11.2)
MβMCC	-4.5(2.8)	291(121)	1599(1159)	95(105)	79(105)	36.9(11.1)
MβPECS	-3.3(4.4)	288(112)	1332(1094)	80(99)	53(96)	36.3(12.4)

Table 6.3: Sounding properties for each MCS radar classification: means and (standard deviations).

Classification	LI	SWEAT	CAPE (J/kg)	CIN (J/kg)	BRN	PW (mm)
embedded	-1.9(5.5)	290(127)	1049(1078)	86(111)	52(111)	34.4(11.8)
not embedded	-4.6(3.2)	319(124)	1743(1175)	79(101)	79(123)	37.4(10.5)
line	-3.9(3.9)	360(129)	1536(1383)	86(99)	56(111)	36.4(12.2)
areal	-3.8(4.0)	291(119)	1559(1091)	78(99)	74(110)	36.9(11.0)
combination	-4.8(3.5)	330(126)	1783(1225)	82(110)	86(144)	37.0(9.7)
merger	-4.4(3.5)	318(125)	1661(1223)	82(105)	77(129)	36.7(10.5)
isolated	-4.0(2.7)	295(113)	1598(1037)	62(101)	77(96)	36.7(10.1)
growth	-3.3(5.2)	306(129)	1483(1106)	83(95)	66(99)	37.8(12.1)
unclassifiable	-4.0(5.0)	391(169)	1747(1333)	57(60)	58(71)	30.3(14.2)

higher CAPE. Line systems also had a statistically significant higher SWEAT index than areal systems, which follows the positive correlation between the SWEAT index and maximum size, since line systems were much larger systems than areal systems on average. Finally, there is even less difference among the average properties of the soundings when the systems are separated according to cluster interaction. The only statistically significant (at the 95% level) differences were the lower LI and higher CAPE for merger systems when compared to growth systems. Other than those parameters, the systems were statistically very similar.

Table 6.4: Properties of average soundings for each satellite classification.

Classification	LI	CAPE (J/kg)	CIN (J/kg)	BRN	PW (mm)
MCC	-4.2	1171	190	35	32.8
PECS	-5.4	1723	112	45	37.1
MβMCC	-5.0	1573	153	60	34.5
MβPECS	-3.5	771	169	19	30.7
All MCSs	-4.5	1263	187	36	36.3

6.2 Properties of average soundings

Another way to look at the sounding data is to take the actual temperature, moisture, and wind profiles from a group of individual soundings and combine them to form an average sounding. Figure 6.4 shows the average sounding for the entire MCS population while Figures 6.5-6.8 display the composite soundings for the various MCS satellite classifications. The temperature and dewpoint temperature profiles are plotted on the skew T/log P diagram along with the wind profile on the right side. In addition, the path of a parcel lifted from the surface is plotted, and the areas corresponding to CAPE and CIN have been shaded. Once again, the type of system that stands out is the MβPECS. These systems formed in much more stable environments than the other types of MCSs. Moreover, MCCs also appear to form in more stable environments when looking at the average sounding as opposed to the sounding averages. Table 6.4 provides a summary of the parameters from the average soundings that are plotted. When compared to Table 6.2, it appears that averaging the soundings has resulted in higher CIN, lower BRNs, and lower PW values.

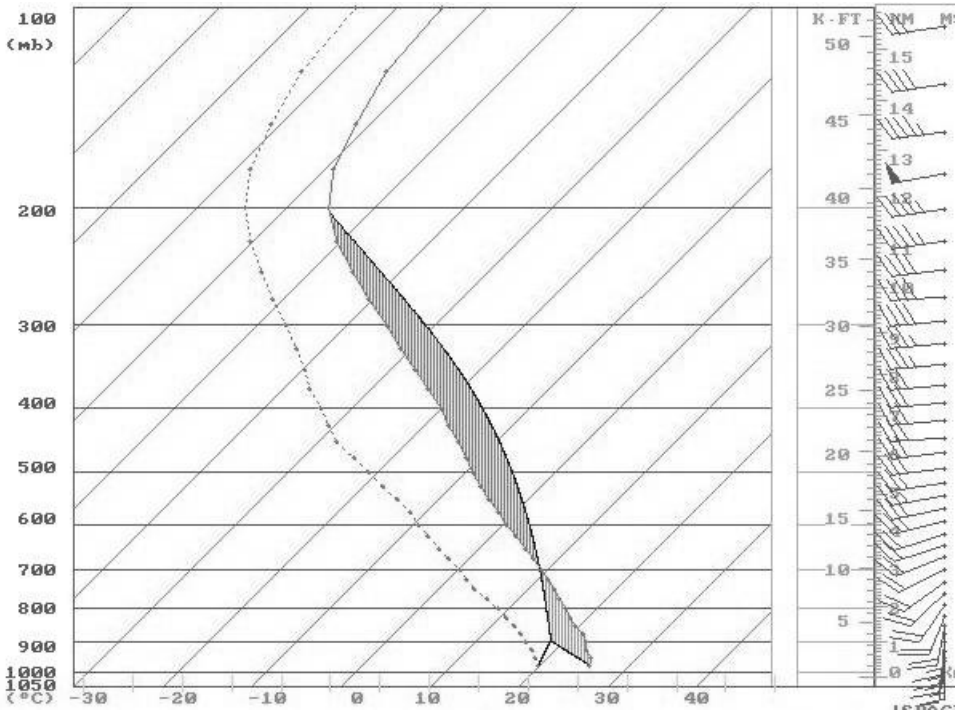

Figure 6.4: Mean sounding for all systems. The temperature, dewpoint, and winds are plotted with the CAPE and CIN shaded.

Figures 6.9-6.17 show the average soundings for the classes of radar development. As expected, there is a significant difference between the average soundings of embedded and unembedded systems. In fact, the CIN of the average sounding for embedded systems is larger than its CAPE indicating large stability. The average sounding for line systems is more unstable (lower LI and higher CAPE) than the average soundings for areal and combination systems, which was not the case when the parameters for the individual soundings were directly averaged. Likewise, the average sounding of the isolated systems also shows more instability than the averaged properties indicated. Also, note that the growth systems, which tended to develop into smaller systems, had a low BRN within the range of supercells found by Weisman and Klemp (1982, 1984, 1986). A summary of the properties of these average soundings is provided in Table 6.5.

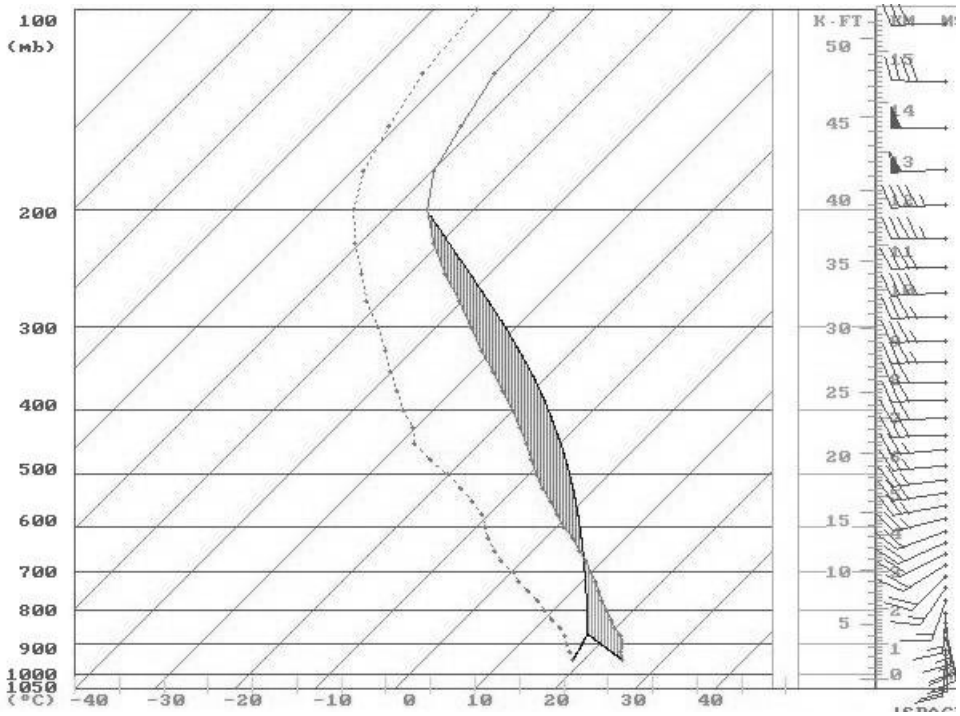

Figure 6.5: Same as Fig. 6.4 except for MCCs.

Examination of soundings did lead to some information about the environments of the MCSs. First of all, larger MCSs tended to last longer, have a higher range of the total totals index, have a higher SWEAT index, and have a more narrow range of precipitable water values. MβPECS formed in more stable environments (higher LI and lower CAPE) compared to the other types of MCSs, and the same can be said for embedded systems. The remainder of the development categories did not have distinguishable environmental characteristics, especially when comparing the averaged properties of the soundings to the properties of the averaged soundings.

6.3 Severe weather reports

The inspection of the stability parameters for these systems leads directly into the discussion of severe weather. MCSs are convective, of course, by definition, so one might expect severe weather from these systems, but do certain types of

Table 6.5: Properties of average soundings for each radar classification.

Classification	LI	CAPE (J/kg)	CIN (J/kg)	BRN	PW (mm)
embedded	-0.9	70	306	2	29.5
not embedded	-5.2	1613	169	48	37.6
line	-5.8	1858	76	39	34.3
areal	-4.2	1218	152	42	33.5
combination	-4.4	1189	228	31	37.1
merger	-4.2	1149	220	38	36.8
isolated	-5.3	1899	109	55	37.3
growth	-4.4	1157	107	23	31.8
unclassifiable	-1.1	189	296	6	31.5

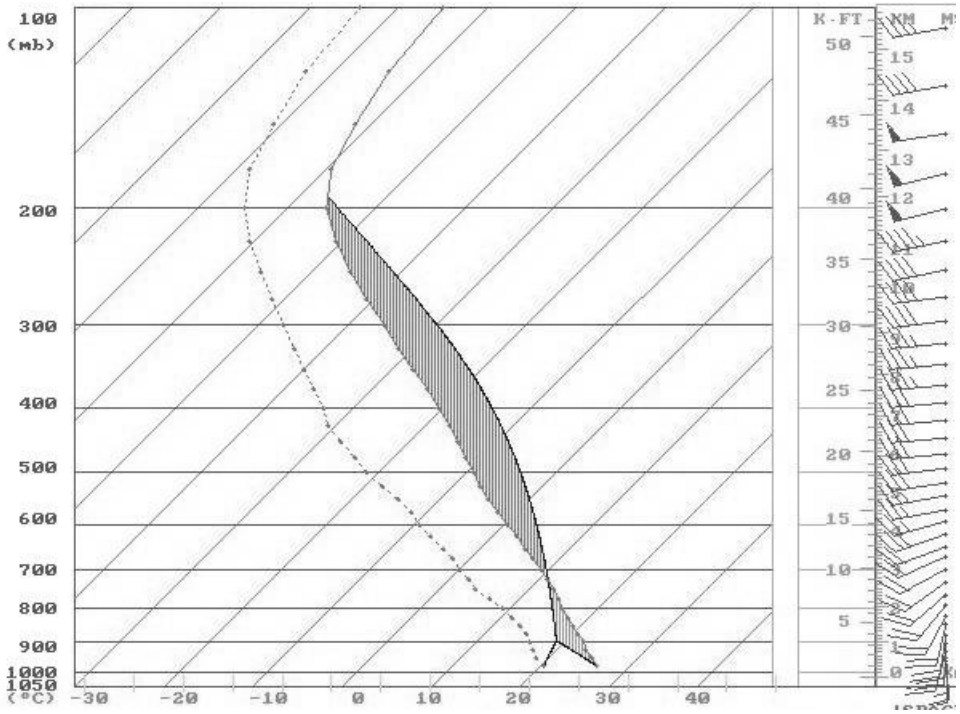

Figure 6.6: Same as Fig. 6.4 except for PECSs.

systems have a propensity to produce severe weather? Table 6.6 provides the total number of severe weather reports for tornadoes, hail, and wind as well as deaths and injuries for each satellite classification. To be reported as severe weather, a tornado must merely be present, hail must be 3/4" in diameter or larger, and winds must be measured at greater than 50 knots at the surface. Clearly, MCCs and PECSs accounted for most of the severe weather reports during the study period. These systems were also more common than the other types of MCSs, so Table 6.7 lists the number of reports *per MCS*. Even when the data are broken down in this manner, it is still obvious that severe weather was more common with MCCs and PECSs. These systems had more than 3 tornadoes and around 25 wind and hail reports per system. Whereas, the smaller systems (MβMCCs and MβPECSs) had many fewer severe weather reports per system with less than 1 tornado and about 8 wind and hail reports. This information reinforces the importance of PECSs on society due to their

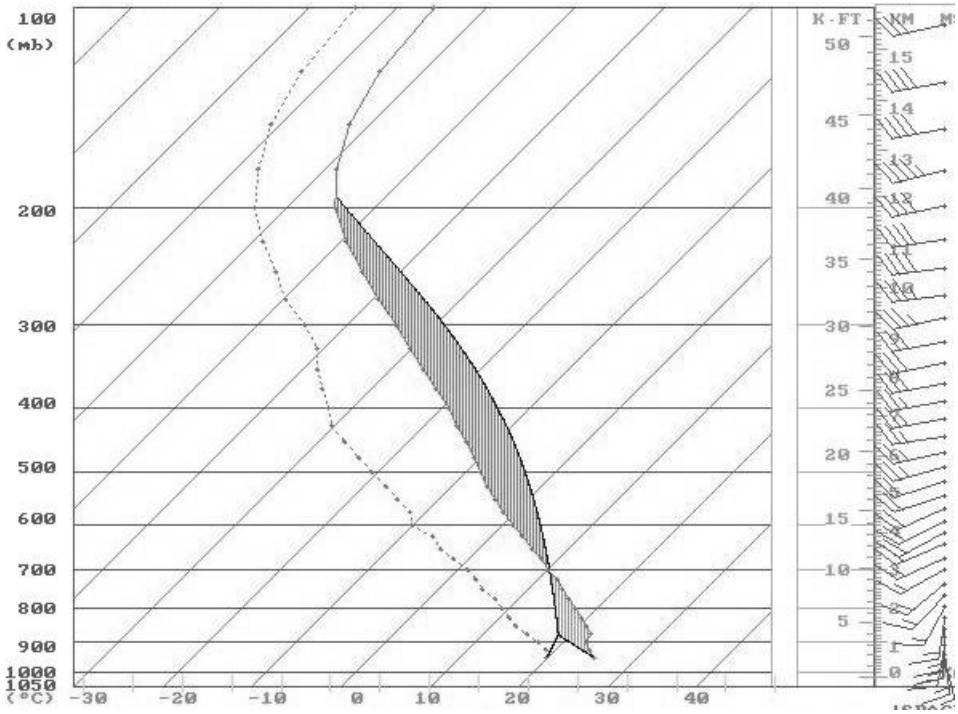

Figure 6.7: Same as Fig. 6.4 except for MβMCCs.

commonness and violent nature. More than half of all severe weather reports and almost 3/4 of the reported deaths and injuries were due to these systems even though the average severe weather indices did not show them to be significantly different from other types of MCSs.

In a similar fashion, the severe weather reports can be classified according to the development of each system to investigate the relationship between development and the occurrence of severe weather. Table 6.8 lists the total number of severe weather reports for each development category while Table 6.9 lists the number of reports per MCS to help interpret the frequency of severe weather for each level of radar development. Severe weather was much more frequent with systems that were not embedded. The areal systems also stand out as they generated significantly less severe weather as shown by the lower number of severe weather reports per MCS. This agrees with the findings of Bluestein et al. (1987) that broken areal squall lines

Table 6.6: Number of severe weather reports for each MCS satellite classification.

Classification	Tornadoes	Hail	Wind	Deaths	Injuries
MCC	248	2119	2075	2	154
PECS	567	4118	4165	12	533
MβMCC	33	375	455	0	12
MβPECS	53	780	759	2	50
All MCSs	901	7392	7454	16	749

Table 6.7: Number of severe weather reports per MCS for each satellite classification.

Classification	Tornadoes	Hail	Wind	Deaths	Injuries
MCC	2.8	23.5	23.1	0.02	1.7
PECS	3.8	27.6	28.0	0.1	3.6
MβMCC	0.5	5.8	7.0	0	0.2
MβPECS	0.6	9.4	9.1	0.02	0.6
All MCSs	2.3	19.1	19.3	0.04	1.9

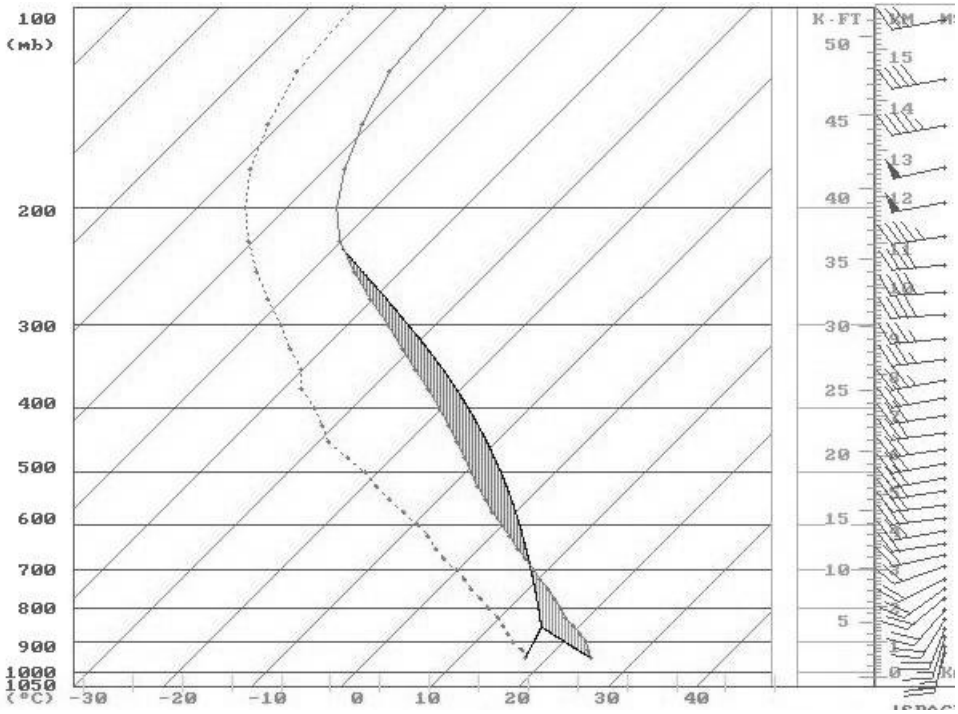

Figure 6.8: Same as Fig. 6.4 except for MβPECSs.

are the least likely development category to be associated with severe weather. Thus, knowing the arrangement of the initial convection may provide some information on the ability of the storm to produce severe weather. Also, note the high frequency of wind reports for the line systems, which is consistent with the bow echo relationship to derechos (Johns and Hirt 1987). Looking at the cluster interaction categories, the merger systems tended to have more severe weather reports than isolated and growth systems, but growth systems were extremely dangerous in their own right as noted by their high injury rate and relatively few severe weather reports.

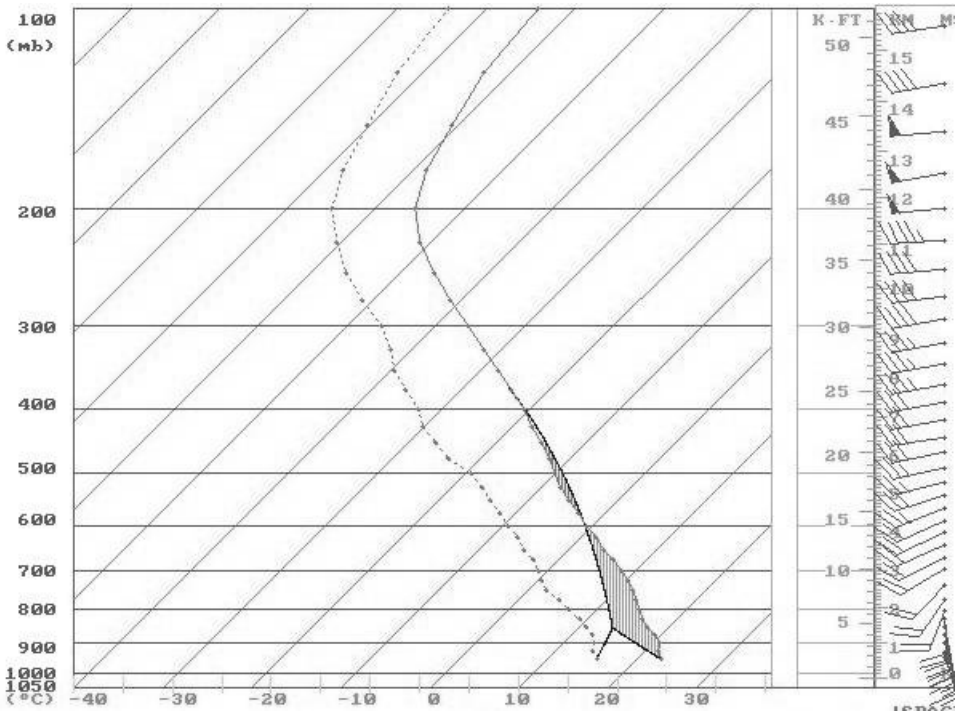

Figure 6.9: Same as Fig. 6.4 except for embedded systems.

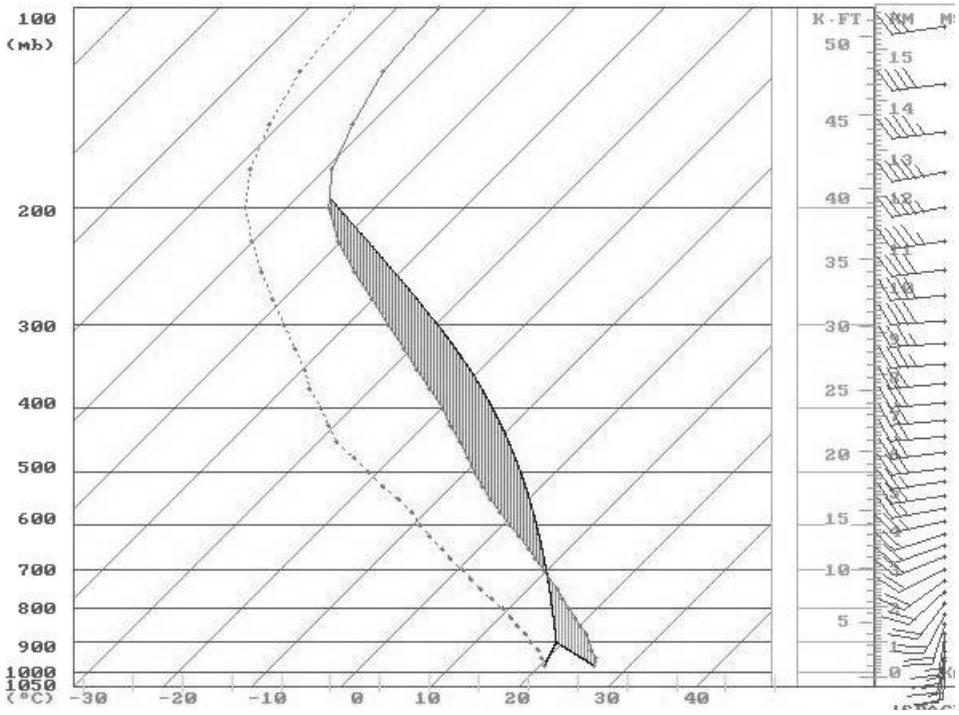

Figure 6.10: Same as Fig. 6.4 except for systems that were not embedded.

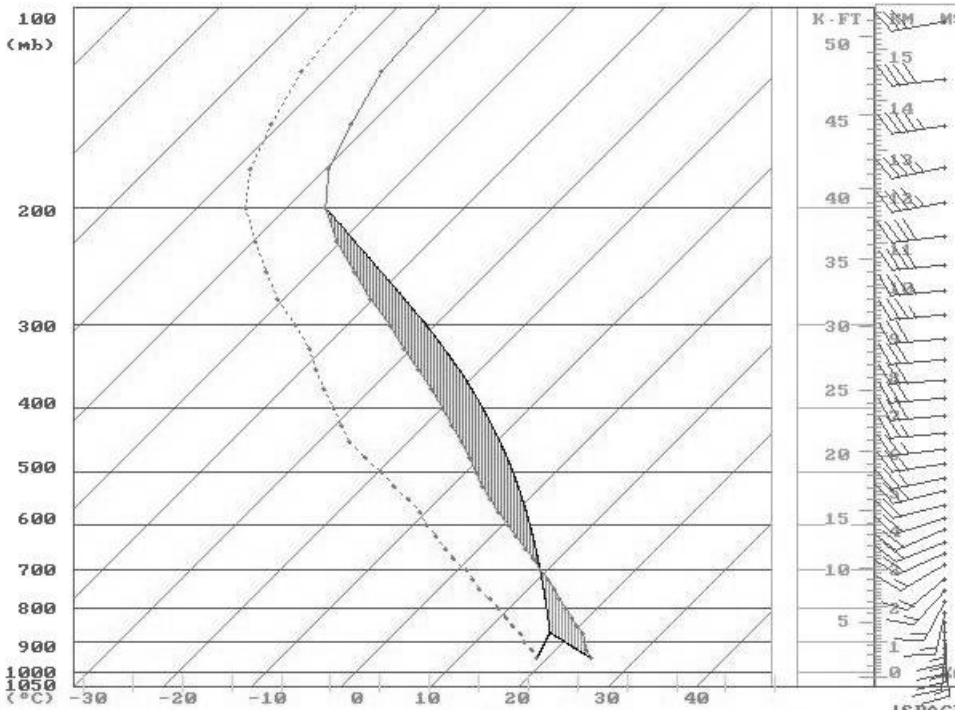

Figure 6.11: Same as Fig. 6.4 except for areal systems.

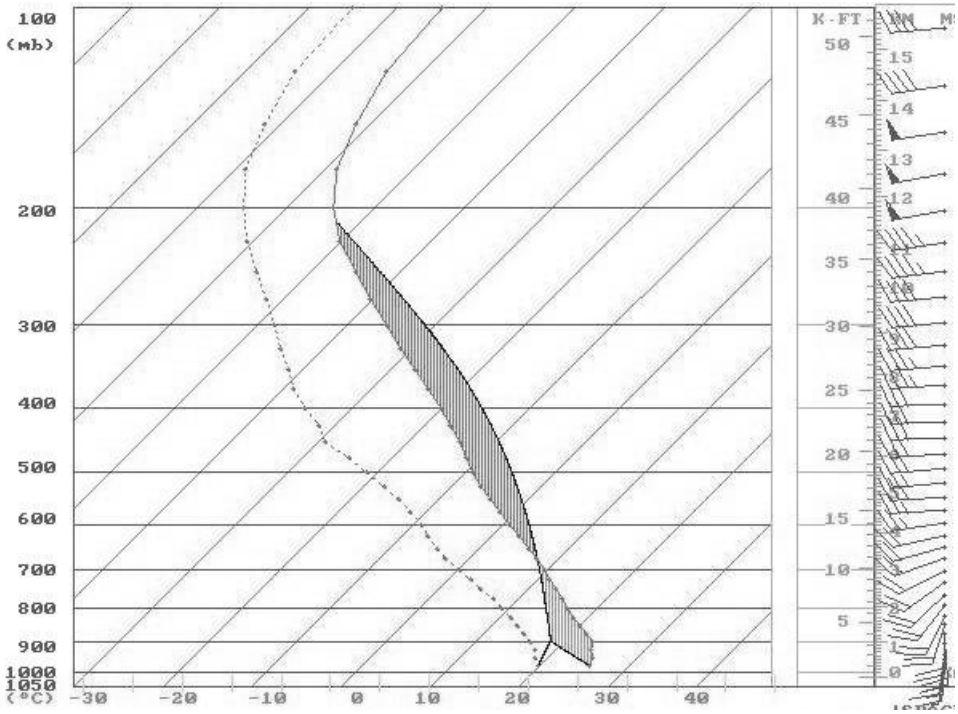

Figure 6.12: Same as Fig. 6.4 except for line systems.

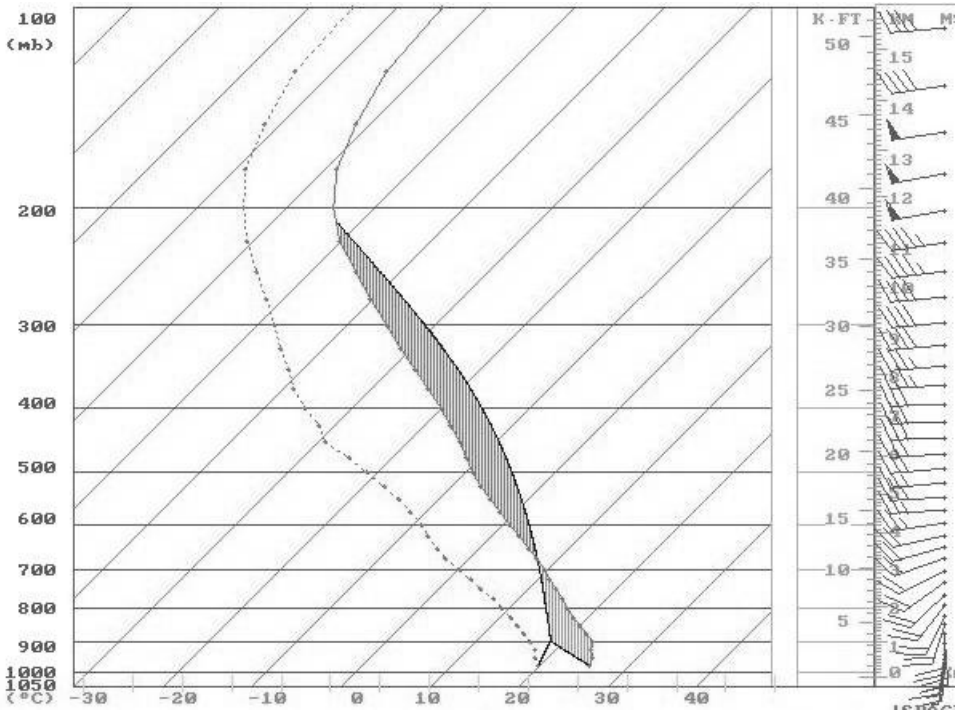

Figure 6.13: Same as Fig. 6.4 except for combination systems.

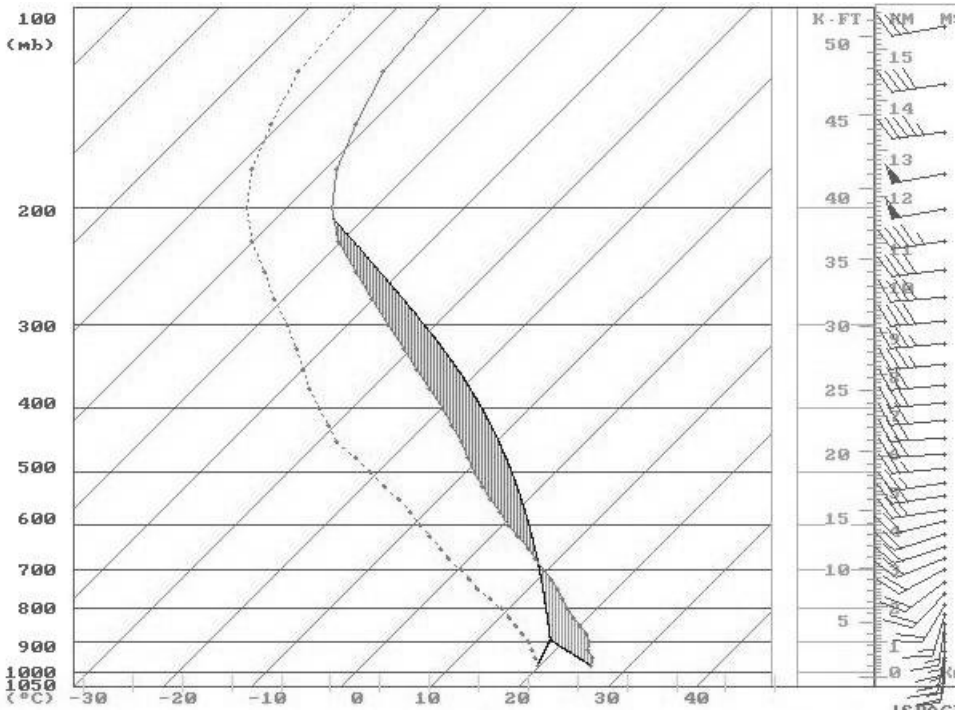

Figure 6.14: Same as Fig. 6.4 except for merger systems.

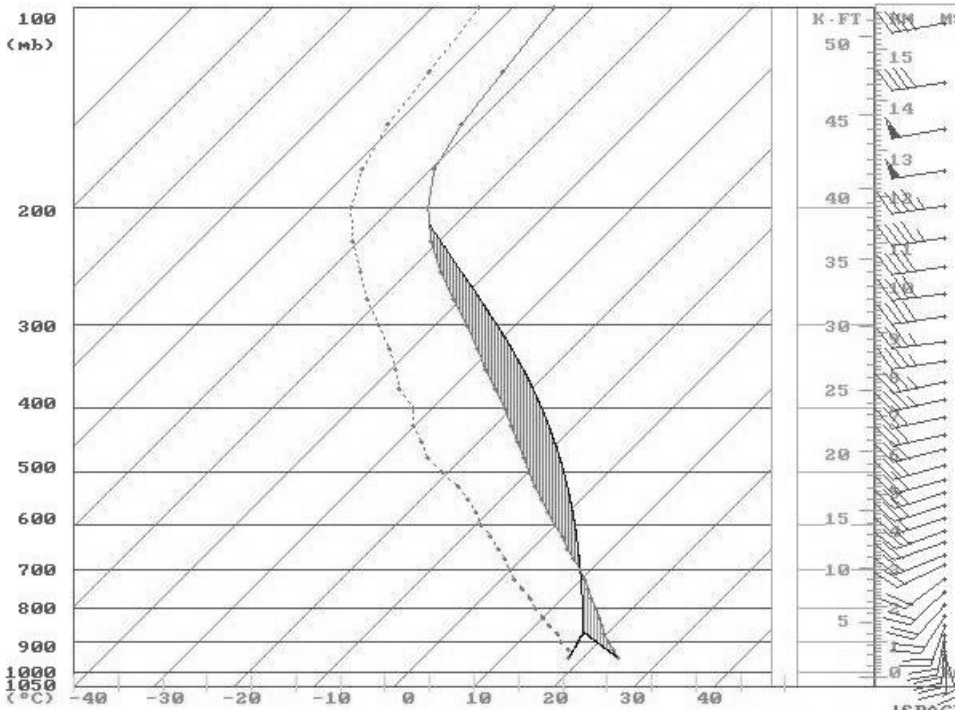

Figure 6.15: Same as Fig. 6.4 except for growth systems.

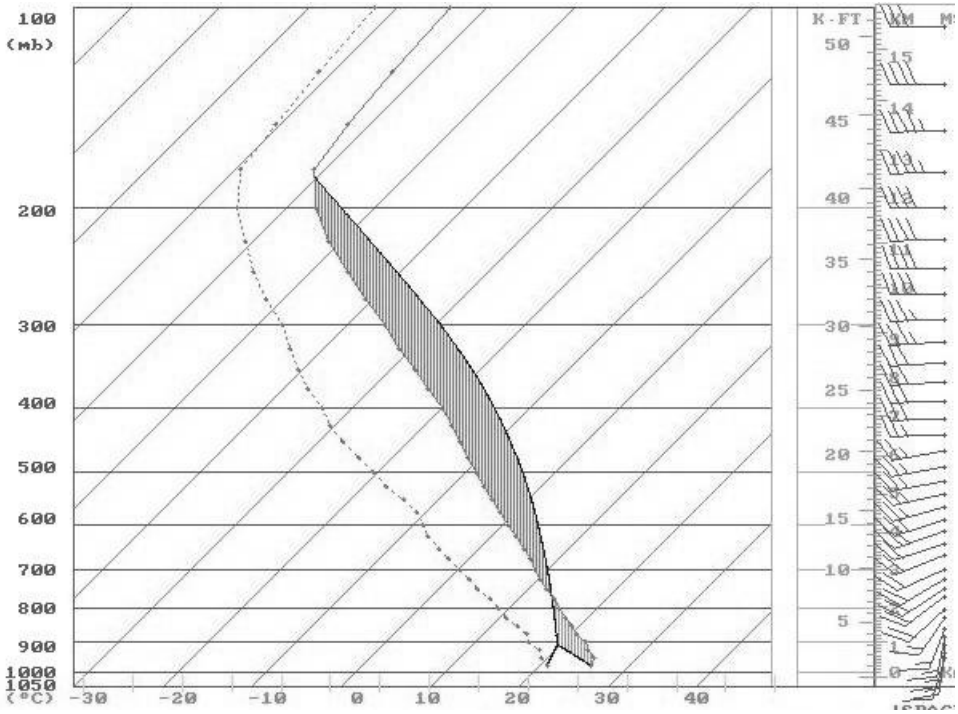

Figure 6.16: Same as Fig. 6.4 except for isolated systems.

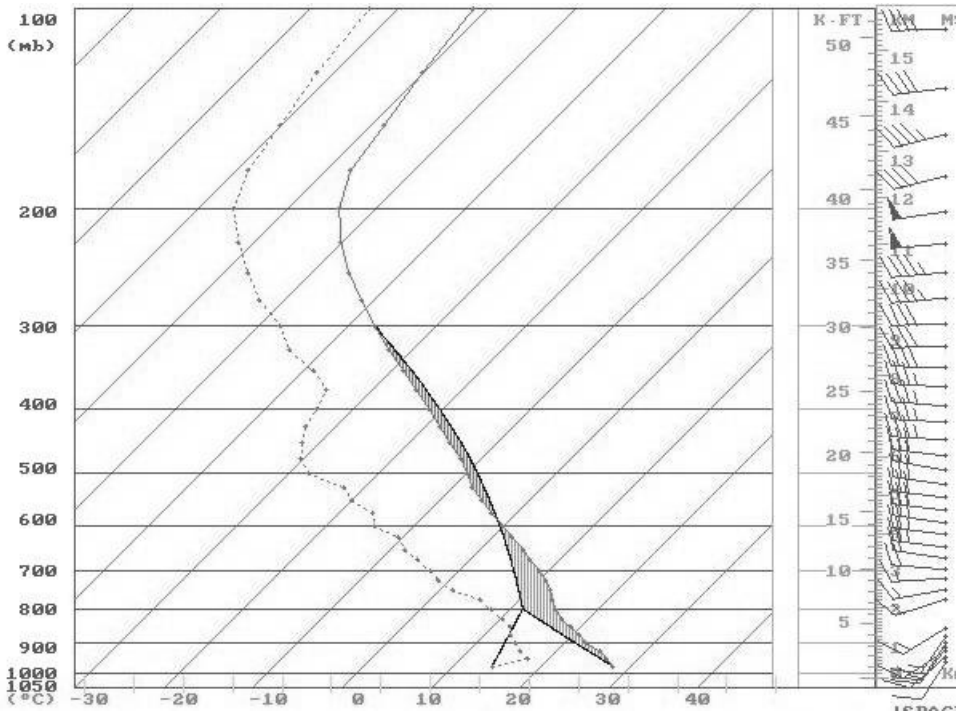

Figure 6.17: Same as Fig. 6.4 except for unclassifiable systems.

Table 6.8: Number of severe weather reports for each radar classification.

Classification	Tornadoes	Hail	Wind	Deaths	Injuries
embedded	64	736	792	0	33
not embedded	811	6452	6386	16	691
line	195	1510	2116	3	226
areal	269	2794	1929	1	113
combination	411	2884	3133	12	385
merger	696	5614	5729	14	491
isolated	59	531	414	0	29
growth	120	1043	1035	2	204
unclassifiable	26	204	276	0	25

Table 6.9: Number of severe weather reports per MCS for each radar classification.

Classification	Tornadoes	Hail	Wind	Deaths	Injuries
embedded	1.0	11.3	12.2	0	0.5
not embedded	2.6	20.7	20.5	0.05	2.2
line	3.1	24.0	33.6	0.05	3.6
areal	1.4	14.0	9.6	0.01	0.6
combination	3.6	25.3	27.5	0.1	3.4
merger	2.5	20.4	20.8	0.05	1.8
isolated	1.8	16.6	12.9	0	0.9
growth	1.7	14.9	14.8	0.03	2.9
unclassifiable	2.6	20.4	27.6	0	2.5

Chapter 7

MCS composite results

The composite products of the satellite and precipitation lifecycles are the last results to be analyzed for this MCS sample. Combining, or compositing, the lifecycles of the various MCS classifications allows for a general overview of each category's lifecycle. The systems were composited by normalizing the lifecycle of each system according to the time it was first classified as a MCS, its time of maximum extent, and the time when it no longer met the definition of a MCS. This normalization allows systems of all durations, growth rates, and decay rates to be composited. In the first section, the MCS tracks are reviewed for each category looking for any geographical biases. Then, the satellite lifecycle composites for each class will be discussed. Finally, the chapter will conclude with an examination of the rainfall lifecycle of each MCS category.

7.1 MCS tracks

Plotting the MCS tracks on a map allows for the investigation of possible geographical preferences for the formation of certain types of MCSs. Figures 7.1-7.13 display the MCS tracks of the various satellite and radar classifications. Some of these

plots are very messy due to the large volume of systems studied. In a way, the amount of "noise" in an area corresponds to higher MCS frequency. For those categories with a fewer number of MCSs, it might be possible to read the system number, which is positioned along the system track at the time of maximum extent. Figure 7.1 shows the tracks of all of the systems, and nearly all of the systems formed to the east of the Rocky Mountains with a fairly even north-south distribution of systems. Figures 7.2 and 7.3 show the tracks of MCCs and PECSs. It appears that the highest frequency of PECS formation was to the east of the MCC maximum, and indeed the average initiation of PECSs was more than 100 km east of the average initiation of MCCs. This agrees with Anderson and Arritt (1998) who also found that PECSs initiated and developed further east than MCCs. MβMCCs and MβPECSs (Figs. 7.4-7.5) do not appear to have a geographical preference of formation.

The remaining figures (Figs. 7.6-7.13) show the MCS tracks for the levels of radar development. Embedded systems tended to form in the very central part of the United States while there was much more activity east of Iowa and Missouri for systems that were not embedded (see Figs. 7.6-7.7). Systems that developed in the southern portion of the United States showed a strong inclination of having an areal arrangement of convective cells as seen in Figures 7.8-7.10. The initiation of areal systems was nearly 150 km south of the initiation of line and combination systems on average. Finally, looking at the systems distinguished by cluster interaction (Figs.7.11-7.12), it appears that a relatively high fraction of systems in Texas were growth, or single cluster, systems.

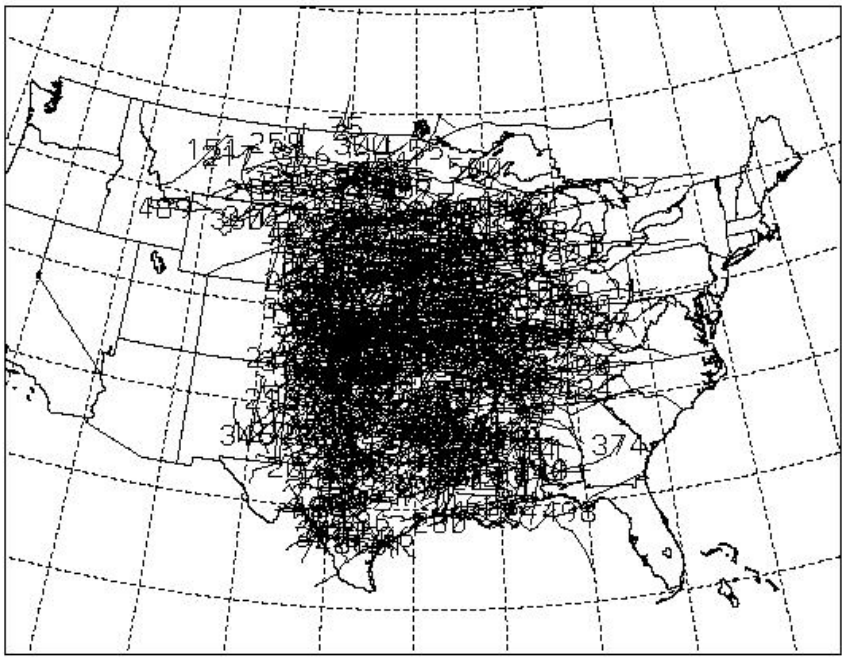

Figure 7.1: Plot of MCS tracks for all systems.

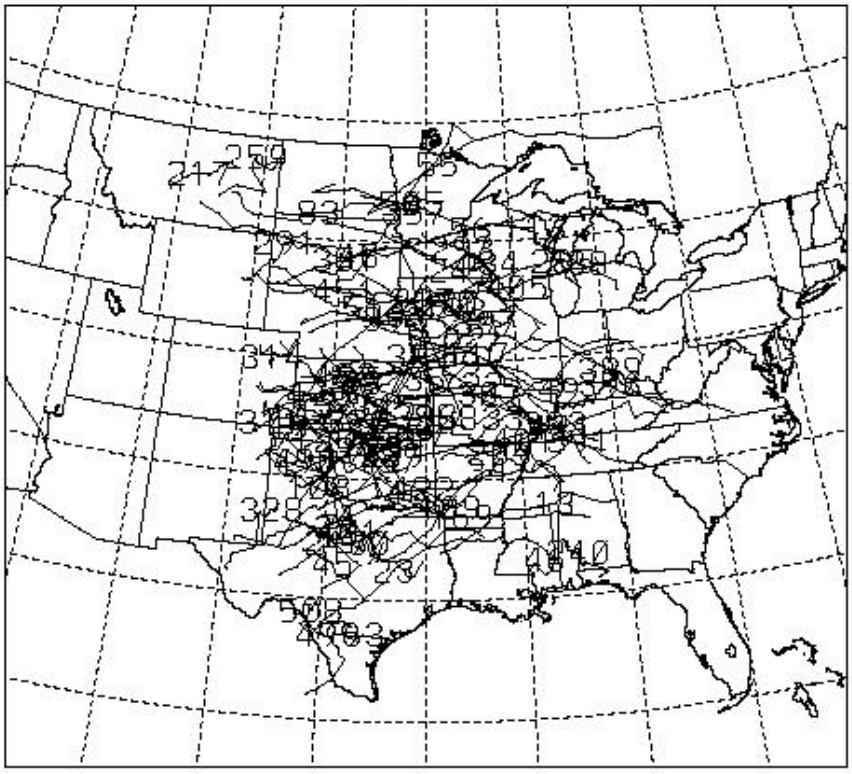

Figure 7.2: Plot of MCC tracks.

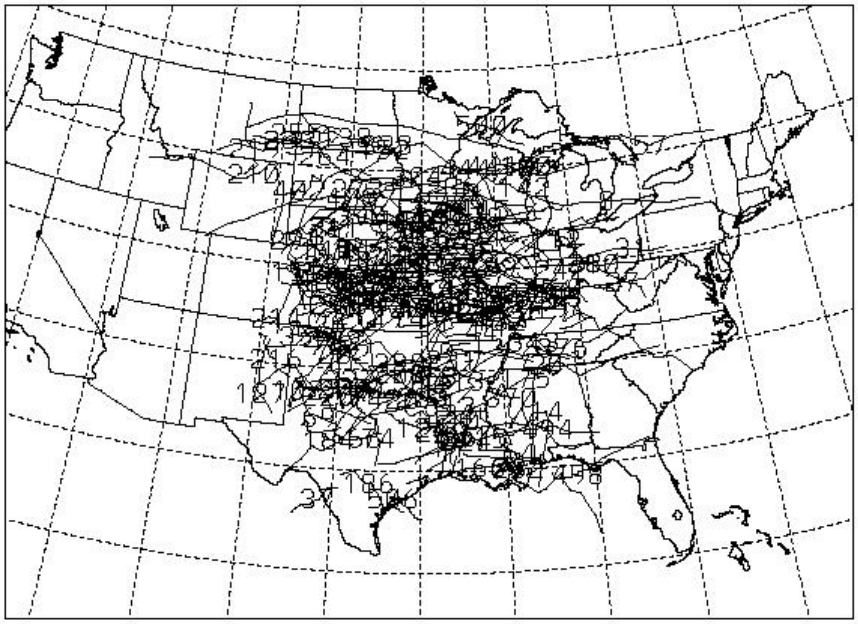

Figure 7.3: Plot of PECS tracks.

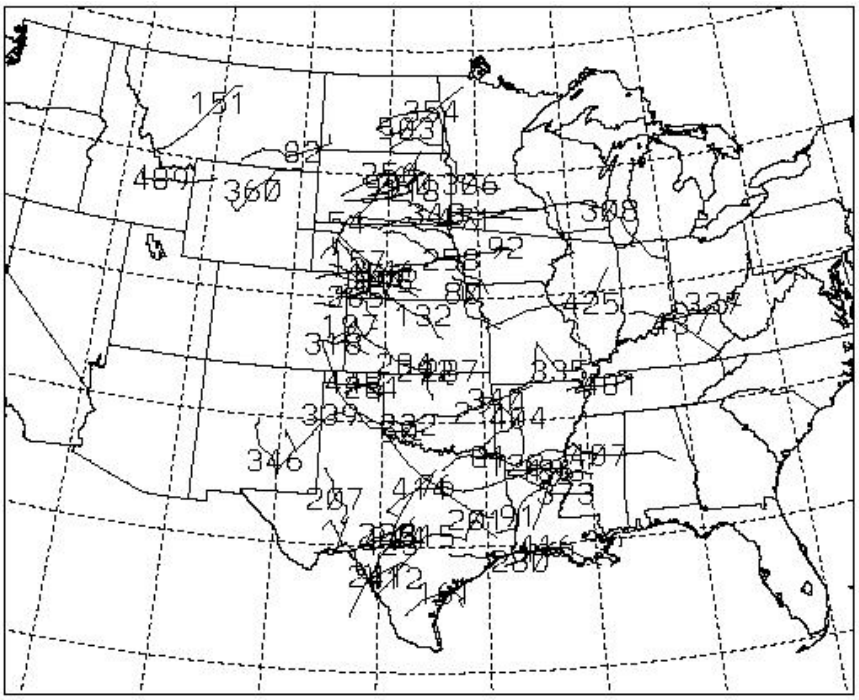

Figure 7.4: Plot of MβMCC tracks.

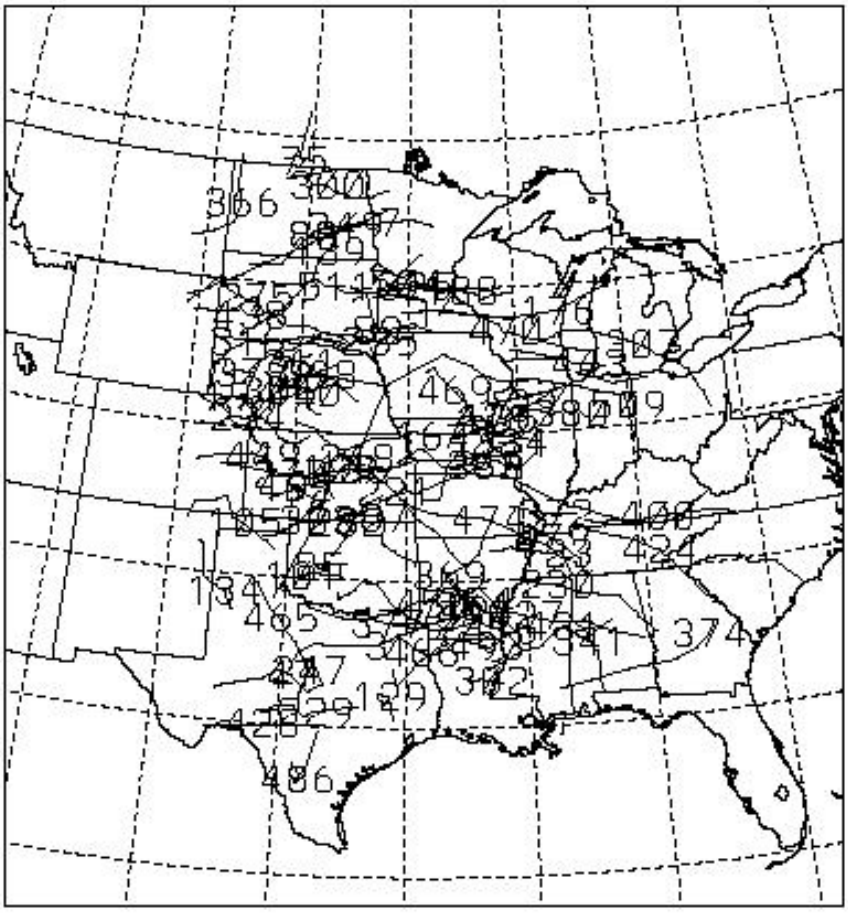

Figure 7.5: Plot of MβPECS tracks.

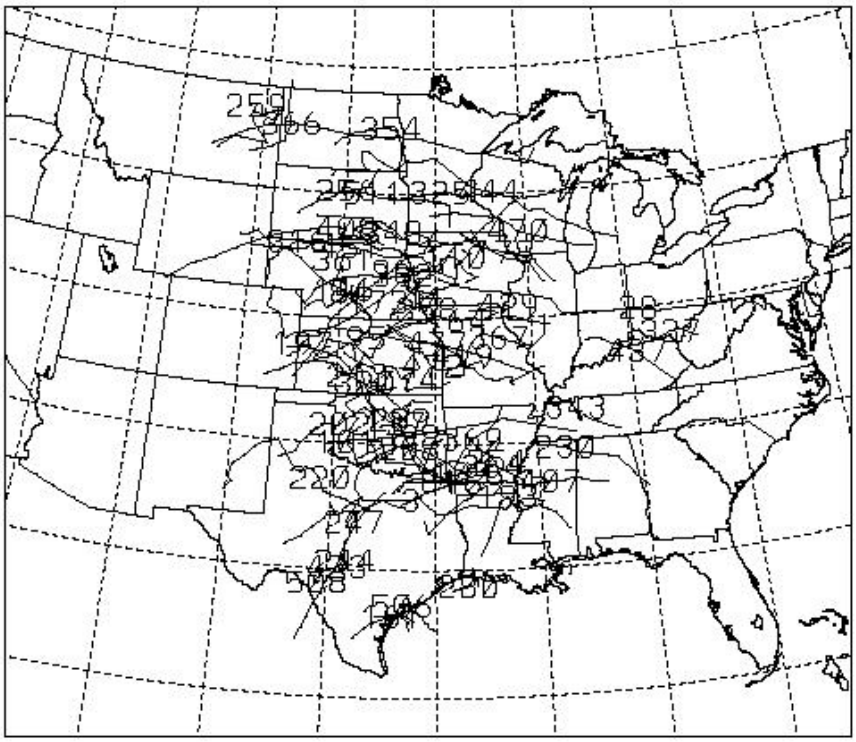

Figure 7.6: Plot of MCS tracks for embedded systems.

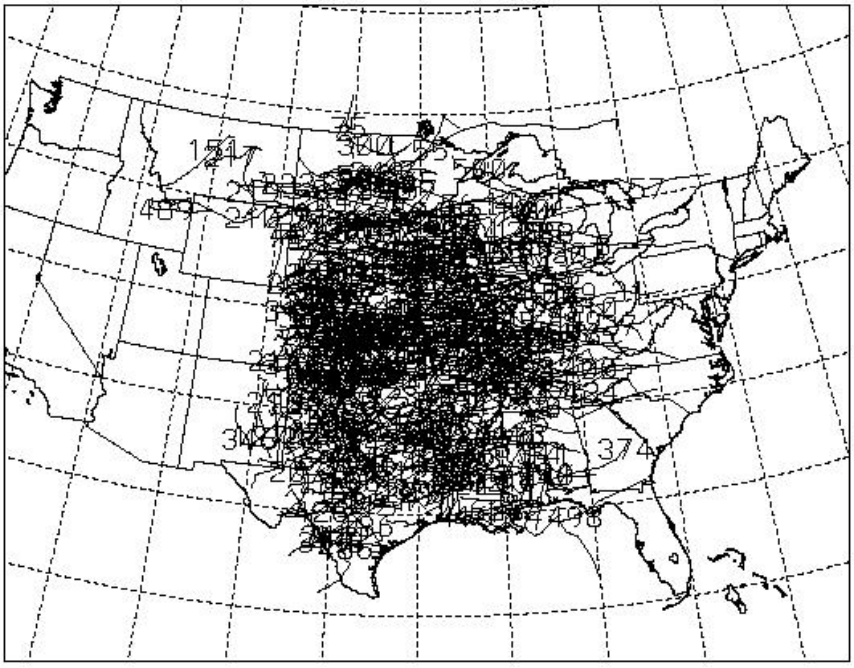

Figure 7.7: Plot of MCS tracks for systems that were not embedded.

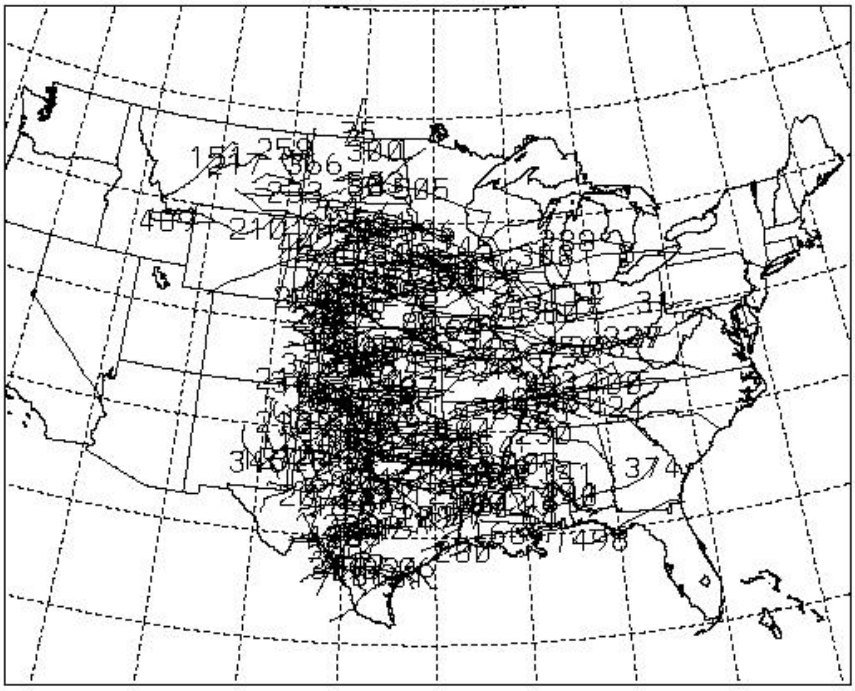

Figure 7.8: Plot of MCS tracks for areal systems.

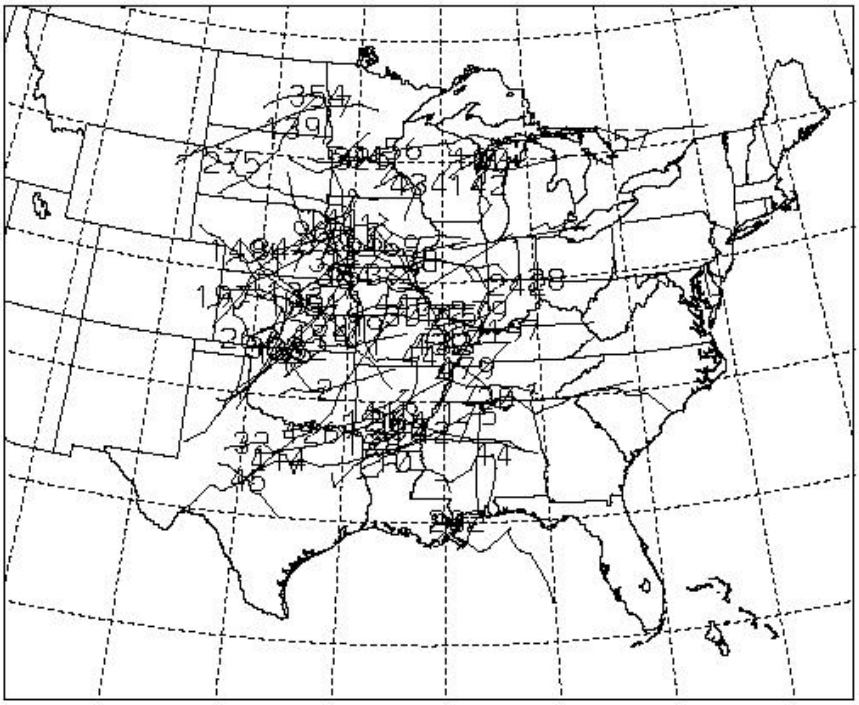

Figure 7.9: Plot of MCS tracks for line systems.

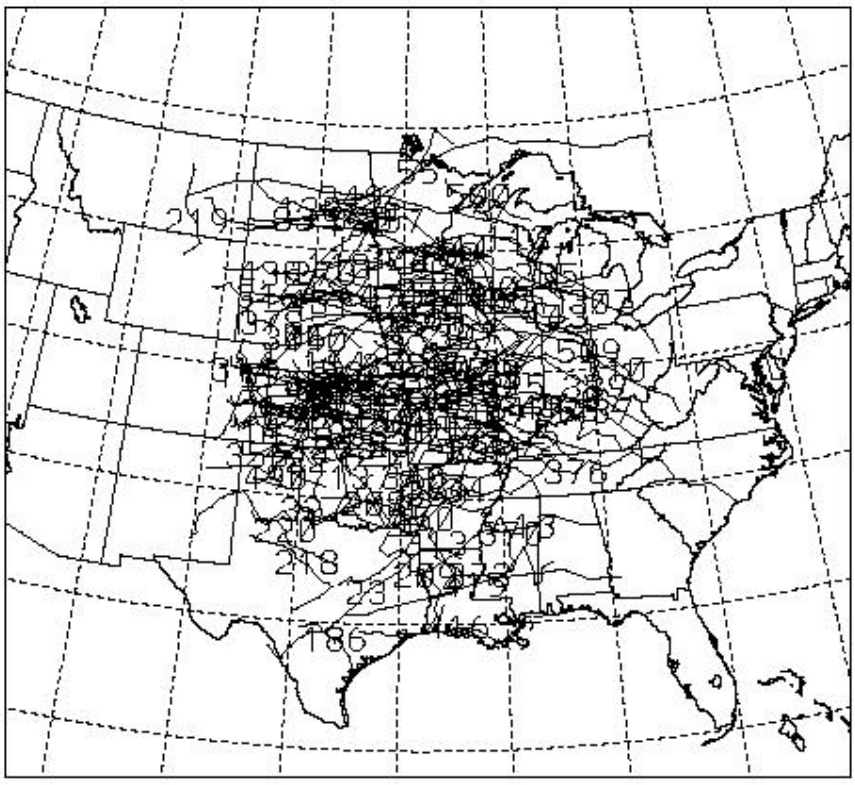

Figure 7.10: Plot of MCS tracks for combination systems.

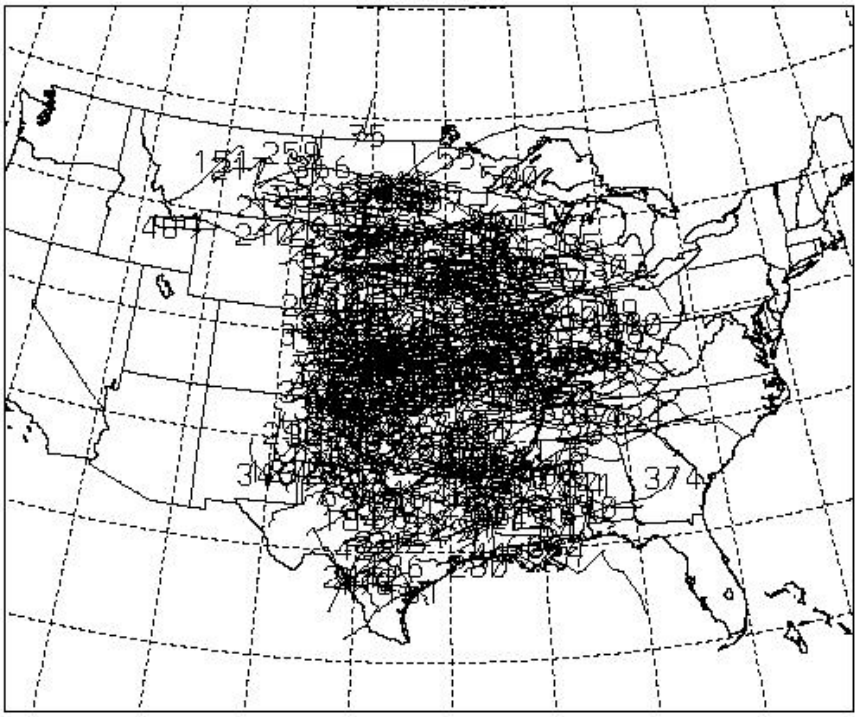

Figure 7.11: Plot of MCS tracks for merger systems.

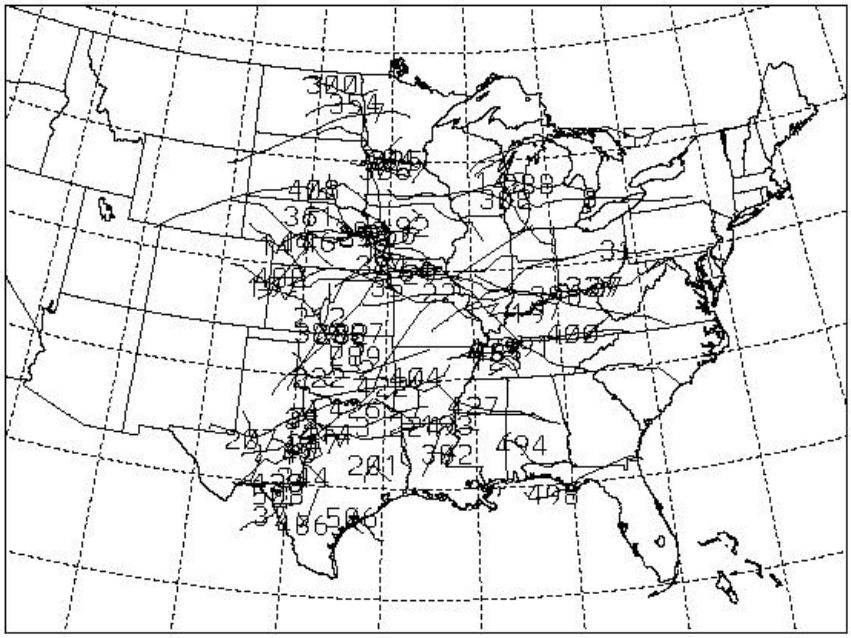

Figure 7.12: Plot of MCS tracks for growth systems.

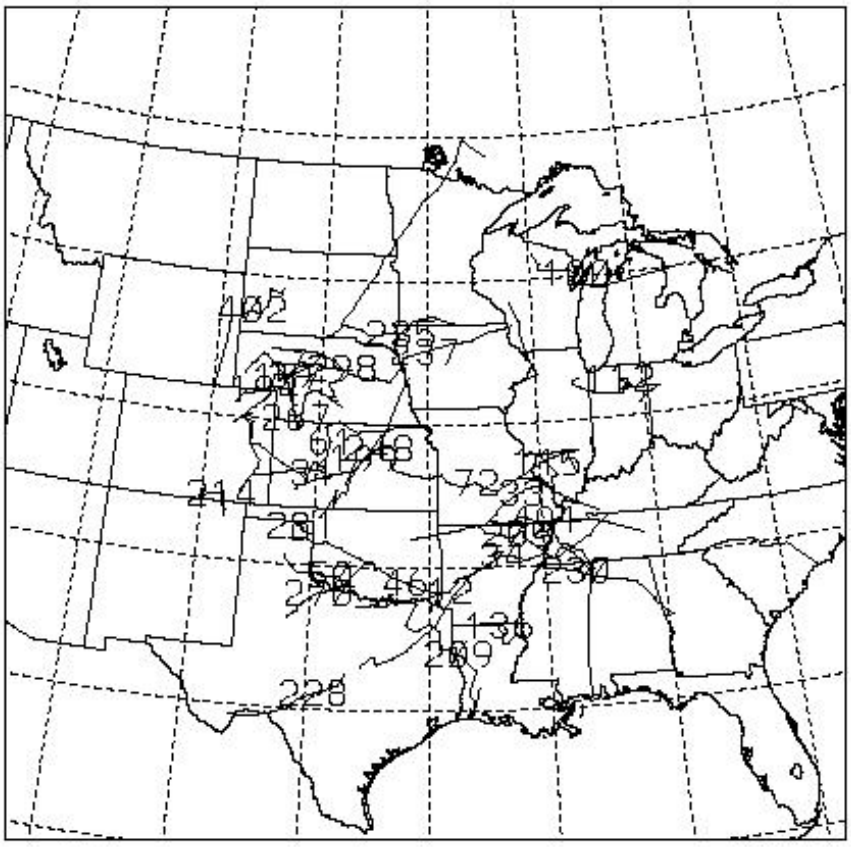

Figure 7.13: Plot of MCS tracks for isolated systems.

7.2 MCS satellite lifecycle

As mentioned previously, the lifecycles of the systems were composited by normalizing the MCS timescale. This allowed the areas at the −52°C, −58°C, −64°C, and −70°C blackbody temperature thresholds to be summed together at each normalized MCS time in order to create a composite lifecycle. Figures 7.14-7.26 show these composites for each MCS classification. In these figures, the areas of the aforementioned IR temperature thresholds are plotted against the MCS timescale with "00" representing the time when the systems first met their MCS definition. A vertical line is also used here to demarcate the beginning of the systems. The middle vertical line indicates the maximum time of the composite; thus, the period between these first two lines represents the growth stage of the systems. The vertical line on the right signifies the end of the systems, so the period between the second two lines represents the decay stage of the systems.

In reviewing Figs. 7.14-7.26, it is apparent that the satellite lifecycles of each MCS category are very similar. The primary differences among them include the length of the cycles and the size of the systems. Otherwise, the shapes and features of each composite are very much alike. One feature in all of the plots is that the areas of colder temperature thresholds reached a maximum before the warmer thresholds. For example, the composite figures show that the area of the −58°C cloud shield peaked before the −52°C area reached a maximum. In addition, the growth stage of MCSs lasted longer than the decay stage. In general, it took about one-half hour longer for a MCS to grow from its initiation to maturity than to dissipate from maturity to termination.

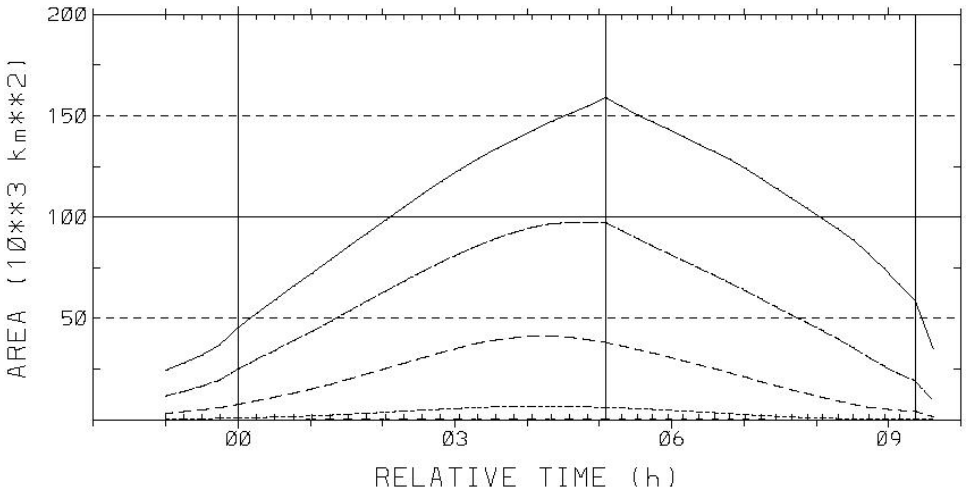

Figure 7.14: Infrared satellite lifecycle composite for all systems. Curves represent the areas of the $-52°C$, $-58°C$, $-64°C$, and $-70°C$ blackbody temperature thresholds. Vertical lines represent start, max, and end times.

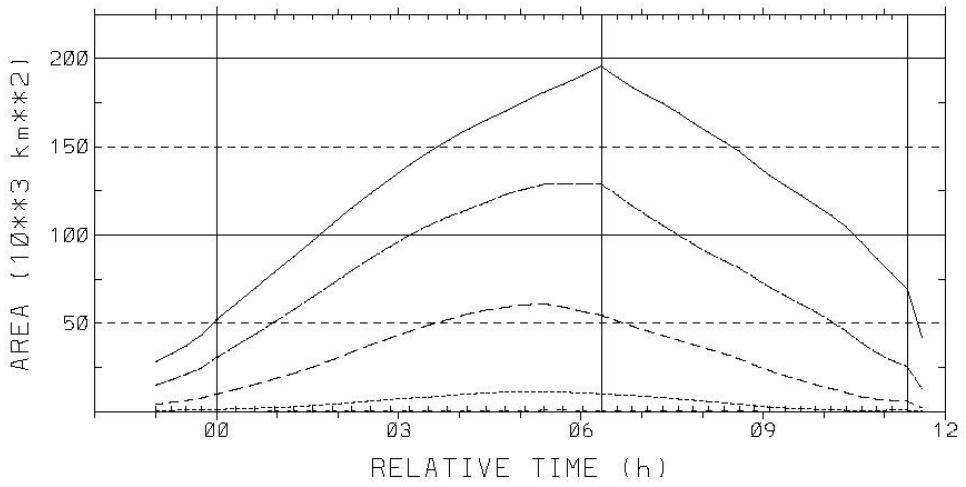

Figure 7.15: Same as Fig. 7.14 except for MCCs.

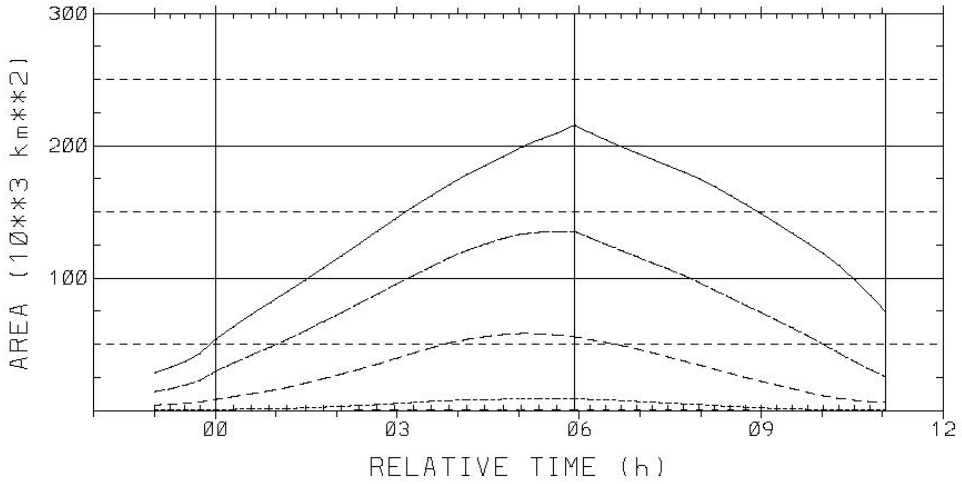

Figure 7.16: Same as Fig. 7.14 except for PECSs.

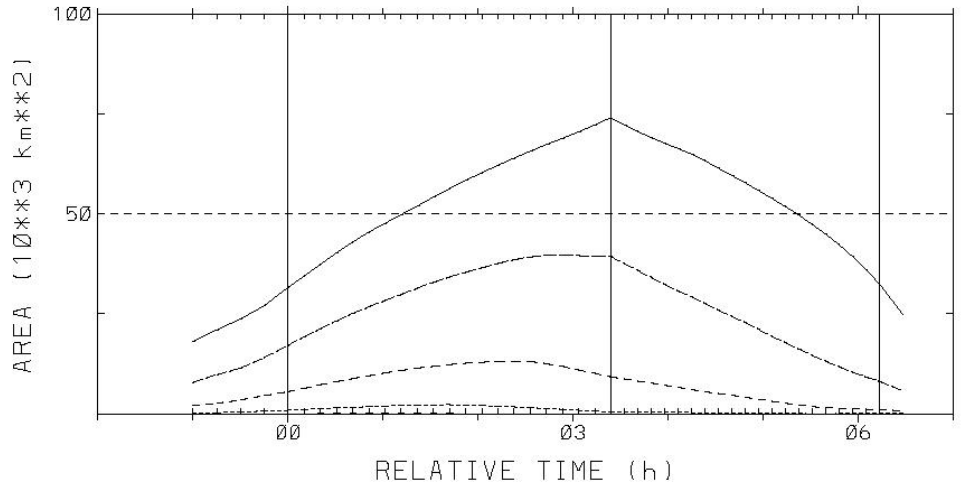

Figure 7.17: Same as Fig. 7.14 except for MβMCCs.

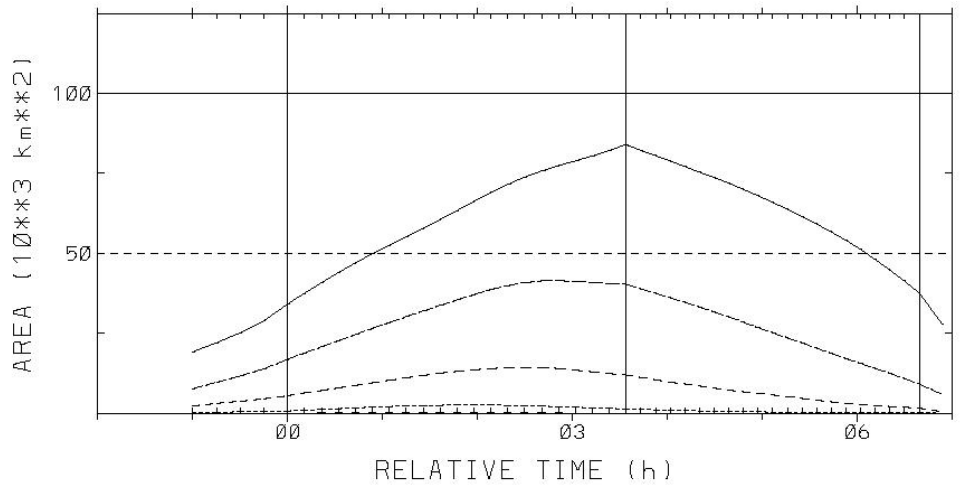

Figure 7.18: Same as Fig. 7.14 except for MβPECSs.

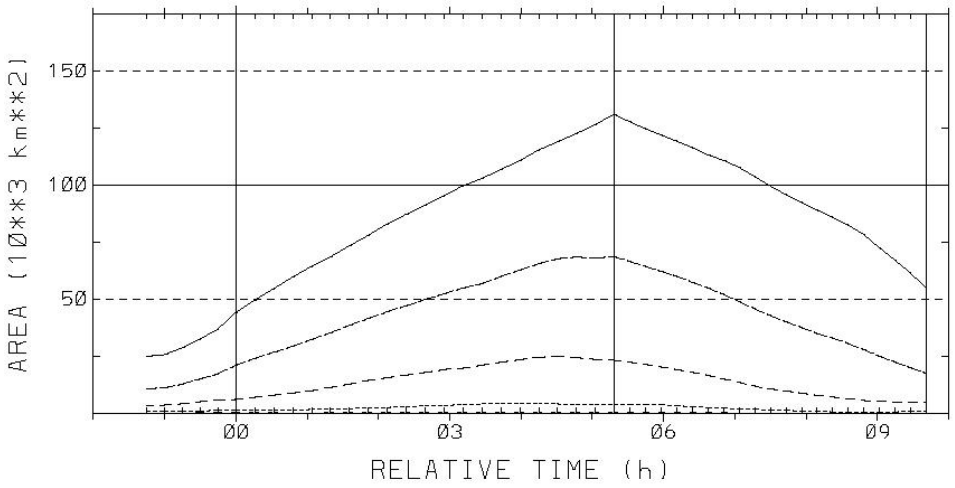

Figure 7.19: Same as Fig. 7.14 except for embedded systems.

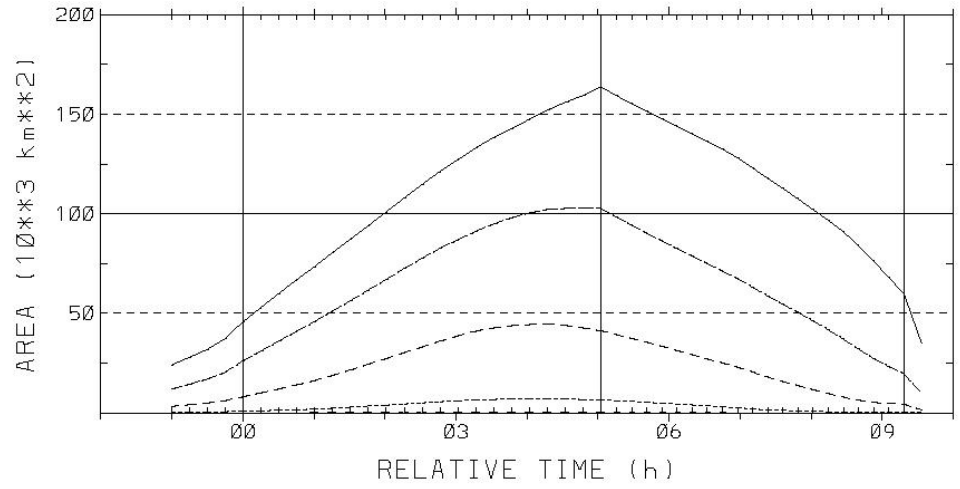

Figure 7.20: Same as Fig. 7.14 except for systems that were not embedded.

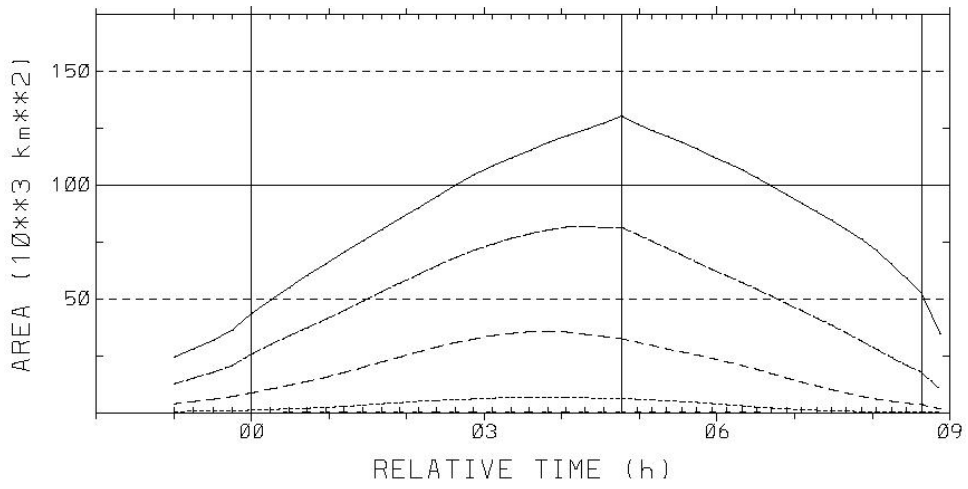

Figure 7.21: Same as Fig. 7.14 except for areal systems.

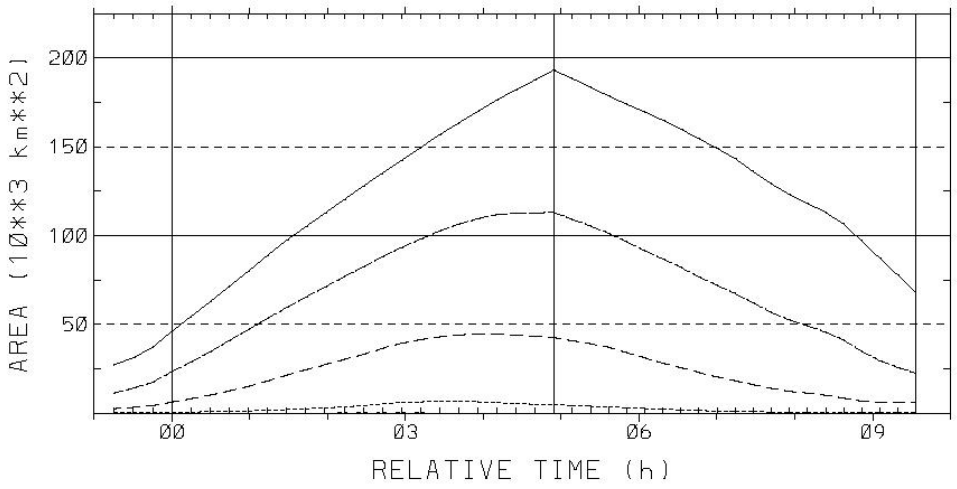

Figure 7.22: Same as Fig. 7.14 except for line systems.

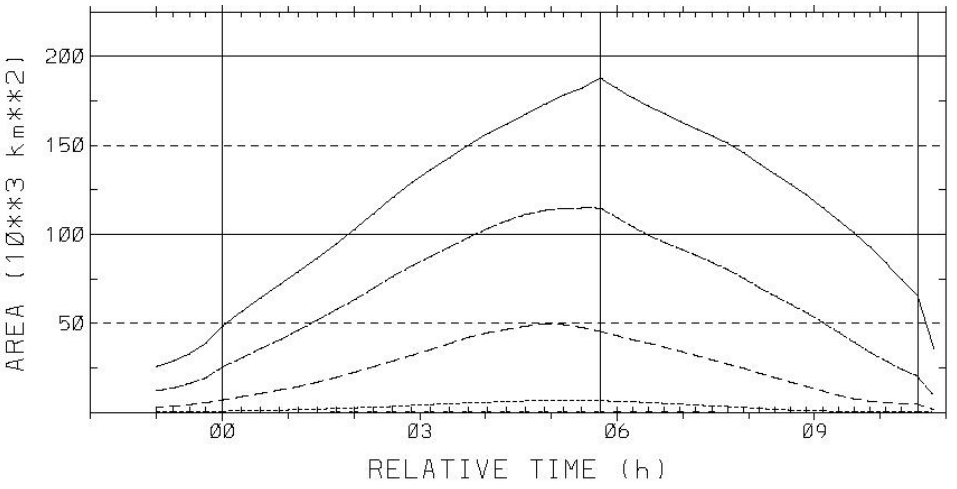

Figure 7.23: Same as Fig. 7.14 except for combination systems.

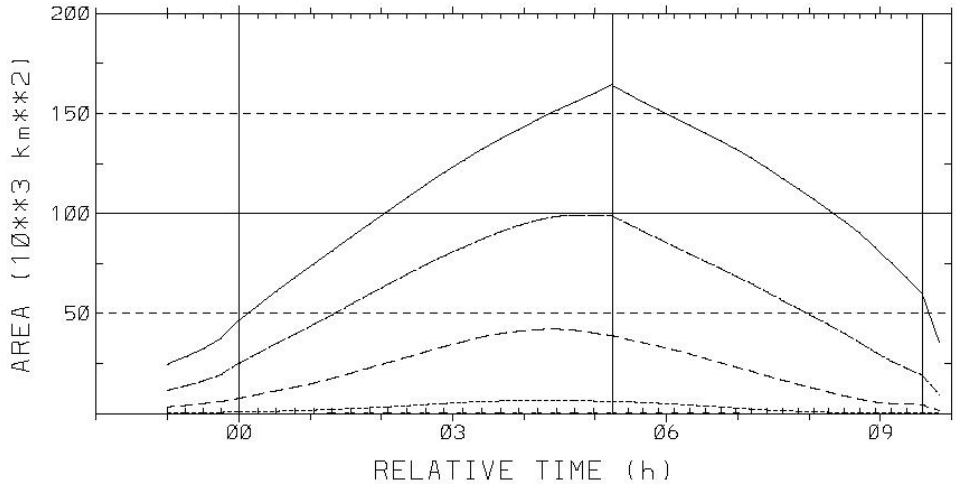

Figure 7.24: Same as Fig. 7.14 except for merger systems.

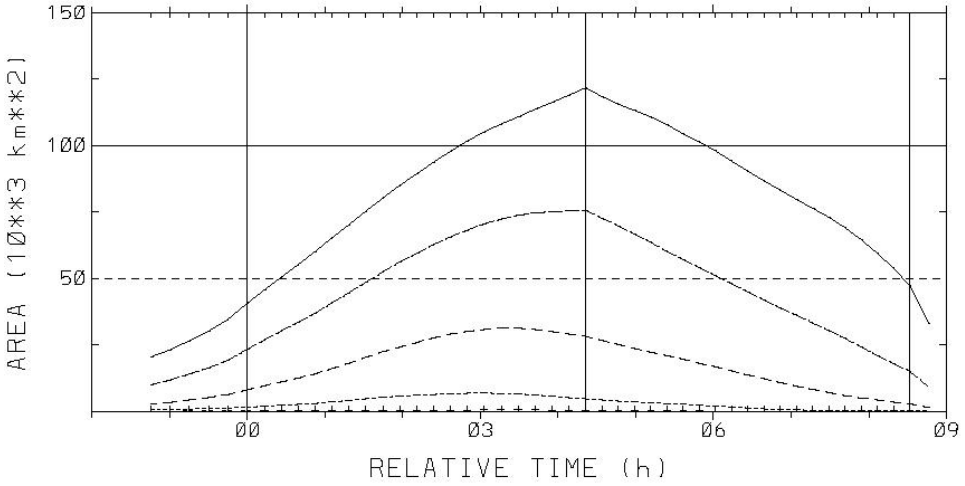

Figure 7.25: Same as Fig. 7.14 except for growth systems.

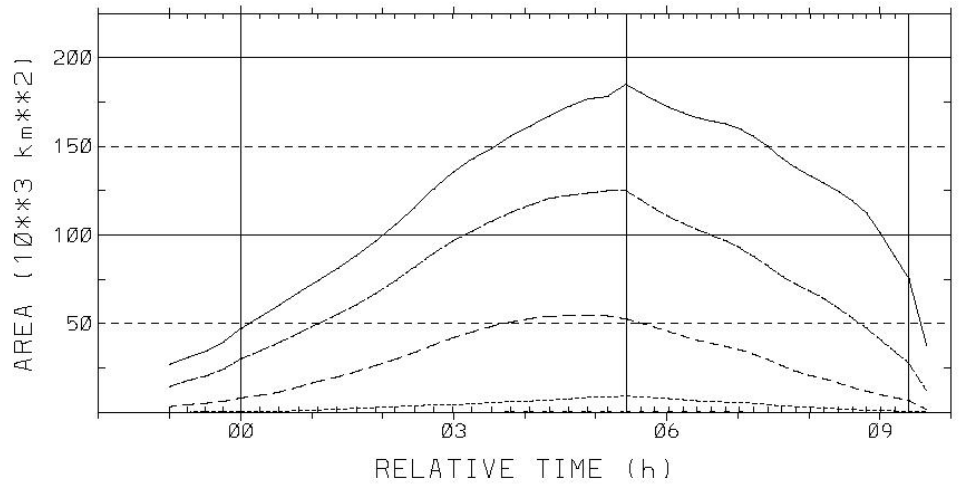

Figure 7.26: Same as Fig. 7.14 except for isolated systems.

7.3 MCS radar lifecycle

The normalized MCS timescale developed to produce composite satellite lifecycles was also used to create composite radar lifecycle plots. Therefore, the vertical lines in Figures 7.27-7.39 still represent the start, maximum, and end times of the *satellite* lifecycle. There are three lines plotted in these figures: the solid line represents volumetric rain rate, V, calculated using the NEXRAD default Z-R relationship as described in Section 3.3.2, the thick, dashed curve represents the precipitation area, A (defined as the reflectivity area $\geq$20 dBZ), and the thin, dashed curve represents the average rain rate, $\bar{R}$, which is calculated as $\bar{R} = V/A$.

Examination of the radar lifecycle plots (Figs. 7.27-7.39) for each category of MCS once again reveals that the systems had very similar lifecycles. The scales vary somewhat between classifications, but the trends and properties of the volumetric rainfall rate, precipitation area, and average rainfall rate were very similar among the categories. The radar lifecycle composite for all systems (Fig. 7.27) shows several common features of an average MCS lifecycle for this study. One feature was that the average rainfall rate reached a maximum very early in the lifecycle at about the time of MCS initiation (left vertical line). At this time, the area of the system was also small, which indicates the presence of developing convective cells. As the system continued to grow, the average rainfall rate decreased signifying an increase in stratiform precipitation. Another feature was that the volumetric rain rate peaked at nearly the same time as the -52°C cloud shield area (middle vertical line) even though the precipitation area continued to grow for approximately another hour. Although the data after MCS termination (right vertical line) were not as reliable due to the sampling of fewer and fewer systems with time, the secondary peak in

average rainfall rate may not be an erroneous feature. Many systems were observed to produce a secondary wave of convective cells along a gust front as they dissipated, which may provide an explanation for this feature.

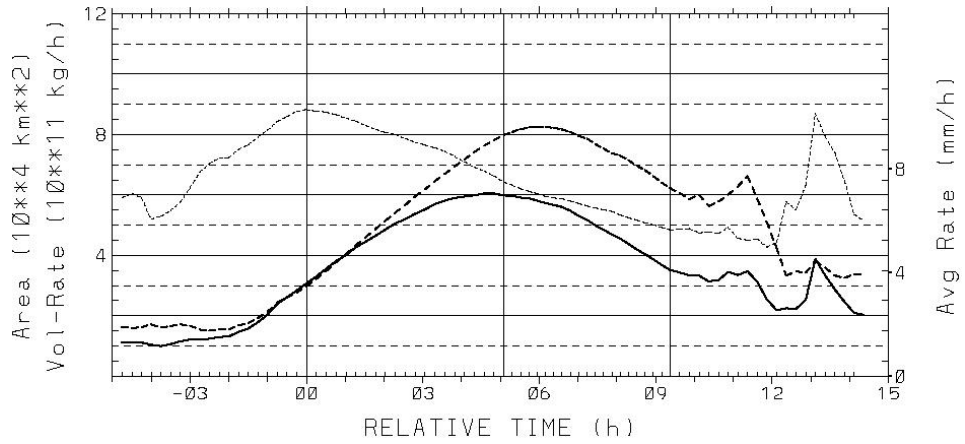

Figure 7.27: Radar lifecycle composite for all systems. Solid curve represents volumetric rain rate, thick, dashed curve represents precipitation area, and thin, dashed curve represents average rain rate. Vertical lines represent start, max, and end times of the *satellite* lifecycle.

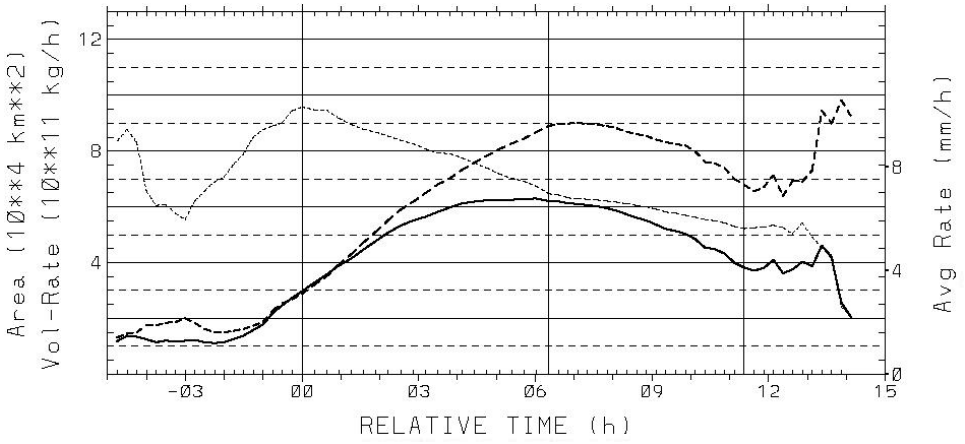

Figure 7.28: Same as Fig. 7.27 except for MCCs.

Additional information about the precipitation characteristics of MCSs were extracted from these composites. For example, the total precipitation mass and convective/stratiform partitioning were calculated to examine some system total precipitation properties of MCSs. The total precipitation mass was calculated from the

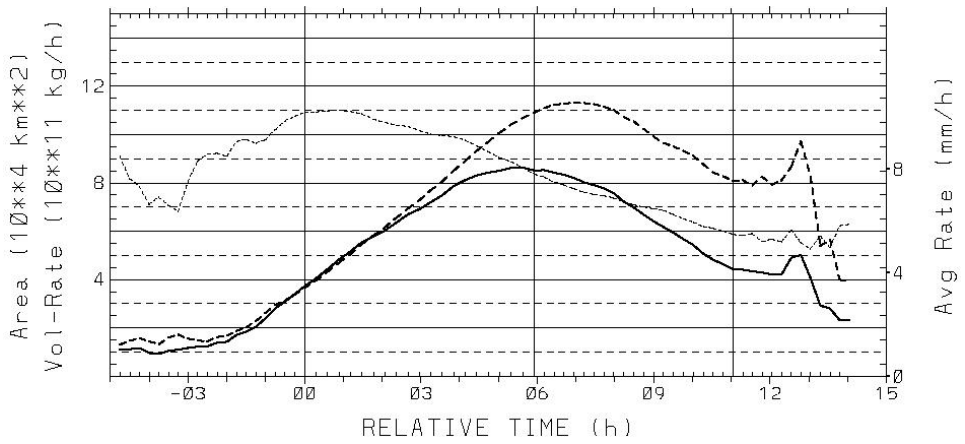

Figure 7.29: Same as Fig. 7.27 except for PECSs.

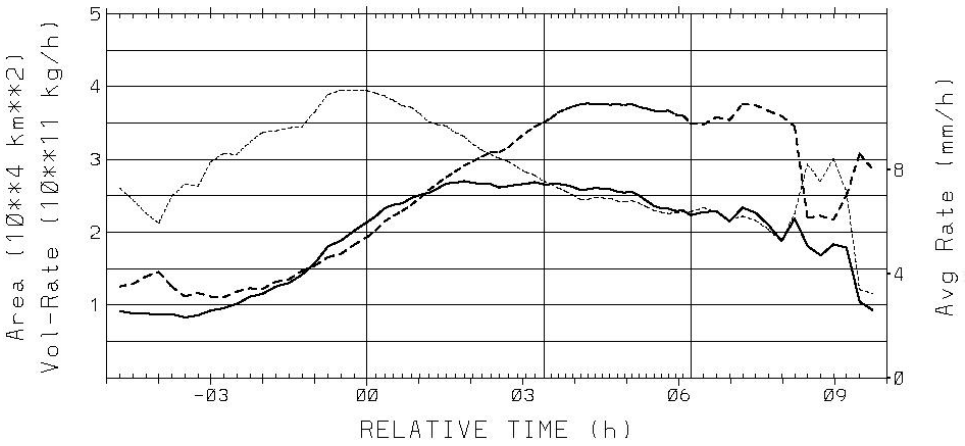

Figure 7.30: Same as Fig. 7.27 except for MβMCCs.

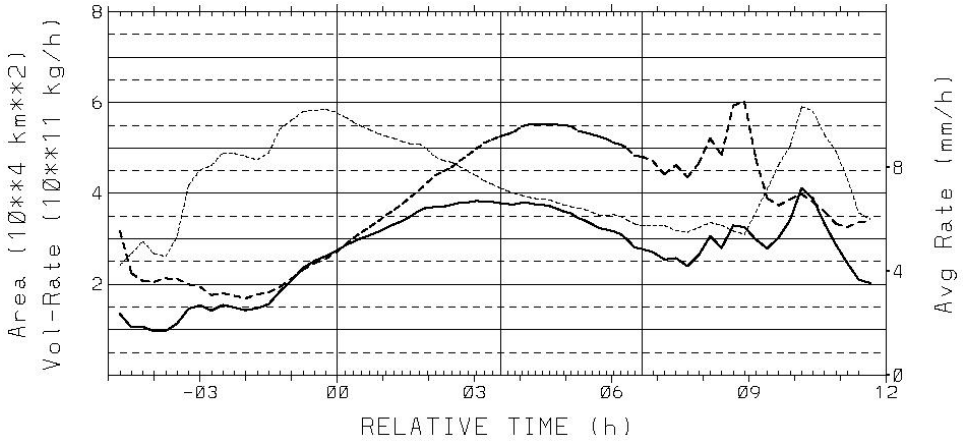

Figure 7.31: Same as Fig. 7.27 except for MβPECSs.

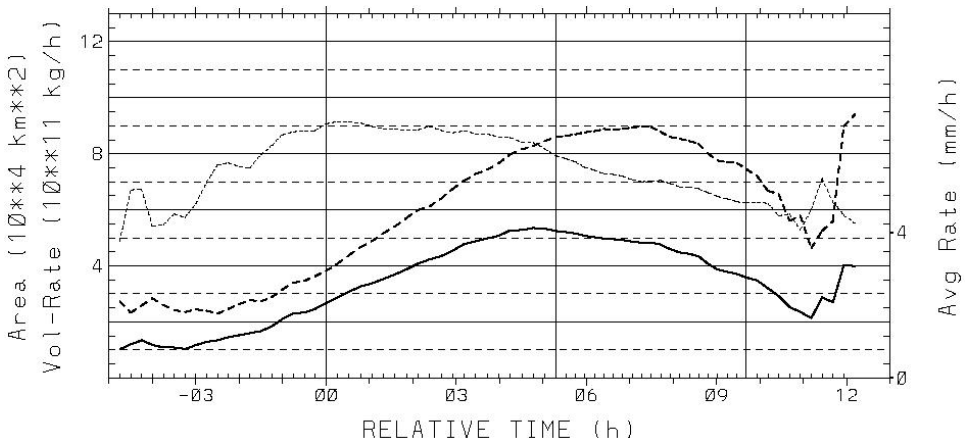

Figure 7.32: Same as Fig. 7.27 except for embedded systems.

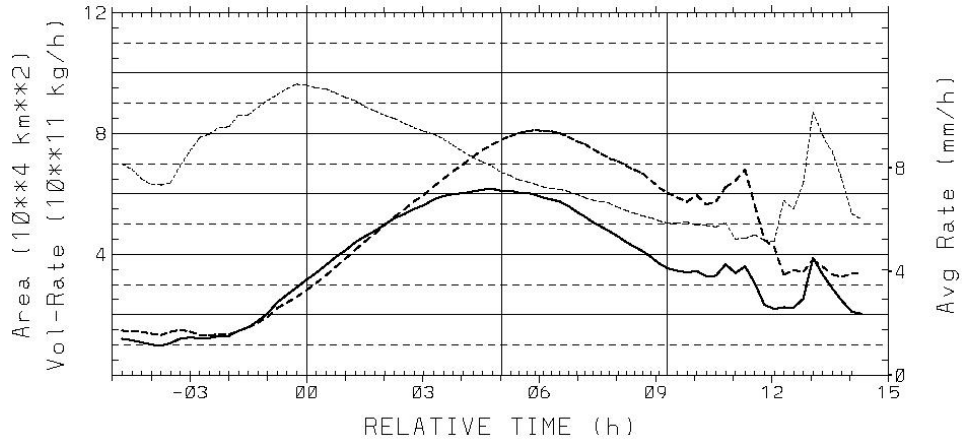

Figure 7.33: Same as Fig. 7.27 except for systems that were not embedded.

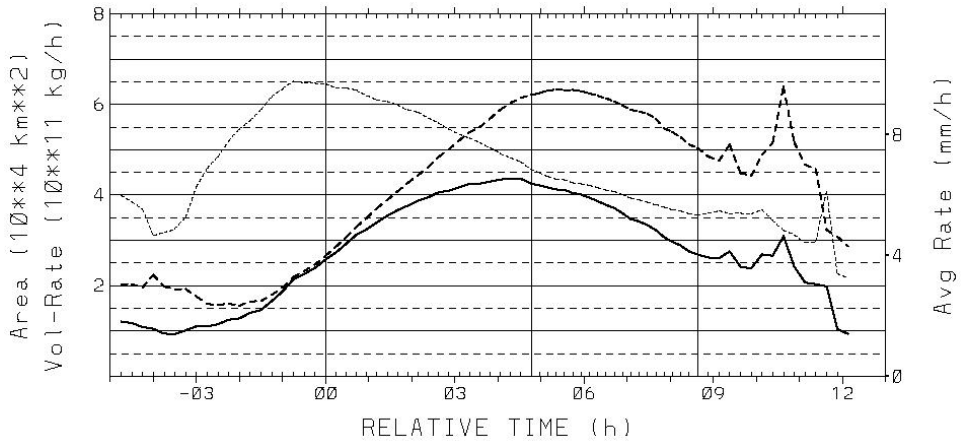

Figure 7.34: Same as Fig. 7.27 except for areal systems.

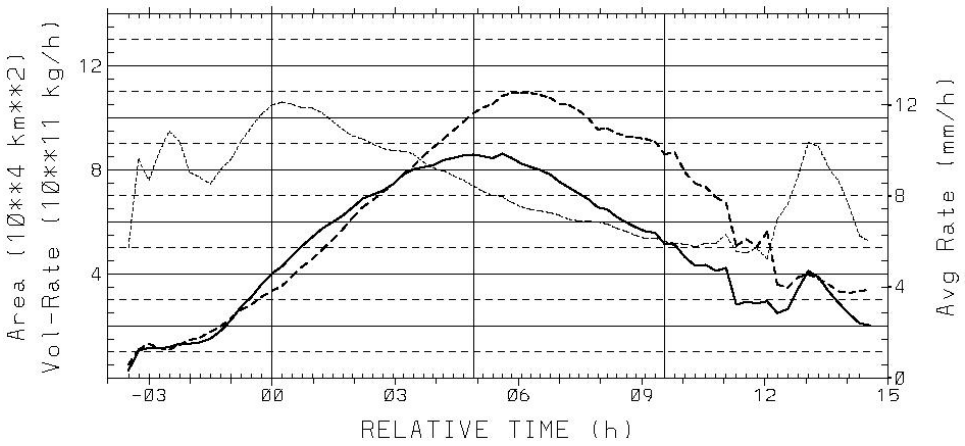

Figure 7.35: Same as Fig. 7.27 except for line systems.

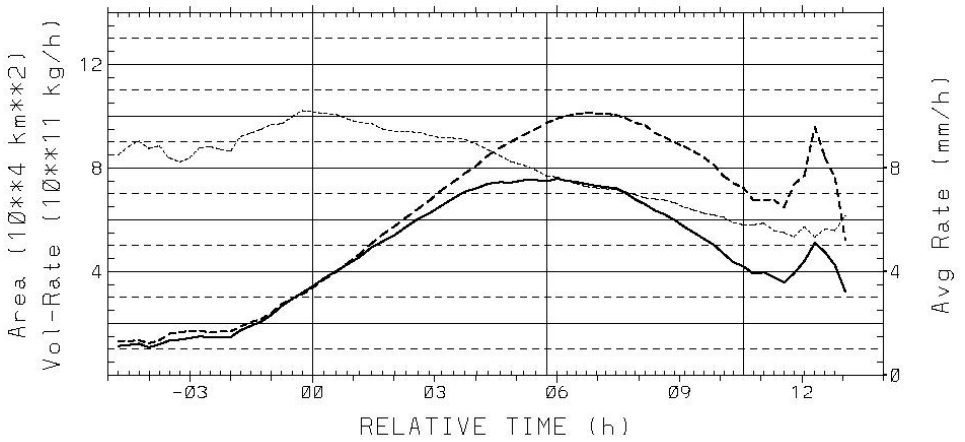

Figure 7.36: Same as Fig. 7.27 except for combination systems.

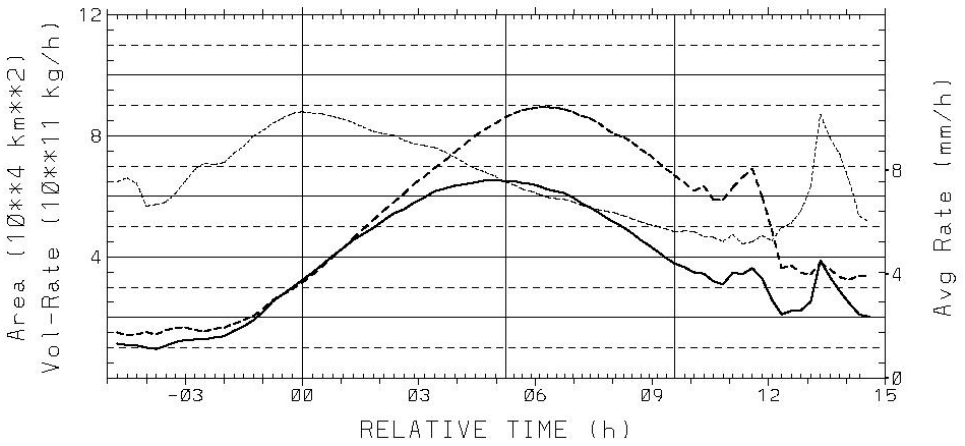

Figure 7.37: Same as Fig. 7.27 except for merger systems.

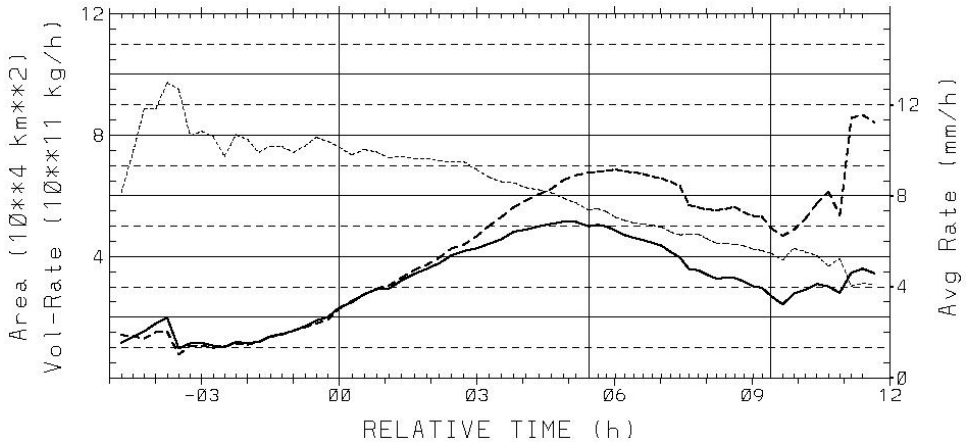

Figure 7.38: Same as Fig. 7.27 except for growth systems.

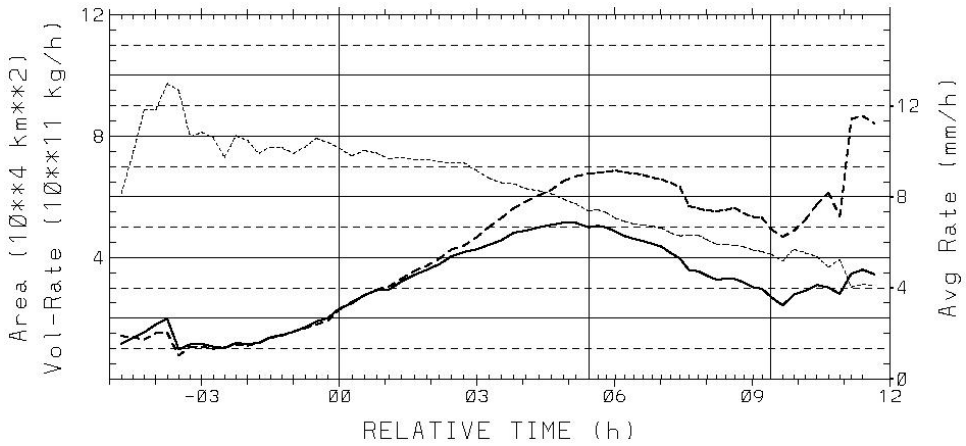

Figure 7.39: Same as Fig. 7.27 except for isolated systems.

radar composites by integrating the volumetric rainfall rate from initiation to termination. The contribution to the total precipitation was divided into convective and stratiform components by choosing a convective reflectivity threshold, where everything less than the threshold was considered stratiform and everything greater than the threshold was considered convective. Steiner et al. (1995) chose 40 dBZ as the convective reflectivity threshold, but they also considered the gradient of the reflectivity field to include some reflectivity centers less than 40 dBZ as convective. Due to the large number of systems considered in this study, the reflectivity gradient was not used to determine convective precipitation; however, a range of convective reflectivity thresholds was selected in an attempt to ascertain a realistic threshold.

Table 7.1 provides the total precipitation mass, average system motion, and convective percentage of precipitation for the entire MCS sample and the satellite classifications. The total precipitation mass for the average MCC is larger than that found by McAnelly and Cotton (1989), but close to the amount for their "large" MCCs. Keep in mind that they estimated the total precipitation mass by hourly rainfall data while the total precipitation mass for this study was estimated using radar data. The larger systems (MCCs and PECSs) were much more prolific rain-producing weather systems than the smaller systems (MβMCCs and MβPECSs) generating more than three times as much precipitation. Examination of the average storm motion reveals that the systems do not move at significantly different speeds. Thus, PECSs would be the most likely MCS to produce the greatest amount of rainfall over a given watershed. Also, notice that the convective contribution to precipitation was nearly identical for each type of MCS regardless of the difference in total precipitation. Houze (1993) claimed that it is typical for stratiform precipitation to account for 25%-50% of the

total rain in MCSs. If this is the case, then the proper convective threshold probably fell somewhere between 40 dBZ and 45 dBZ for this MCS sample.

Similarly, Table 7.2 shows the total precipitation mass, average system motion, and convective percentage for the levels of radar development. First of all, again notice that the convective contribution to precipitation was nearly identical for all categories, except for the embedded systems. As expected, these systems had a higher percentage of stratiform precipitation since by definition they form in an area of stratiform precipitation. When reviewing the total precipitation, there was not much difference between embedded systems and those that did not develop in an area of stratiform precipitation. The areal systems produced much less precipitation than systems with other types of cell arrangement, which is not surprising since they were also found to be smaller and shorter-lived. However, they also moved more slowly than line systems allowing more precipitation to fall over the same area. Finally, systems with merging convective clusters produced much more precipitation than growth or isolated systems. Interestingly, isolated systems had larger cloud shields on average than merger systems, but they produced much less total rainfall indicating the lack of interaction between convective clusters in these systems.

Table 7.1: Total precipitation mass, average motion, and percentage of convective precipitation for the composite of each MCS satellite classification.

	Total Precip. Mass (10^{11} kg)	Average Motion (km/hr)	Convective Percentage for reflectivity thresholds of: **35 dBZ**	**40 dBZ**	**45 dBZ**
All MCSs	47.0	45.0	88.5	75.1	58.0
MCC	60.5	49.3	87.9	73.9	56.8
PECS	75.0	45.8	88.8	75.3	58.0
MβMCC	15.8	40.4	89.2	76.6	60.1
MβPECS	23.0	42.7	88.3	75.5	58.6

Table 7.2: Total precipitation mass, average motion, and percentage of convective precipitation for the composite of each radar development level.

	Total Precip. Mass (10^{11} kg)	Average Motion (km/hr)	Convective Percentage for reflectivity thresholds of: **35 dBZ**	**40 dBZ**	**45 dBZ**
embedded	43.0	44.3	85.0	67.5	47.2
not embedded	47.6	44.6	89.2	76.4	59.8
areal	32.0	40.7	87.6	73.6	56.6
line	67.0	51.8	89.7	76.9	59.3
combination	65.3	47.6	88.8	75.3	58.1
merger	51.9	45.2	88.5	74.9	57.7
growth	32.4	45.4	88.5	76.7	61.0
isolated	37.6	37.4	88.7	76.7	61.0
unclassifiable	52.0	63.2	89.3	77.6	62.2

In addition to analyzing the total precipitation and convective/stratiform partitioning for each type of system, some parameters were calculated using both radar and satellite characteristics to estimate how proficient the systems were at producing precipitation. One such parameter provides the ratio of the average precipitation area to the average cloud shield area (at the $-52°$C temperature threshold). Another parameter estimates the average depth of precipitation produced by a system over its lifetime. This theoretical average depth corresponds to the amount of precipitation that would fall over the system's average cloud shield area provided that it remained stationary throughout its lifecycle. These quantities were calculated from the composites by integrating the volumetric rain rate, precipitation area, and cloud shield area over the lifetime of the systems.

The composite lifecycle characteristics for the satellite classifications are provided in Table 7.3. The duration, average cloud shield area, and average precipitation area are included in this table as they were used to calculate the other precipitation

parameters, which are also listed in the table. First of all, the composite of all MCSs shows that on average almost 60% of the cold cloud shield area had underlying precipitation. MβPECSs were the only type of MCS to vary significantly from that percentage. They were relatively efficient systems as nearly three-fourths of the cloud shield produced precipitation on average. However, since they did not persist as long as the larger systems, their theoretical average depth was less than MCCs and PECSs. With an average theoretical depth of 5 cm, PECSs were once again the most impressive systems while MβMCCs were less impressive producing less than 3 cm of precipitation on average.

Table 7.4 reveals the same information except for the categories of development. Although embedded systems have not demonstrated much importance, they were effective at producing rain. Almost 80% of the cloud shield produced precipitation in these systems resulting in a theoretical average depth of 4.6 cm, which, surprisingly, was larger than for systems that were not embedded. This provides evidence that even though embedded systems may not generate a significant amount of severe weather, they are very important for the production of precipitation over the agricultural region of the central United States. It is also noteworthy to point out that embedded systems and MβPECSs, which formed in the most stable environments (see Chapter 6), also had the highest ratio of precipitation area to cloud shield area. Investigation of the cell arrangement categories shows that once again systems with an areal arrangement of convective cells had much different properties than systems with linearly arranged convection. Although they only had a slightly lower precipitation area ratio, their theoretical depth was more than 1.5 cm less than line and combination systems. This indicates that they were relatively ineffective at producing precipitation. Finally, the interaction of convective clusters had a large influence on the ability of the MCSs to

generate precipitation. Isolated systems had a very low precipitation area fraction, as expected, and produced less than 3 cm of rainfall on average. The most effective means of generating precipitation was by the merging of multiple convective clusters.

Table 7.3: Composite lifecycle characteristics for each MCS satellite classification.

	Duration (hr)	Avg. Cloud Shield Area (10^3 km^2)	Avg. Precip. Area (10^3 km^2)	Theoretical Avg. Precip. Depth (cm)	Ratio of Precip. Area to Cloud Shield Area
All MCSs	9.4	111.5	65.3	4.2	0.59
MCC	11.4	135.5	71.8	4.5	0.53
PECS	11.1	148.4	86.6	5.1	0.58
MβMCC	6.2	55.7	31.9	2.8	0.57
MβPECS	6.7	63.2	46.4	3.6	0.73

Table 7.4: Composite lifecycle characteristics for each level of radar development.

	Duration (hr)	Avg. Cloud Shield Area (10^3 km^2)	Avg. Precip. Area (10^3 km^2)	Theoretical Avg. Precip. Depth (cm)	Ratio of Precip. Area to Cloud Shield Area
embedded	9.7	93.5	73.6	4.6	0.79
not embedded	9.3	114.8	63.5	4.2	0.55
areal	8.6	94.4	51.9	3.4	0.55
line	9.6	132.0	84.0	5.1	0.64
combination	10.6	129.1	78.7	5.1	0.61
merger	9.6	114.8	70.4	4.5	0.61
growth	8.5	87.7	50.1	3.7	0.57
isolated	9.4	130.7	52.1	2.9	0.40
unclassifiable	9.3	126.3	69.1	4.1	0.55

Chapter 8

Summary and conclusions

8.1 Summary

The analysis of a sample of MCSs was presented in this thesis. The systems were first identified and classified according to infrared satellite characteristics into four categories: MCCs, PECSs, MβMCCs, and MβPECSs. Then, the systems were reanalyzed with 2-km national composite radar reflectivity data to examine the development stages at a higher spatial and temporal resolution. The development of each system was categorized by a three-level process based on the presence of stratiform precipitation, arrangement of convective cells, and interaction of convective clusters. Finally, further analyses of each category were conducted based on the environment, severe weather reports, satellite lifecycle, and rainfall lifecycle in an attempt to discover differences among the various categories.

8.2 Conclusions

Dividing the MCSs according to satellite and radar characteristics resulted in a multitude of ways to view and analyze data. Certainly, not every division resulted

in new and useful information, but a few interesting and valuable results did appear. Examination of the basic characteristics for the satellite classifications showed that:

- PECSs were the largest and most common type of MCS.
- Two-thirds of the systems were smaller than average even though a majority of the systems fell into the larger satellite classifications (MCCs and PECSs).
- Larger systems peaked early in the convective season (May) while the smaller systems peaked later in the convective season (July).

Some useful results also came from analyzing the general characteristics of the radar classifications of development:

- More than half of the systems were either areal merger or combination merger systems.
- Less than 20% of the systems were embedded, half of the systems were areal, and more than 70% were merger systems.
- Embedded, areal, and growth systems were statistically smaller than the other categories in their respective levels. Areal systems also had shorter durations than systems with other types of cell arrangement.
- Embedded and line systems were most common in April when strong baroclinic forcing remained.

In addition to possessing knowledge about the common features of these systems, it is also desirable to know something about their predictability. Thus, some severe weather parameters were reviewed to determine the types of environments that produce these systems. Unfortunately, few strong signals appeared:

- On average, the MCSs developed in environments with a moderate potential to produce thunderstorms.

- The TT and SWEAT indices tended to be greater for larger systems.

- The range of PW decreased for larger systems possibly indicating a narrow window of PW values needed for the production of massive MCSs.

- MβPECSs and embedded systems developed in more stable environments than the other systems. The remaining systems had no detectable differences among their environments.

Closely related to the issue of the nurturing environment is the ability of the system to produce severe weather. Severe weather affects society significantly; therefore, each MCS classification was examined for an inclination of producing violent storms:

- PECSs were the type of MCS most likely to be associated with severe weather.

- The smaller satellite classifications had many fewer severe weather reports per system than the larger systems.

- Embedded and areal systems were less likely to be associated with severe weather than other systems in their respective levels.

Finally, the systems were composited to determine the geographical biases and lifecycle characteristics for each category.

- PECS initiated and developed farther east than MCCs.

- A majority of the systems in the southern part of the U.S. had an areal arrangement of convective cells.

- The composite satellite lifecycles showed that the colder cloud top temperature thresholds reached a maximum area before the warmer thresholds with the growth stage lasting longer than the decay stage.

- The average rainfall rate peaked early in the radar lifecycle while the precipitation area reached a maximum after the system attained its maximum extent.

- The convective/stratiform partitioning of precipitation was nearly identical for all systems except for embedded systems, which had a higher percentage of stratiform precipitation.

- The systems that formed in the most stable environments, MβPECS and embedded systems, also had the largest ratio of precipitation area to cloud shield area.

- MCCs and PECSs generated much more precipitation than the smaller satellite-defined systems.

- Embedded, line, and merger systems were the most proficient systems at producing precipitation in their respective levels of development while areal and isolated systems were the least proficient systems.

Overall, a large sample of MCSs over the central United States was analyzed and classified. Common patterns of MCS development were identified, and a classification scheme was devised to categorize a large number of assorted MCSs. Hopefully,

this scheme will prove to be flexible and practical enough for use in future MCS studies. The levels of radar development may have important implications on real-time forecasting, especially the arrangement of convective cells. Given that the initial convection is spread out over an area (i.e. an areal system), the systems tended to be smaller, shorter-lived, less severe, and less effective at producing precipitation than MCSs with linearly arranged convection. Bluestein et al. (1987) also found these types of systems to be less likely associated with severe weather. A forecaster could use this information to assist in issuing warnings and making short-term forecasts as these extremely difficult decisions have a large impact on society.

8.3 Suggestions for future research

Even though much has been learned about MCSs over the past twenty-five years, there still remains much to understand. This research was another attempt to extract information about MCSs by categorizing them and investigating the differences among the classifications. As Doswell (1991) commented, "a taxonomy of convective systems can become a valuable contribution to our understanding of such storm systems and their recognition by field forecasters." The focus of this research was to develop extensive classification schemes that would at least be a small step toward enhancing our knowledge of MCSs.

Although hundreds of systems were considered in this study, the findings should be tested and verified with an even larger MCS sample to create a true climatology. Only at that point can broad generalizations be made about MCSs. Not only should more systems be tested, but the systems in this study were analyzed using only satellite, radar, and sounding data. Thus, a more detailed examination of the synop-

tic and storm environments using model reanalysis data would likely provide useful information about the MCSs.

The frequency of MCSs forming across the central United States is astounding as one MCS is located over this region on average per day during the warm season. The focus of this study was to examine the differences among past systems to gain insight on future systems, but what can be said about their predictability? Often supercells and MCSs develop in similar environments, but these environments do not always yield MCSs. This poses a significant forecasting problem as MCSs can have a much larger impact on society than supercells due to their greater physical extent. An investigation of both the synoptic scale and mesoscale features that influence the formation of each system would be invaluable in understanding how nature discriminates between the systems. Such information would also be important in understanding the development process outlined in this thesis.

The greatest contribution to further the understanding of MCSs will be to increase the density and quality of the observation network. This will allow for the analysis of mesoscale features important to MCS development that cannot currently be resolved by the observation network (Stensrud and Fritsch 1994). In addition, this dense network would provide invaluable data for mesoscale models to more accurately simulate these systems, which would most certainly lead to further understanding of MCS development. Undoubtedly, progress will continue as insight gained from this study and studies similar to it build toward understanding mesoscale convective systems.

Appendix A

Sounding Indices

***All temperatures are in degrees Celsius.**

Lifted Index (LI)

$$LI = T_e - T_p$$

where T_e is the environmental temperature at 500 mb
where T_p is the theoretical temperature a parcel of air would have at 500 mb if it was lifted from the surface

LI	Thunderstorm Potential
>-3	Weak
-3 to -5	Moderate
< -5	Strong

Total Totals Index (TT)

$$TT = (T_{850} + T_{d850}) - (2 * T_{500})$$

where T_{850} is the temperature at 850 mb
where T_{d850} is the dewpoint temperature at 850 mb
where T_{500} is the temperature at 500 mb

TT	Thunderstorm Potential
<45	Weak
45 to 55	Moderate
> 55	Strong

K Index (KI)

$$KI = (T_{850}\text{-}T_{500}) + T_{d850} - (T_{700}\text{-}T_{d700})$$

where T_{850} is the temperature at 850 mb
where T_{500} is the temperature at 500 mb
where T_{d850} is the dewpoint temperature at 850 mb
where T_{700} is the temperature at 700 mb
where T_{d700} is the dewpoint temperature at 700 mb

KI	Thunderstorm Potential
<25	Weak
25 to 35	Moderate
> 35	Strong

SWEAT Index (SWEAT)

$$SWEAT = (12*T_{d850}) + (20*(TT\text{-}49)) + (2*W_{850}) + W_{500} + (125*[\sin(D_{500}\text{-}D_{850})+.2])$$

where T_{d850} is the dewpoint temperature at 850 mb
where TT is the total totals index and
(TT-49) is set to zero if negative
where W_{850} is the wind speed at 850 mb in knots
where W_{500} is the wind speed at 500 mb in knots
where D_{850} is the wind direction at 850 mb
where D_{500} is the wind direction at 500 mb

SWEAT	Thunderstorm Potential
<300	Weak
300 to 399	Moderate
400 to 599	Strong
> 600	High

Bibliography

Anderson, C. J. and R. W. Arritt, 1998: Mesoscale convective complexes and persistent elongated convective systems over the United States during 1992 and 1993. *Mon. Wea. Rev.*, **126**, 578–599.

Augustine, J. A., 1985: An automated method for the documentation of cloud-top characteristics of mesoscale convective systems. NOAA Tech. Memo. ERL ESG-10, Dept. of Commerce, Boulder, CO, 121 pp.

Augustine, J. A. and K. W. Howard, 1988: Mesoscale convective complexes over the United States during 1985. *Mon. Wea. Rev.*, **116**, 685–701.

Blanchard, D. O., 1990: Mesoscale convective patterns of the southern High Plains. *Bull. Amer. Meteor. Soc.*, **71**, 994–1005.

Bluestein, H. B. and M. H. Jain, 1985: Formation of mesoscale lines of precipitation: Severe squall lines in Oklahoma during the spring. *J. Atmos. Sci.*, **42**, 1711–1732.

Bluestein, H. B. and C. R. Parks, 1983: A synoptic and photographic climatology of low-precipitation severe thunderstorms in the Southern Plains. *Mon. Wea. Rev.*, **111**, 2034–2046.

Bluestein, H. B., G. T. Marx, and M. H. Jain, 1987: Formation of mesoscale lines of precipitation: Non-severe squall lines in Oklahoma during the spring. *Mon. Wea. Rev.*, **115**, 2719–2727.

Brooks, R. H., C. A. Doswell, and J. Cooper, 1994: On the environments of tornadic and nontornadic mesocyclones. *Wea. Forecasting*, **9**, 606–618.

Cotton, W. R., M. S. Lin, R. L. McAnelly, and C. J. Tremback, 1989: A composite model of mesoscale convective complexes. *Mon. Wea. Rev.*, **117**, 765–783.

Doswell, C. A., 1991: Comments on mesoscale convective patterns of the southern High Plains. *Bull. Amer. Meteor. Soc.*, **72**, 389–390.

Fritsch, J. M., R. J. Kane, and C. R. Chelius, 1986: The contribution of mesoscale convective weather systems to the warm-season precipitation in the United States. *J. Climate Appl. Meteor.*, **25**, 1333–1345.

Fujita, T. T., 1978: Manual of downburst identification for project NIMROD. Satellite and Mesometeorology Research Paper No. 156, Dept. of Geophysical Sciences, Univ. of Chicago, 104 pp. [NTIS PB-286048].

Fulton, R. A., J. P. Breidenbach, D.-J. Seo, D. A. Miller, and T. O'Bannon, 1998: The WSR-88D rainfall algorithm. *Wea. Forecasting*, **13**, 377–395.

Hilgendorf, E. R. and R. H. Johnson, 1998: A study of the evolution of mesoscale convective systems using WSR-88D data. *Wea. Forecasting*, **13**, 437–452.

Houze, R. A., Jr., 1993: *Cloud Dynamics*. Acadmeic Press, 573 pp.

Houze, R. A., Jr., B. F. Smull, and P. Dodge, 1990: Mesoscale organization of spring-time rainstorms in Oklahoma. *Mon. Wea. Rev.*, **118**, 613–654.

Johns, R. H. and W. D. Hirt, 1987: Derechos: widespread convectively induced windstorms. *Wea. Forecasting*, **2**, 32–49.

Knupp, K. R. and W. R. Cotton, 1987: Internal structure of a small mesoscale convective system. *Mon. Wea. Rev.*, **115**, 629–645.

Loehrer, S. M. and R. H. Johnson, 1995: Surface pressure and precipitation life cycle characteristics of PRE-STORM mesoscale convective systems. *Mon. Wea. Rev.*, **123**, 600–621.

Maddox, R. A., 1980: Mesoscale convective complexes. *Bull. Amer. Meteor. Soc.*, **61**, 1374–1387.

Maddox, R. A., 1983: Large-scale meteorological conditions associated with midlatitude, mesoscale convective complexes. *Mon. Wea. Rev.*, **111**, 126–140.

Maddox, R. A., D. M. Rogers, and K. W. Howard, 1982: Mesoscale convective complexes over the United States during 1981 – An annual summary. *Mon. Wea. Rev.*, **115**, 2298–2321.

McAnelly, R. L. and W. R. Cotton, 1985: The precipitation lifecycle of mesoscale convective complexes. Preprints*, 6th Conf. Hydrometeorology*, Amer. Meteor. Soc., 197-204.

McAnelly, R. L. and W. R. Cotton, 1986: Meso-β scale characteristics of an episode of meso-α scale convective complexes. *Mon. Wea. Rev.*, **114**, 1740–1770.

McAnelly, R. L. and W. R. Cotton, 1989: The precipitation life cycle of mesoscale convective complexes over the central United States. *Mon. Wea. Rev.*, **117**, 784–808.

Orlanski, I., 1975: A rational subdivision of scales for atmospheric processes. *Bull. Amer. Meteor. Soc.*, **56**, 527–530.

Parker, M. D., 1999: May 1996 and May 1997 linear mesoscale convective systems of the Central Plains: Synoptic meteorology and a reflectivity-based taxonomy. Dept. of Atmospheric Science Paper No. 675, Colorado State University, Fort Collins, CO, 185 pp.

Parker, M. D. and R. H. Johnson, 2000: Organizational modes of midlatitude mesoscale convective systems. *Mon. Wea. Rev.*, **128**, 3413–3436.

RAOB Program, 1997: *RAOB: The Complete RAwinsonde OBservation Program: User's Guide*. Environmental Research Services. Version 4.0.

Rasmussen, E. N. and R. B. Wilhelmson, 1983: Relationships between storm characteristics and 1200 GMT hodographs, low-level shear, and stability. Preprints, *13th Conf. on Severe Local Storms*, Amer. Meteor. Soc., 55-58.

Schiesser, H. H., R. A. Houze, Jr., and H. Huntrieser, 1995: The mesoscale structure of severe precipitation systems in Switzerland. *Mon. Wea. Rev.*, **123**, 2070–2097.

Steiner, M., R. A. Houze, Jr., and S. E. Yuter, 1995: Climatological characterization of three-dimensional storm structure from operational radar and rain gauge data. *J. Appl. Meteor.*, **34**, 1978–2007.

Stensrud, D. K. and J. M. Fritsch, 1994: Mesoscale convective systems on weakly forced large-scale environment. Part II: Generation of a mesoscale initial condition. *Mon. Wea. Rev.*, **122**, 3326–3344.

Weisman, M. L. and J. B. Klemp, 1982: The dependence of numerically simulated convective storms on vertical wind shear and buoyancy. *Mon. Wea. Rev.*, **110**, 504–520.

Weisman, M. L. and J. B. Klemp, 1984: The structure and classification of numerically simulated convective storms in directionally varying wind shears. *Mon. Wea. Rev.*, **112**, 2479–2498.

Weisman, M. L. and J. B. Klemp, 1986: Characteristics of isolated convective storms. *Mesoscale Meteorology and Forecasting*, P. S. Ray, Ed., Amer. Meteor. Soc., 331-358.

Woodley, W. L., A. R. Olsen, A. Herndon, and V. Wiggert, 1975: Comparison of gage and radar methods of convective rain measurement. *J. Appl. Meteor.*, **14**, 909–928.

Zipser, E. J., 1982: Use of a conceptual model of the life cycle of mesoscale convective sysystems to improve very-short-range forecasts. *Nowcasting*, K. Browning, Ed., Academic Press, 191-204.